University of Naples Federico II

Photo-Switchable Bio-Interfaces for the Dynamic Control of Cell Behaviour

PhD Thesis

PhD Program in Industrial Product and Process Engineering (XXXV cycle)

Francesca Mauro

Supervisor

Prof. Paolo A. Netti

Advisors

Dr. Carlo F. Natale

Dr. Eng. Valeria Panzetta

Coordinator

Prof. Andrea D'Anna

Novembre 2019- Gennaio 2023

PHOTO-SWITCHABLE BIO-INTERFACES FOR THE DYNAMIC CONTROL OF CELL BEHAVIOUR

A THESIS SUBMITTED IN PARTIAL FULFILLMENT OF THE REQUIREMENT FOR THE DEGREE OF DOCTOR OF PHILOSOPHY IN

INDUSTRIAL PRODUCTS AND PROCESS ENGINEERING

Author

Francesca Mauro

Supervisor

Prof. Paolo A. Netti

Advisors

Dr. Carlo F. Natale

Dr. Eng. Valeria Panzetta

Coordinator

Prof. Andrea D'Anna

Table of Contents

Abstract

The external cellular environment carries out a crucial role in affecting and dictating cellular functions thus influencing several biological processes such as morphogenesis, tissue regeneration and repair. The bidirectional communication between cells and the extracellular matrix (ECM) occurs through the transmission of biochemical/biophysical signals at sub-micrometric level involving different sub-cellular components such as focal adhesions, cytoskeleton structures and the nucleus, activating then a series of biological events that can eventually affect cellular fate. Indeed, the extracellular matrix has a peculiar 3D organization dictated by the spatial organization of fibres bundles, providing a specific geometry that is involved in shaping tissue architecture and functions. Moreover, the ECM is a dynamic entity and its properties change during time (*i.e.* tissue growth, disease progression) representing a fundamental aspect that should be taken into account in order to design more reliable bio-interfaces able to impact cell function and fate. Numerous studies have been done in order to investigate cellular response to external stimuli, but the majority includes the presentation of static signals. Thus, the aim of my PhD project is focused on the realization of dynamic bio-interfaces that reliably replicate the native extracellular environment for *in-vitro* cell culturing. To this purpose, photo-deformable azopolymer material has been chosen to cover glass-bottom petri-dishes and provide dynamic platform for cells. Indeed, azobenzene-based materials have the ability to change the shape of surface topography in response to light, as a consequence of mass movement triggered by the *trans-cis* photoisomerization of the azo-moiety. Precisely, by illuminating their surface with a linearly polarized light, a linear pattern, in the form of parallel ridges/grooves can be imprinted on the azopolymer surface and easily erased with a non-polarized or circularly polarized light. We investigated the behaviour of human breast epithelial cells (MCF10A) in response to *in-situ* linear light-induced topography patterning, in terms of cell and nuclear

morphology and mechanical properties, in order to spatiotemporally control and guide their functions. Additionally, we found that the transmission of topographic signal can have an impact also on the internal organization of cell nucleus, stating that the propagation of macroscopic deformation can reach the internal nuclear structures up to chromatin level. Then, the photo-switching properties of azopolymer were exploited in order to transmit cyclic topographical signals by finely presenting/removing a linear pattern with the aim to examine the effectiveness of the dynamic platform to reverse cells behaviour.

Chapter 1

Introduction

1.1. Cell-Material Interaction

In their native environment, cells are surrounded by the extracellular matrix (ECM) with which they communicate through the transmission of biochemical and biophysical cues [1]. The cell-ECM crosstalk occurs in a bilateral manner, with cells generating forces that remodel and alter ECM structure and organization [2], and ECM physical properties transduced into cell biological events that eventually affect cell functions, such as spreading, migration, morphogenesis, proliferation and differentiation, through a process known as mechano-transduction [3]. One mechanism through which cells interact with the ECM is signalling via matrix adhesion molecules and receptors such as integrins [4], which are transmembrane proteins enabling cells to be anchored to the ECM, promoting their adhesions and transmission of information to e from the ECM. The integrins also provide the site of formation of Focal Adhesions (FAs), which are constituted by a highly organized ensemble of cytoplasmic proteins (talin, paxillin, zyxin and vinculin) that represent the mechanosensitive complexes through which cells sense and probe the extracellular environment. Indeed, FAs connect integrins to cell cytoskeleton actin filaments to form the adhesion complexes, which play a fundamental role in the transmission of external signals [5]. In details, integrins can transmit mechanical forces to ECM through cell actomyosin contractility or, conversely, from external environment to cell cytoskeleton actin contractile filaments, thus regulating its architecture [6]. Indeed, actin filaments are reported to function as the mechano-sensor for tensile forces applied to cells [7]. Furthermore, it is nowadays well-known that cell cytoskeleton can transmit these external mechanical forces to the nucleus through

nuclear transmembrane proteins (LINC complexes), influencing its shape and chromatin organization [8], confirming the role of nucleus as mechano-sensitive organelle in the process of mechano-transduction [9,10]. Additionally, the native extracellular environment has been demonstrated to be a dynamic entity, continuously undergoing remodelling, assembly and degradation processes during growth and in disease progression [11–14]. In summary, the cell-ECM crosstalk regulates, through integrins, cell functions in terms of adhesion, migration, proliferation, morphology and differentiation. The control of these processes occurs in a dynamic way since ECM is constantly undergoing remodelling, assembly and degradation during the normal processes of development and wound repair. For this reason, the realization of dynamic bio-interfaces, able to recapitulate reliably the native extracellular environment and to provide precise signals both in space and in time in order to investigate cell behaviour, represent an ongoing challenge for applications in tissue engineering.

1.2. Topography Activation of Cell Mechano-transduction

Biophysical signals are associated with mechanical forces generated from ECM rigidity and topographical cues which characterize the geometrical structure of ECM. Matrix topography is involved in shaping tissue architecture and plays an essential role in cellular and tissue organization. Topographical features in matrix can be present at different length scales (*i.e.* from nano- to microscale) and shape (*e.g.* fibers, pores) inducing local (*i.e.* at FAs) and global (*i.e.* cell spreading and shape) changes in cell behaviour. Changes in topographical features at the scale of single cell size (*i.e.* microscale) may influence the degree of cell spreading and give signals associated with contact guidance such as during cell migration along a fibrillar matrix [15]. For example, the basement membrane, an ubiquitous ECM structure separating cell layers from interstitial ECM, regulates a series of tissue functions, including polarization and compartmentalization [16]. Also, ultrastructural analysis of ex vivo rat myocardium revealed that within the

myocardium, cells are highly elongated and oriented along matrix fibres direction, suggesting a strong influence of ECM architecture in guiding myocardial organization during tissue development [17]. Many cellular structure as integrin/FA sites, G-protein, ion channels, cytoskeleton components and membrane biomolecules have been identified as potential mechano-sensors, able to convert external physical signal into biochemical process [18]. Thus, it is necessary to better understand the interaction, and the related biological phenomena, between cells and its external environment in order to study and predict cells' behaviours. To this aim, in the past years many studies have been conducted in order to investigate cell response to external physical signals through the fabrication of Cell Instructive Materials (CIMs) which were supposed to recapitulate the *in-vivo* ECM [19]. The most widely studied topographies are grooves and grids, protrusions and pit arrays. For example, cells exposed to grooved substrates usually acquire an elongated morphology and alignment to groove direction, reproducing the native tissue organization and promoting cell attachment and polarization state [20–22].

1.2.1. Focal Adhesions Signalling

The first mechanosensitive subcellular structures that probe the external ECM physic-chemical properties are the focal adhesions, which are connected to integrins that directly interact with ECM adhesive proteins such as fibronectin, vitronectin and laminin [23]. Topographic patterns provide sites that are readily accessible for cell lamellipodia and filopodia, such as the top of ridges or pillars, as well as the bottom of grooves and pits. The accessibility of a given region to the cell membrane and its protrusions depends on the geometric features of the pattern, *i.e.* the depth and pitch. Several works reported that in the presence of microgroove patterns, focal adhesions form predominantly on the top of the ridge due to the restriction imposed by lateral barrier [24–26], which also affect FAs orientation and alignment [27–29]. Moreover, Ventre M. *et al.* showed that

topographic geometrical characteristics can influence FAs formation and growth ultimately dictating cell adhesion and polarization. More precisely, cells can sense the adjacent topographic features only if these are separated by a distance on the length scale of cell filopodia extension (Fig 1.1 A) [30].

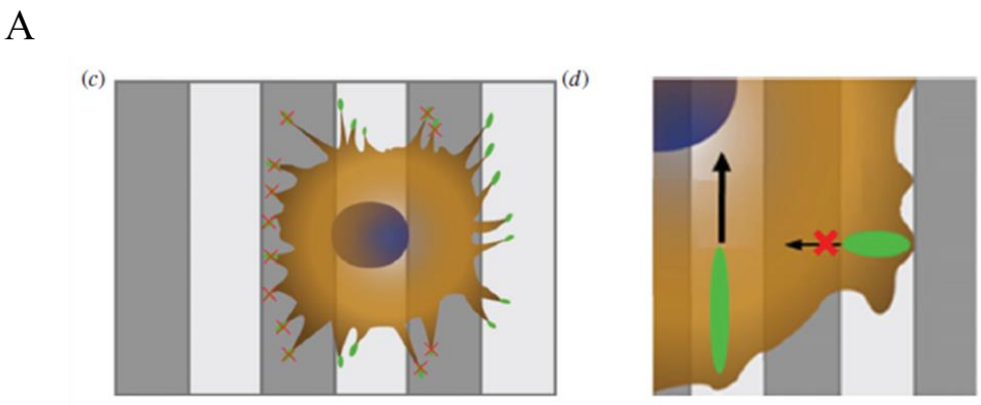

Figure 1.1 A) Graphic representation of filopodia probing topography mechanisms. If the distance is larger, filopodia cannot bridge several ridges (left), while on narrower topographic features (right), FAs can overpass the ridge dimension and grow significantly [30].

1.2.2. Cell Cytoskeleton Assembly

The process of physical signals mechano-transduction is a stepwise mechanism. After probing external environment, focal adhesions transmit the information to the inner cytoskeleton, which regulate cell shape, maintain its structural integrity and also contribute to cell mechanical properties [31]. The cytoskeleton network is composed of three main types of polymers: actin filaments, microtubules and intermediate filaments. Both actin filaments and microtubules provide suitable tracks for molecular motors that move preferentially in one direction. These motors are members of the dynein or kinesin families for microtubules and the large family of myosin proteins for actin filaments. Further, myosin motors also act on the bundles of aligned actin filaments in stress fibres, allowing the cells to contract, and sense, their external environment [32]. Several studies reported the effect of topographical cues on cell morphology following cytoskeleton re-

organization which is able to align and orient cells along a specific direction dictated by the underlying pattern [33–37] (Fig. 1.2 A) through the process known as contact guidance [38]. Yim E.K.F *et al.* showed that a 350 nm gratings of tissue-culture polystyrene (TCPS) and polydimethylsiloxane (PDMS) can modulate human mesenchymal stem cells (hMSC) morphology, with elongated hMSCs exhibiting an aligned actin cytoskeleton, while on unpatterned controls, spreading cells resulted randomly oriented [39] (Fig. 1.2 B).

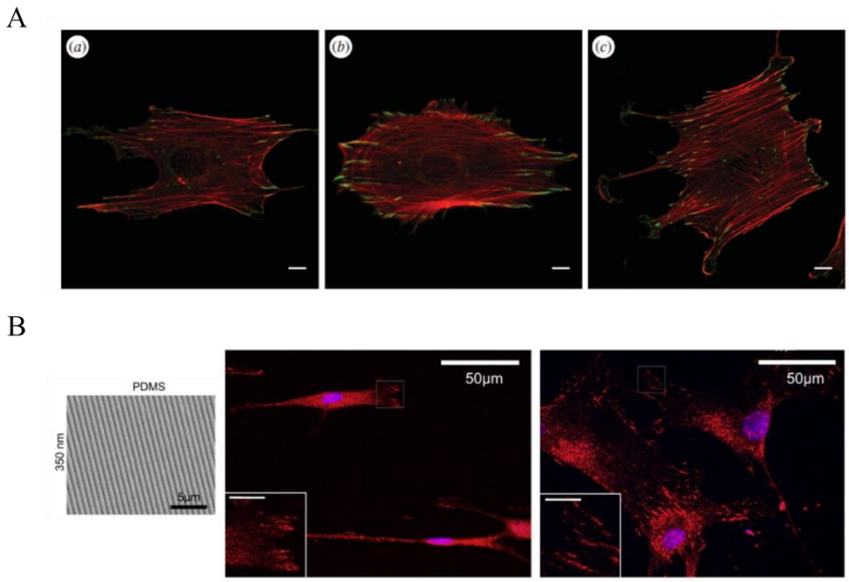

Figure 1.2. Representative confocal images of cells morphology modulation on micropatterned surfaces. A) Confocal images of MC3T3 cells cultivated on oxygen plasma-treated substrates for 4 h on (a) 2 µm pattern, (b) 5 µm and (c) flat surfaces [30]. B) hMSC focal adhesions (vinculin, red) organization on PDMS 350 nm gratings (left) and flat PDRM substrate (right) [39].

1.2.3. Nucleus Organization

Forces applied to cells are then transmitted through cytoskeleton actin fibres to the different inner cellular organelles. The nucleus is the largest and stiffest organelle in eukaryotic cell and is composed of a nuclear interior, containing DNA that is wrapped around histones, which in turn are organized into higher-order structures, classified as either open, transcriptionally active euchromatin or

condensed, inactive heterochromatin, and a nuclear envelope (NE) [40]. The NE act as a barrier for genetic material protection and is constituted by two lipid layers known as the inner and outer nuclear membrane (INM and ONM, respectively). The INM is directly connected to nuclear lamina, which is a meshwork of intermediate filaments separated into A-type and B-type. Lamin A-type contribute mainly to nuclear stiffness and integrity [41]. Further, the NE is connected to cell cytoskeleton through nuclear transmembrane proteins (LINC complexes), which allow the transmission of external mechanical signals to the nucleus. Indeed, the NE and actin cytoskeleton are considered as active partners in regulating several cell functions, such as gene expression, nuclear shape and stiffness, cell migration and division [42] (Fig. 1.3 A). Although recent studies have pointed out the emergent role of nucleus as mechanosensory element which alone activate downstream cellular biological functions in response to external mechanical forces [43–45], it is well known that cell cytoskeleton actin filaments is able to transmit mechanical stresses to the nucleus affecting its shape and chromatin organization [46–52]. Wang K. *et al.* used engineered nano-topographies of various shapes (gratings and pillars) and dimensions (feature size, spacing and height), to study human primary fibroblasts behaviour in response to the topographical stimuli. They found a correlation between nuclear deformation and cell functions such as cell proliferation, transfection and extracellular matrix protein type I collagen production [53] (Fig. 1.3 B). Additionally, numerous studies proved the role of topography in regulating gene-expression as consequence of nuclear deformation, eventually dictating specific cell final commitment [54–60] (Fig. 1.3 C).

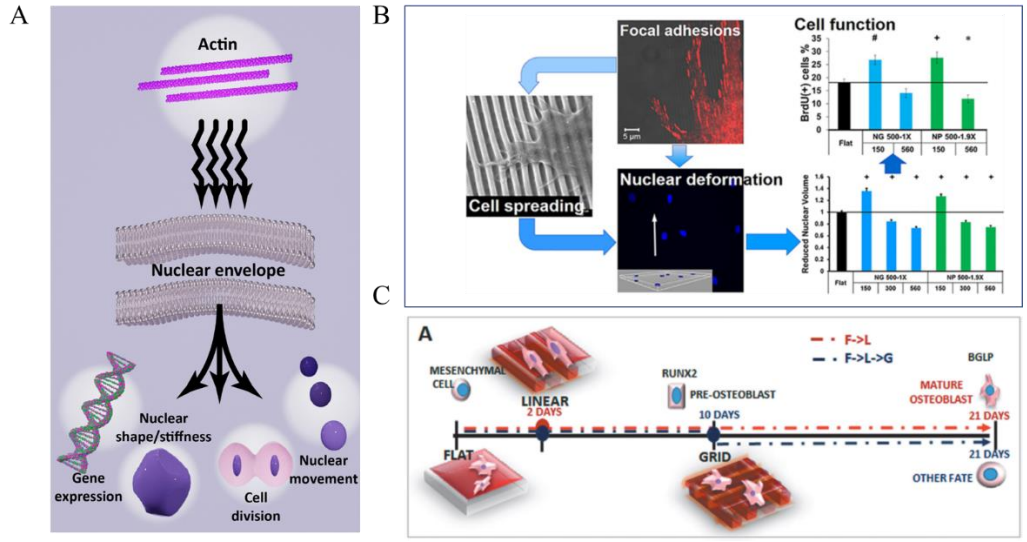

Figure 1.3. A) Schematization of interaction between actin cytoskeleton and nuclear envelope [42]. B) The effect of nano topography on nuclear shape, cell spreading and functions [53]. C) Graphic representation of topographic modulation of poly-disperse red1-metacrylate (PDR1m) azopolymer into linear pattern (red dashed line) and from linear to grid surface variation (blue dashed line), which resulted in hMSC differentiation into different lineages [60].

1.3. Static Topography Cell-Instructive Materials (CIMs)

Numerous technologies were implemented aiming to imprint topographic features on top of substrate surface enabling the investigation of the role of topography in cell–material interaction [61–64]. The main goals in biomaterials' design is to recapitulate the structure and function of the native ECM by realizing substrates with micron, submicron and nanoscale topographies of diverse shapes. The cell response to topographies depends on cell type, cell-cell interactions, and the geometry of the patterns, with those having dimensions in the range of 70 nm up to 2-5 μm exhibiting the most relevant effects on cell behaviour [65–67]. Several studies have been conducted in order to study the effect of presenting static topographical signals to cells. Liliensiek S.J *et al.* fabricated polyurethane substrates containing anisotropically ordered ridge and groove structures and isotropically ordered pores from 200 nm to 2000 nm in size. They investigated

the impact of biomimetic length-scale topographic cues on orientation/elongation, proliferation and migration on four human vascular endothelial cell-types from large and small diameter vessels. Indeed, the basement membrane of extracellular matrix has several factors, including a complex three-dimensional topography, which affect endothelial cell functions that are all important for the remodelling of matrix, formation of new vessels during both development and wound healing as well as for the interaction of native endothelial cells with implanted prosthetic scaffolds. They found that all cell-types exhibited orientation and alignment, higher rates of proliferation and preferential migration along the ridges and grooves, with the most pronounced response on anisotropically ordered ridges of 800 nm [33]. Hamilton *et al.* investigated the adhesion, spreading and migration of human periodontal ligament (PDL) fibroblasts in response to continuous and discontinuous topographic cues in the nanometric range. They reported that PDL fibroblasts were able to adhere spread on all the surfaces, with initial slower spreading and focal adhesion formation on discontinuous nanogrooves, while they resulted highly elongated on both types of nanogrooves after 24 h post seeding [68]. Moreover, hydrogels represent important class of materials that can be fabricated, implemented with surface microstructures, to mimic the 3D native cellular environment [69–71]. For example, Hong H. *et al.* fabricated a 3D hydrogel with Digital light processing 3D printing of silk fibroin for tissue engineering applications. In particular, they proved that the SF hydrogel allows to ensure viability, proliferation and differentiation to chondrogenesis of encapsulated cells up to 4 weeks of *in-vitro* cultivation [72].

1.4. Dynamic Topography CIMs

The introduction of dynamicity into “cell-instructive” platforms has led to the design and realization of innovative bio-interfaces able to mimic the time-varying properties of the native extracellular environment in a more reliable way. To this aim, several “smart” or “stimuli-responsive” materials were developed, which

have the ability to modulate their properties in response to an external trigger, *e.g.* electrical, thermal, optical, or mechanical stimulus [73,74]. These responsive materials have attracted extensive attention due to their potential to achieve high levels of spatio-temporal control over biological processes, including the control over reversibility of the transmitting signals. Lam *et al.* reported the first application of a dynamic topography variation using reversible poly(dimethylsiloxane) (PDMS) surfaces. A wavy micropattern, obtained by plasma oxidizing, was realized and removed applying and releasing compressive stress in presence of C2C12 myoblast cells, affecting their organization and morphology (Fig. 1.4 A) [75]. Furthermore, another approach to develop dynamic platforms was constituted by shape-memory polymers (SMPs), which gained great attention in the biomedical field [76,77]. SMPs are active materials that have the ability to maintain a temporary shape and return to the original shape under external stimuli (*e.g.*, heat, electricity, light, magnetism) [78]. Additionally, the integration of controllable nano/microstructures into materials can improve the performance of SMPs in various applications [79]. For example, Gong T. *et al.* fabricated a cross-linked poly(ε-caprolactone) (c-PCL) polymer, where, on its surface, microgrooves were imprinted through thermal embossing micro imprint lithography. SMPs are deformed at a high temperature and then cooled down under a fixed strain to memorize the temporary shape by locking the deformed polymer chains, and later recover to the permanent shape by a triggering event, such as heat. Compressed and stretched surfaces were analysed in order to investigate different topographical features on cell behaviour. Dynamic changes of microgrooves could effectively regulate cellular and nuclear shape via altering cell alignment, elongation, and spreading. Moreover, they showed that the expression of myogenic marker genes (β-MHC and cTNNt2) was significantly increased on the dynamic patterned surface when compared to the one on the static surfaces, with respect to the osteogenic markers Runx2, OPN, and OCN, stating that a dynamically altering micropatterned surface and the resultant

convergent force can regulate signal transduction of stem cells and subsequently guide stem cell differentiation into myogenic lineages (Fig. 1.4 B) [80].

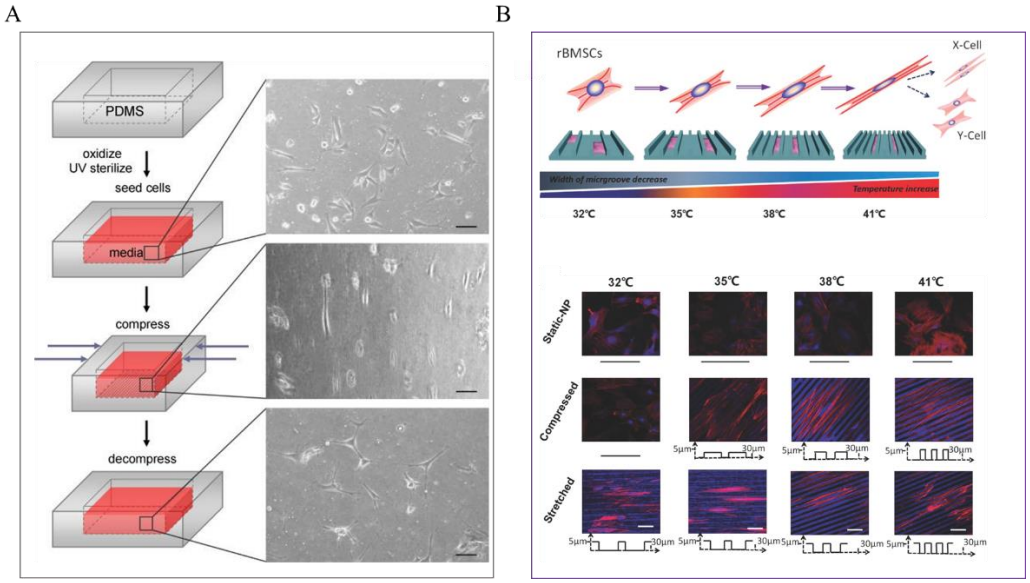

Figure 1.4. A) Graphic representation of the reversible behaviour of the PDMS cell culture substrate (left). Optical microscopy images of muscle cells on the micro structured substrate, showing cells alignment along the waves, which returned to random orientation on the flat surface after decompression [75]. B) Scheme of shape memory effect (top) on rat bone marrow mesenchymal stem cell (rBMSC) morphology in response to surface dynamic variation induced by temperature switching. Confocal images of immunolabeled cells with rhodamine-phalloidin stained F-actin and DAPI stained nuclei on the static non-patterned surface and dynamic surface, including compressed and stretched micro-grooved surfaces (down) [80].

1.5. Azobenzene

Azobenzene molecules have unique optical properties which can be exploited for a large variety of applications [81]. The molecular structure of azobenzene is characterized by two phenyl rings held together by the azo-linkage (–N=N–). Isomerization of the azobenzene between the thermodynamically stable *trans*-form and the meta-stable *cis*-form occurs upon the absorption of a photon within its absorption band and involves changes in geometry and polarity of the molecule, which passes from the planar spatial configuration in the *trans* isomer to the non-planar in the *cis* isomer [82]. The photoisomerization from *trans* to *cis*

isomer upon UV/visible light irradiation is a reversible process in which the *cis* isomer can be isomerized to the *trans* form by thermal relaxation or by a new illumination in the *cis*-absorption band. There are three classes of azobenzene characterized by the substitution of functional groups of the phenyl rings, which defines the different absorption spectra and photophysical response: the azobenzene-type molecules, the amino-azobenzene type, and the pseudo-stilbenes (Fig. 1.5 A) [83]. Azobenzene-type molecules are similar to the parent azobenzene molecule characterized by a *cis* lifetime of days. The amino-azobenzene type molecules which are ortho or para substituted with an electron-donating group, characterized by an intermediate lifetime in the dark. Pseudo stilbenes, which are substituted at 4 and 4´ positions with an electron-donating group and electron withdrawing group, have red-shifted absorption band and a very rapid *cis*-to-*trans* reconfiguration since their absorption spectra overlap (Fig. 1.5 B). Among them, pseudo stilbenes have the best photo-switching properties, resulting as the most used azobenzene type molecules.

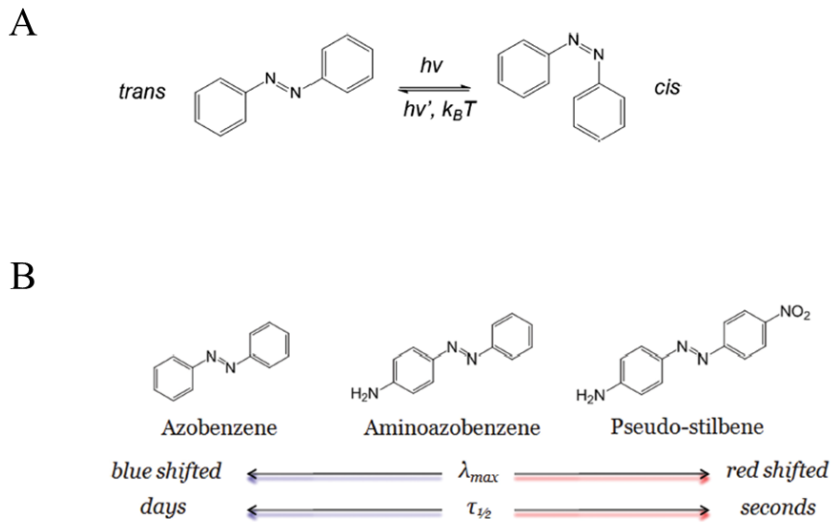

Figure 1.5. A) Chemical structure of azobenzene molecule and *trans-cis* isomerization upon light illumination and *cis-trans* back reaction upon thermal relaxation or light irradiation [84]. B) the three classes of azobenzene type molecules with their absorbance band and cis-state lifetime in the dark [84].

1.5.1. Azobenzene Photo-orientation and Birefringence

The isomerization of the azobenzene molecules can be photo-activated also by a linearly polarized light. In particular, when the photo-isomerization between the two isomeric states occur continuously, as in pseudo-stilbenes azobenzene, a series of motion can take place at molecular, nanoscale and micrometre (macroscopic) levels [85]. In more details, only azobenzene molecules with a transition dipole axis oriented along the light polarization direction can absorb the incident light and then photo-isomerize. However, the probability of absorption varies as $\cos 2\phi$, where ϕ is the angle between the light polarization and the azobenzene dipole axis [86]. Therefore, azo-molecules orientated parallel to the light polarization will absorb, while the chromophores with dipole axis perpendicular to the light will not move. After several photoisomerization cycles, the azo moiety will be stochastically oriented orthogonal to light polarization, resulting in a reduction of the population of *trans* isomers aligned in the direction of polarization. This statistical reorientation gives rise to very strong birefringence (anisotropy in refractive index) and dichroism (anisotropy in absorption spectrum) [86].

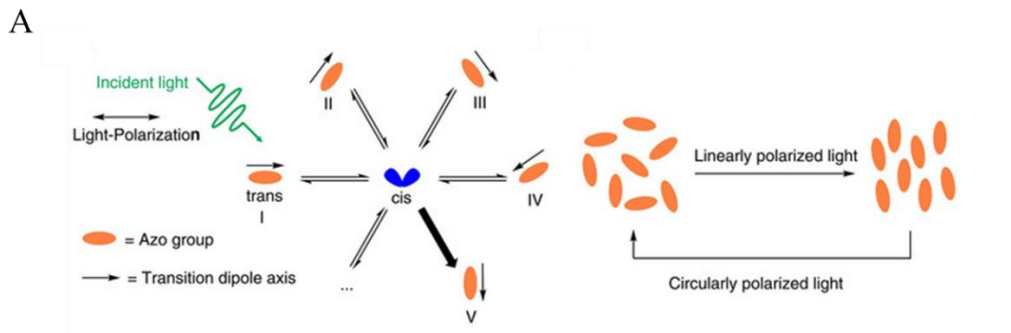

Figure 1.6. A) Photo-orientation of azobenzene molecule induced by irradiation with a linearly polarized light. The *trans* isomers oriented parallel to the light polarization will absorb photons and isomerize, while the isomers with a dipole axis orthogonal will not absorb. Multiple switches will result in the alignment of the *trans* population in the direction perpendicular to light polarization. The initial isotropic condition can be restored by circularly polarized light [87].

1.5.2. Azobenzene Photo-mechanics

The microscopic movements of the polymer chain, as a consequence of azo molecule photoisomerization, promote a macroscopic mass transport at the surface of polymer thin film at temperatures far below the polymers glass transition temperatures Tg. In polymers containing pseudo-stilbene azobenzene-type as side chains, the cyclic isomerization of azobenzene involving the polymer chains induces a massive movement of the polymer material. Several theories have emerged in order to clarify the origin of the interesting mechanism behind the macroscopic mass transport of the azopolymer matrix [88–90]. Saphiannikova and co-workers proposed a re-orientation model, assuming that the light-induced re-orientation of the azobenzene side chains induces a re-organization of polymer backbone generated by the formation of a mechanical stress which in turn produce a mass migration [91]. This theory assumes that the material remains in the solid state during light illumination. The Karageorgiev's group, instead, supports an isothermal directional photo-fluidization model stating that the cyclic isomerization of azobenzenes may cause an isothermal transition from an isotropic solid to an anisotropic liquid [92]. However, other explanations were discussed which still remains under debate nowadays [87,93].

1.5.3. Light-induced Surface Mass Transport in Azobenzene-based Materials

The integration of azo-molecules within different polymer matrix has led to the development of attractive azobenzene-based materials with potent photo-switchable properties. Indeed, the photo-isomerization of the azo-molecules, as a consequence of light illumination, generates a macroscopic mass movement on the surface of azo-materials, which can be exploited in several fields of application. For example, they acquired large employ in photonics, as Bragg reflectors, as light couplers and spectral filters, optoelectronic devices, and

recorder holograms [94,95]. Further, the possibility to modify the chemical and physical properties of the molecule allows to formulate innovative systems with specific and modular physical, chemical and mechanical properties. The formation of stable surface relief gratings (SRGs) induced on azopolymer film by the irradiation of an interference pattern generated by two laser beams was reported for the first time in 1995 by Natansohn's [96] and Trypathy's [97] groups independently. These sinusoidal-shaped structures were observed in different types of azo-materials, such as amorphous polymers [98,99], side chain liquid crystalline polymers [100,101], supramolecular systems [102], amorphous molecular materials [103]. There materials are extremely versatile since different optical techniques can be used to realize SRGs on their surface. Although the most common method to induce the light-triggered surface mass movement in azobenzene-based materials is the interference lithography in Lloyd's mirror configuration [97], other systems can be employed, such as holographic light irradiation, 1D Gaussian laser beam [104] and one-beam irradiation [105].

1.5.4. Azopolymers as Dynamic Bio-interfaces for Cell Culturing

The high demand for the development of dynamic platforms for cell culture experiments has led to the design of smart materials that reliably recapitulate the native extracellular microenvironment. Specifically, systems with tuneable physical, chemical and mechanical properties are extremely appealing since they allow to control both in space and in time the transmission of precise instructions to cells in order to guide their functions. Azobenzene-type materials are commonly employed for the realization of dynamic bio-interfaces because of their ability to change the shape of surface topography in response to light. Moreover, light responsive systems are largely preferred in biological applications because, among all external stimuli used to activate smart materials, light provides high spatial/temporal precision and is not harmful for cells, giving the possibility for *in-situ* investigation of cell behaviour. Therefore, the light-induced azo-materials

surface reliefs provides a physical nano/micro pattern, which can be exploited as guidance structures to orient and align cells along preferential directions. Although preliminary studies were conducted in static conditions, in which cells were seeded on patterned azopolymer surfaces to study the effect of the physical signal on cell behaviour [106–109], in the last decade, with the advanced comprehension of azo-materials properties and their interactions with biological systems, materials incorporating azo-molecules were even more used to realize photo-switchable dynamic platforms [58,60,110–117]. Rianna C. *et al.* used poly-disperse red1-methacrylate (pDR1m) azopolymer to provide dynamic *in-situ* variation of topographical cues, to NIH 3T3 fibroblast, in order to precisely control cell orientation and migration in a spatio-temporal regulated manner (Fig. 1.7 A) [118]. Also, Puliafito A. *et al.* presented an approach to spatio-temporally control substrate topographies starting from a pre-patterned azopolymeric structure on a glass-bottom Petri dish. In detail, they modified the topography elongating micropillars along a direction parallel to the laser polarization, with a single exposure of the target area with living cells attached to the substrate and observed that both cancer cells and kidney epithelial cells are able to sense the local deformation direction and orient and migrate accordingly [119]. Also, with the need to recreate a dynamic 3D microenvironment, photo-actuating hydrogels have gained great attention [120]. For example, Pennacchio F. *et al.* developed a gelatin based hydrogel containing azobenzene cross-linker stimulated by light illumination, which generated nuclear deformations of confined NIH-3T3 cells upon light-triggered expansion of gelatin microstructures (Fig. 1.7 B) [121].

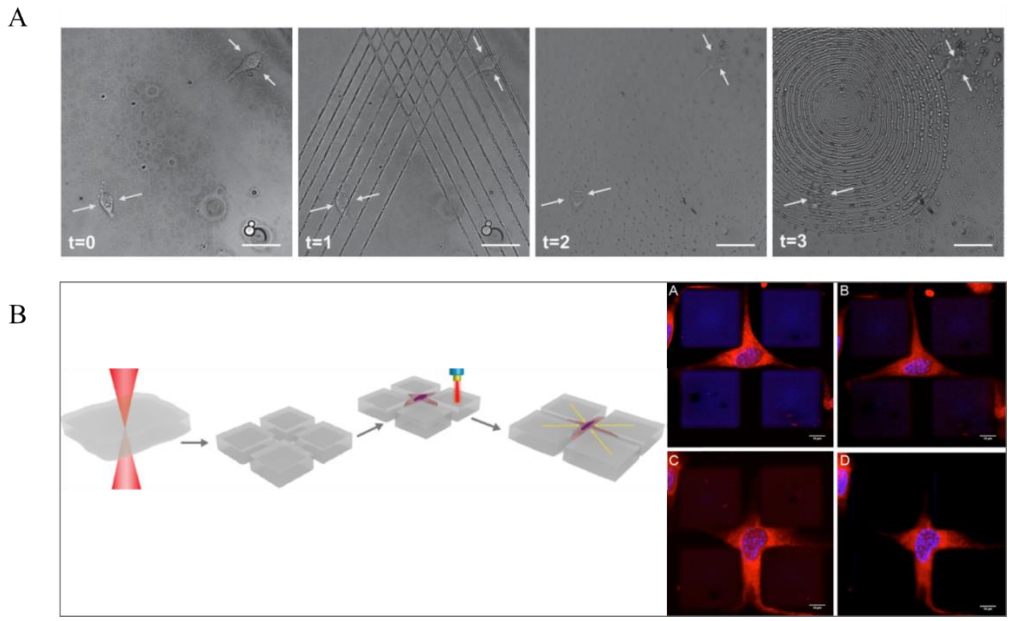

Figure 1.7 A) Confocal images of two NIH 3T3 cells seeded on flat pDR1m surface (t = 0), the same area exposed to a first light-induced pattern inscription (t = 1), pattern erasure (t = 2) and second patten inscription (t = 3), showing the feasibility of the dynamic photo-switching of the azopolymer [118]. B) Graphic representation of the light-induced stimulation of the gelatin-azobenzene based hydrogel (left) and confocal images of CellTracker deep red (cell body, red) and hoechst (nuclei, blue) stained NIH-3T3 living cells before light irradiation (a,c) and after 10 min of multiphoton stimulation (b,d) [121].

1.6. Aim and Outline of the Thesis

In-vivo studies of cellular external microenvironment during years have revealed the presence of biochemical and biophysical elements which characterize the properties of the extracellular matrix (ECM) and influence the behaviour of the nearby cells, defining the communication between cells and their surrounding ECM. In particular, the geometrical features of the ECM, in the form of fibrillar matrix, were shown to dictate a preferential direction along which cells polarize and elongate, eventually affecting their functions such as migration, proliferation and differentiation. Thus, in order to better understand the way external physical signals are transmitted to cells and transduced into biological functions, scientific community tried to design and develop functionalized materials with specific

chemical, physical and mechanical properties, able to replicate the native aspects of the ECM. Nowadays, it is well-known that the interaction between cells and the ECM is a process mediated by cell transmembrane proteins, which anchored to the ECM, thus promoting the formation and growth of mechanosensitive proteins that are responsible to transmit the external signals to the inner subcellular structures finally activating a cascade of biochemical events through the mechanism of mechano-transduction. The majority of these studies were conducted in static conditions, which are not suitable for miming the highly dynamic nature of the ECM that continuously undergoes remodelling processes during growth and in diseases, thus modulating both in space and in time the presentation of physical cues to cells. Therefore, in recent years much more effort was done in order to engineer cell culturing substrates with controllable material properties through the application of an external trigger. These are known as "smart" or "stimuli-responsive" materials. However, concerning topography, few works were performed providing cell culture platforms with "on-demand" regulated dynamic surface topography variation and even less with reconfigurable surfaces able to deliver cyclic stimulation to cells. Thus, the aim of this thesis is to realize a photo-switchable platform for cell culturing experiments which allows to control the presentation of topographical signals in a spatiotemporal manner in order to investigate cell behaviour in response to dynamic and cyclic variation of topographical stimuli. To this purpose, photo-responsive azopolymer material was employed to cover glass-bottom Petri-dish, which enables the *in-situ* light-induced surface patterning and removal.

In **Chapter 1**, an introduction of the intriguing communication mechanism between cells and their extracellular environment is presented with a main focus on the topography cues transmission from outside, through focal adhesions, to the inner cellular structures, until the nucleus. Further, advances in fabrication methods of cell-instructive materials (CIMs) for application in tissue engineering

in both static and dynamic conditions are reported. Additionally, the optical properties of azobenzene molecules as well as the fascinating process of surface patterning of photo-responsive azobenzene containing materials are discussed along with their applications in the biological field. In **Chapter 2**, the realization of light-induced topographic pattern on the azopolymer surface by means of a Gaussian beam of a confocal laser scanning microscope is proposed. In addition, different optical methods are investigated in order to erase the imprinted pattern, with the aim to induce multiple light triggered azopolymer surface variations. Lastly, characterization of azopolymer behaviour in wet environments is carried out. In **Chapter 3**, a study on the effect of *in-situ* light-induced topography patterning of azopolymer surface on human breast epithelial cells (MCF10A) is reported. In details, the time evolution of cell behaviour in response to the transmission of the topographical signals at a specific time of cell growth is studied in terms of focal adhesions morphology and assembly, cell shape and cytoskeleton organization. In addition, the impact of the light-induced topographical signal on nuclear morphology and inner structure organization is also investigated, in terms of nuclear shape, chromosome arrangement and chromatin condensation state. Further, investigation on cell growth and proliferation rate induced by the nano topography is carried out. Lastly, cell and nuclear mechanical properties variations upon azopolymer surface photo-patterning are also evaluated. In **Chapter 4**, the photo-switchable properties of azopolymer are exploited in order to regulate the presentation/removal of topography signal both in space and in time, thus providing cyclic topographic stimuli to MCF10A cells with the aim to control and guide their behaviour. Specifically, a single flat-to-pattern-to-flat surface variation is performed in presence of living cells in order to test cell capability to reverse their functions upon topographical signal removal. Moreover, for the first time, the impact of multiple topography photo-switching on cell behaviour is investigated in order to examine cell responsiveness also to long time topography stimulation. **In**

Conclusion and Future Perspectives, a summary of the main results obtained in this thesis is presented and future applications are proposed.

1.7. References

1. Ventre M, Causa F, Netti PA. Determinants of cell-material crosstalk at the interface: towards engineering of cell instructive materials. J R Soc Interface. 2012;9: 2017–2032.
2. Kanchanawong P, Calderwood DA. Organization, dynamics and mechanoregulation of integrin-mediated cell-ECM adhesions. Nat Rev Mol Cell Biol. 2022. doi:10.1038/s41580-022-00531-5
3. Martino F, Perestrelo AR, Vinarský V, Pagliari S, Forte G. Cellular mechanotransduction: From tension to function. Front Physiol. 2018;9: 824.
4. Hubmacher D, Apte SS. The biology of the extracellular matrix: novel insights. Curr Opin Rheumatol. 2013;25: 65–70.
5. Khalili AA, Ahmad MR. A review of cell adhesion studies for biomedical and biological applications. Int J Mol Sci. 2015;16: 18149–18184.
6. Ingber DE Cellular mechanotransduction: putting all the pieces together again. FASEB J. 2006;20: 811–827.
7. Ohashi K, Fujiwara S, Mizuno K. Roles of the cytoskeleton, cell adhesion and rho signalling in mechanosensing and mechanotransduction. J Biochem. 2017;161: 245–254.
8. Ramdas NM, Shivashankar GV. Cytoskeletal control of nuclear morphology and chromatin organization. J Mol Biol. 2015;427: 695–706.
9. Burridge K, Monaghan-Benson E, Graham DM. Mechanotransduction: from the cell surface to the nucleus via RhoA. Philos Trans R Soc Lond B Biol Sci. 2019;374: 20180229.
10. Janota CS, Calero-Cuenca FJ, Gomes ER. The role of the cell nucleus in mechanotransduction. Curr Opin Cell Biol. 2020;63: 204–211.
11. Gattazzo F, Urciuolo A, Bonaldo P. Extracellular matrix: a dynamic microenvironment for stem cell niche. Biochim Biophys Acta. 2014;1840: 2506–2519.
12. Rozario T, DeSimone DW. The extracellular matrix in development and morphogenesis: a dynamic view. Dev Biol. 2010;341: 126–140.
13. Lu P, Weaver VM, Werb Z. The extracellular matrix: A dynamic niche in cancer progression. J Exp Med. 2012;209: i1–i1.
14. Daley WP, Peters SB, Larsen M. Extracellular matrix dynamics in development and regenerative medicine. J Cell Sci. 2008;121: 255–264.
15. Frantz C, Stewart KM, Weaver VM. The extracellular matrix at a glance. J Cell Sci. 2010;123: 4195–4200.
16. Young JL, Holle AW, Spatz JP. Nanoscale and mechanical properties of the physiological cell–ECM microenvironment. Exp Cell Res. 2016;343: 3–6.

17. Kim D-H, Lipke EA, Kim P, Cheong R, Thompson S, Delannoy M, et al. Nanoscale cues regulate the structure and function of macroscopic cardiac tissue constructs. Proc Natl Acad Sci U S A. 2010;107: 565–570.
18. Mack PJ, Kaazempur-Mofrad MR, Karcher H, Lee RT, Kamm RD. Force-induced focal adhesion translocation: effects of force amplitude and frequency. Am J Physiol Cell Physiol. 2004;287: C954-62.
19. Koçer G, Jonkheijm P. About chemical strategies to fabricate cell-instructive biointerfaces with static and dynamic complexity. Adv Healthc Mater. 2018;7: e1701192.
20. Lenhert S, Meier M-B, Meyer U, Chi L, Wiesmann HP. Osteoblast alignment, elongation and migration on grooved polystyrene surfaces patterned by Langmuir-Blodgett lithography. Biomaterials. 2005;26: 563–570.
21. Dalby MJ, Riehle MO, Yarwood SJ, Wilkinson CDW, Curtis ASG. Nucleus alignment and cell signaling in fibroblasts: response to a micro-grooved topography. Exp Cell Res. 2003;284: 274–282.
22. Dalby MJ, McCloy D, Robertson M, Agheli H, Sutherland D, Affrossman S, et al. Osteoprogenitor response to semi-ordered and random nanotopographies. Biomaterials. 2006;27: 2980–2987.
23. García AJ. Get a grip: integrins in cell-biomaterial interactions. Biomaterials. 2005;26: 7525–7529.
24. Meyle J, G�ltig K, Brich M, H�mmerle H, Nisch W. Contact guidance of fibroblasts on biomaterial surfaces. J Mater Sci Mater Med. 1994;5: 463–466.
25. Matsuzaka K, Walboomers F, de Ruijter A, Jansen JA. Effect of microgrooved poly-l-lactic (PLA) surfaces on proliferation, cytoskeletal organization, and mineralized matrix formation of rat bone marrow cells. Clin Oral Implants Res. 2000;11: 325–333.
26. den Braber ET, de Ruijter JE, Ginsel LA, von Recum AF, Jansen JA. Orientation of ECM protein deposition, fibroblast cytoskeleton, and attachment complex components on silicone microgrooved surfaces. J Biomed Mater Res. 1998;40: 291–300.
27. Teixeira AI, Nealey PF, Murphy CJ. Responses of human keratocytes to micro- and nanostructured substrates. J Biomed Mater Res A. 2004;71: 369–376.
28. Teixeira AI, McKie GA, Foley JD, Bertics PJ, Nealey PF, Murphy CJ. The effect of environmental factors on the response of human corneal epithelial cells to nanoscale substrate topography. Biomaterials. 2006;27: 3945–3954.
29. Natale CF, Ventre M, Netti PA. Tuning the material-cytoskeleton crosstalk via nanoconfinement of focal adhesions. Biomaterials. 2014;35: 2743–2751.
30. Ventre M, Natale CF, Rianna C, Netti PA. Topographic cell instructive patterns to control cell adhesion, polarization and migration. J R Soc Interface. 2014;11: 20140687.

31. Handorf AM, Zhou Y, Halanski MA, Li W-J. Tissue stiffness dictates development, homeostasis, and disease progression. Organogenesis. 2015;11: 1–15.
32. Fletcher DA, Mullins RD. Cell mechanics and the cytoskeleton. Nature. 2010;463: 485–492.
33. Liliensiek SJ, Wood JA, Yong J, Auerbach R, Nealey PF, Murphy CJ. Modulation of human vascular endothelial cell behaviors by nanotopographic cues. Biomaterials. 2010;31: 5418–5426.
34. Jiang Y, Lu S, Zeng Y. Dermal fibroblast behaviour on micropatterned substrates with different pattern geometries. J Tissue Eng Regen Med. 2011;5: 402–409.
35. Kim D-H, Provenzano PP, Smith CL, Levchenko A. Matrix nanotopography as a regulator of cell function. J Cell Biol. 2012;197: 351–360.
36. Li Y, Huang G, Zhang X, Wang L, Du Y, Lu TJ, et al. Engineering cell alignment in vitro. Biotechnol Adv. 2014;32: 347–365.
37. Natale CF, Lafaurie-Janvore J, Ventre M, Babataheri A, Barakat AI. Focal adhesion clustering drives endothelial cell morphology on patterned surfaces. J R Soc Interface. 2019;16: 20190263.
38. Weiss P. Experiments on cell and axon orientation in vitro; the role of colloidal exudates in tissue organization. J Exp Zool. 1945;100: 353–386.
39. Yim EKF, Darling EM, Kulangara K, Guilak F, Leong KW. Nanotopography-induced changes in focal adhesions, cytoskeletal organization, and mechanical properties of human mesenchymal stem cells. Biomaterials. 2010;31: 1299–1306.
40. Maurer M, Lammerding J. The driving force: Nuclear mechanotransduction in cellular function, fate, and disease. Annu Rev Biomed Eng. 2019;21: 443–468.
41. Pennacchio FA, Nastały P, Poli A, Maiuri P. Tailoring cellular function: The contribution of the nucleus in mechanotransduction. Front Bioeng Biotechnol. 2020;8: 596746.
42. Davidson PM, Cadot B. Actin on and around the nucleus. Trends Cell Biol. 2021;31: 211–223.
43. Guilluy C, Osborne LD, Van Landeghem L, Sharek L, Superfine R, Garcia-Mata R, et al. Isolated nuclei adapt to force and reveal a mechanotransduction pathway in the nucleus. Nat Cell Biol. 2014;16: 376–381.
44. Szczesny SE, Mauck RL. The nuclear option: Evidence implicating the cell nucleus in mechanotransduction. J Biomech Eng. 2017;139: 021006.
45. Kirby TJ, Lammerding J. Emerging views of the nucleus as a cellular mechanosensor. Nat Cell Biol. 2018;20: 373–381.
46. Maniotis AJ, Chen CS, Ingber DE. Demonstration of mechanical connections between integrins, cytoskeletal filaments, and nucleoplasm that stabilize nuclear structure. Proc Natl Acad Sci U S A. 1997;94: 849–854.

47. Khatau SB, Hale CM, Stewart-Hutchinson PJ, Patel MS, Stewart CL, Searson PC, et al. A perinuclear actin cap regulates nuclear shape. Proc Natl Acad Sci U S A. 2009;106: 19017–19022.
48. Versaevel M, Grevesse T, Gabriele S. Spatial coordination between cell and nuclear shape within micropatterned endothelial cells. Nat Commun. 2012;3: 671.
49. Vishavkarma R, Raghavan S, Kuyyamudi C, Majumder A, Dhawan J, Pullarkat PA. Role of actin filaments in correlating nuclear shape and cell spreading. PLoS One. 2014;9: e107895.
50. Guilluy C, Burridge K. Nuclear mechanotransduction: forcing the nucleus to respond. Nucleus. 2015;6: 19–22.
51. Keeling MC, Flores LR, Dodhy AH, Murray ER, Gavara N. Actomyosin and vimentin cytoskeletal networks regulate nuclear shape, mechanics and chromatin organization. Sci Rep. 2017;7: 5219.
52. Damodaran K, Venkatachalapathy S, Alisafaei F, Radhakrishnan AV, Sharma Jokhun D, Shenoy VB, et al. Compressive force induces reversible chromatin condensation and cell geometry-dependent transcriptional response. Mol Biol Cell. 2018;29: 3039–3051.
53. Wang K, Bruce A, Mezan R, Kadiyala A, Wang L, Dawson J, et al. Nanotopographical modulation of cell function through nuclear deformation. ACS Appl Mater Interfaces. 2016;8: 5082–5092.
54. Teo BKK, Ankam S, Chan LY, Yim EKF. Nanotopography/mechanical induction of stem-cell differentiation. Methods Cell Biol. 2010;98: 241–294.
55. Watari S, Hayashi K, Wood JA, Russell P, Nealey PF, Murphy CJ, et al. Modulation of osteogenic differentiation in hMSCs cells by submicron topographically-patterned ridges and grooves. Biomaterials. 2012;33: 128–136.
56. Iannone M, Ventre M, Formisano L, Casalino L, Patriarca EJ, Netti PA. Nanoengineered surfaces for focal adhesion guidance trigger mesenchymal stem cell self-organization and tenogenesis. Nano Lett. 2015;15: 1517–1525.
57. Newman P, Galenano-Niño JL, Graney P, Razal JM, Minett AI, Ribas J, et al. Relationship between nanotopographical alignment and stem cell fate with live imaging and shape analysis. Sci Rep. 2016;6. doi:10.1038/srep37909
58. Fedele C, De Gregorio M, Netti PA, Cavalli S, Attanasio C. Azopolymer photopatterning for directional control of angiogenesis. Acta Biomater. 2017;63: 317–325.
59. Natale CF, Angrisano T, Pistelli L, Falco G, Calabrò V, Netti PA, et al. Topographic cues impact on embryonic stem cell Zscan4-metastate. Front Bioeng Biotechnol. 2020;8: 178.
60. De Martino S, Cavalli S, Netti PA. Photoactive interfaces for spatio-temporal guidance of mesenchymal stem cell fate. Adv Healthc Mater. 2020;9: e2000470.

61. Gaubert HE, Frey W. Highly parallel fabrication of nanopatterned surfaces with nanoscale orthogonal biofunctionalization imprint lithography. Nanotechnology. 2007;18: 135101.
62. Tseng Q, Wang I, Duchemin-Pelletier E, Azioune A, Carpi N, Gao J, et al. A new micropatterning method of soft substrates reveals that different tumorigenic signals can promote or reduce cell contraction levels. Lab Chip. 2011;11: 2231–2240.
63. Cai S, Wu C, Yang W, Liang W, Yu H, Liu L. Recent advance in surface modification for regulating cell adhesion and behaviors. Nanotechnol Rev. 2020;9: 971–989.
64. Mirbagheri M, Adibnia V, Hughes BR, Waldman SD, Banquy X, Hwang DK. Advanced cell culture platforms: a growing quest for emulating natural tissues. Mater Horiz. 2019;6: 45–71.
65. Loesberg WA, te Riet J, van Delft FCMJM, Schön P, Figdor CG, Speller S, et al. The threshold at which substrate nanogroove dimensions may influence fibroblast alignment and adhesion. Biomaterials. 2007;28: 3944–3951.
66. Lamers E, van Horssen R, te Riet J, van Delft FC, Luttge R, Walboomers XF, et al. The influence of nanoscale topographical cues on initial osteoblast morphology and migration. Eur Cell Mater. 2010;20: 329–343.
67. Nguyen AT, Sathe SR, Yim EKF. From nano to micro: topographical scale and its impact on cell adhesion, morphology and contact guidance. J Phys Condens Matter. 2016;28: 183001.
68. Hamilton DW, Oates CJ, Hasanzadeh A, Mittler S. Migration of periodontal ligament fibroblasts on nanometric topographical patterns: influence of filopodia and focal adhesions on contact guidance. PLoS One. 2010;5: e15129.
69. Khademhosseini A, Langer R. Microengineered hydrogels for tissue engineering. Biomaterials. 2007;28: 5087–5092.
70. Tibbitt MW, Anseth KS. Hydrogels as extracellular matrix mimics for 3D cell culture. Biotechnol Bioeng. 2009;103: 655–663.
71. Unal AZ, West JL. Synthetic ECM: Bioactive synthetic hydrogels for 3D tissue engineering. Bioconjug Chem. 2020;31: 2253–2271.
72. Hong H, Seo YB, Kim DY, Lee JS, Lee YJ, Lee H, et al. Digital light processing 3D printed silk fibroin hydrogel for cartilage tissue engineering. Biomaterials. 2020;232: 119679.
73. Mrinalini M, Prasanthkumar S. Recent advances on stimuli-responsive smart materials and their applications. ChemPlusChem. 2019;84: 1103–1121.
74. Gao S, Tang G, Hua D, Xiong R, Han J, Jiang S, et al. Stimuli-responsive bio-based polymeric systems and their applications. J Mater Chem B Mater Biol Med. 2019;7: 709–729.
75. Lam MT, Clem WC, Takayama S. Reversible on-demand cell alignment using reconfigurable microtopography. Biomaterials. 2008;29: 1705–1712.

76. Delaey J, Dubruel P, Van Vlierberghe S. Shape-memory polymers for biomedical applications. Adv Funct Mater. 2020;30: 1909047.
77. Zhao W, Liu L, Zhang F, Leng J, Liu Y. Shape memory polymers and their composites in biomedical applications. Mater Sci Eng C Mater Biol Appl. 2019;97: 864–883.
78. Xin X, Liu L, Liu Y, Leng J. Mechanical models, structures, and applications of shape-memory polymers and their composites. Acta Mech Solida Sin. 2019;32: 535–565.
79. Zhang F, Xia Y, Liu Y, Leng J. Nano/microstructures of shape memory polymers: from materials to applications. Nanoscale Horiz. 2020;5: 1155–1173.
80. Gong T, Zhao K, Yang G, Li J, Chen H, Chen Y, et al. The control of mesenchymal stem cell differentiation using dynamically tunable surface microgrooves. Adv Healthc Mater. 2014;3: 1608–1619.
81. Fedele C, Ruoko T-P, Kuntze K, Virkki M, Priimagi A. New tricks and emerging applications from contemporary azobenzene research. Photochem Photobiol Sci. 2022;21: 1719–1734.
82. De Martino S, Mauro F, Netti PA. Photonic applications of azobenzene molecules embedded in amorphous polymer. Riv Nuovo Cimento. 2020;43: 599–629.
83. Rau H. Photoisomerization of Azobenzenes. Photoreactive Organic Thin Films. Elsevier; 2002. pp. 3–47.
84. Goulet-Hanssens A, Barrett CJ. Photo-control of biological systems with azobenzene polymers. J Polym Sci A Polym Chem. 2013;51: 3058–3070.
85. Natansohn A, Rochon P. Photoinduced motions in azo-containing polymers. Chem Rev. 2002;102: 4139–4175.
86. Yager KG, Barrett CJ. Novel photo-switching using azobenzene functional materials. J Photochem Photobiol A Chem. 2006;182: 250–261.
87. Weis P, Tian W, Wu S. Photoinduced liquefaction of azobenzene-containing polymers. Chemistry. 2018;24: 6494–6505.
88. Sekkat Z. Photoreactive Organic Thin Films. San Diego, CA: Academic Press; 2002.
89. Lee S, Kang HS, Park J-K. Photofluidization: Directional photofluidization lithography: Micro/nanostructural evolution by photofluidic motions of azobenzene materials (adv. Mater. 16/2012). Adv Mater. 2012;24: 2062–2062.
90. Mahimwalla Z, Yager KG, Mamiya J-I, Shishido A, Priimagi A, Barrett CJ. Azobenzene photomechanics: prospects and potential applications. Polym Bull (Berl). 2012;69: 967–1006.
91. Saphiannikova M, Toshchevikov V, Ilnytskyi J, Heinrich G. Photo-induced deformation of azobenzene polymers: theory and simulations. In: Zamboni R, Kajzar F, Szep AA, Lewis C, Burgess D, Gruneisen MT, et al., editors. Optics and Photonics for Counterterrorism and Crime Fighting VII; Optical

Materials in Defence Systems Technology VIII; and Quantum-Physics-based Information Security. SPIE; 2011. doi:10.1117/12.897375
92. Karageorgiev P, Neher D, Schulz B, Stiller B, Pietsch U, Giersig M, et al. From anisotropic photo-fluidity towards nanomanipulation in the optical near-field. Nat Mater. 2005;4: 699–703.
93. Yadavalli NS, Loebner S, Papke T, Sava E, Hurduc N, Santer S. A comparative study of photoinduced deformation in azobenzene containing polymer films. Soft Matter. 2016;12: 2593–2603.
94. Priimagi A, Shevchenko A. Azopolymer-based micro- and nanopatterning for photonic applications. J Polym Sci B Polym Phys. 2014;52: 163–182.
95. Natansohn A, Rochon P. Photoinduced motions in azobenzene-based amorphous polymers: Possible photonic devices. Adv Mater. 1999;11: 1387–1391.
96. Paterson J, Natansohn A, Rochon P, Callender CL, Robitaille L. Optically inscribed surface relief diffraction gratings on azobenzene-containing polymers for coupling light into slab waveguides. Appl Phys Lett. 1996;69: 3318–3320.
97. Kim DY, Tripathy SK, Li L, Kumar J. Laser-induced holographic surface relief gratings on nonlinear optical polymer films. Appl Phys Lett. 1995;66: 1166–1168.
98. Viswanathan NK, Kim DY, Bian S, Williams J, Liu W, Li L, et al. Surface relief structures on azo polymer films. J Mater Chem. 1999;9: 1941–1955.
99. Yager KG, Barrett CJ. All-optical patterning of azo polymer films. Curr Opin Solid State Mater Sci. 2001;5: 487–494.
100. Zettsu N, Ogasawara T, Mizoshita N, Nagano S, Seki T. Photo-triggered surface relief grating formation in supramolecular liquid crystalline polymer systems with detachable azobenzene unit. Adv Mater. 2008;20: 516–521.
101. Zettsu N, Seki T. Highly efficient photogeneration of surface relief structure and its immobilization in cross-linkable liquid crystalline azobenzene polymers. Macromolecules. 2004;37: 8692–8698.
102. Koskela JE, Vapaavuori J, Ras RHA, Priimagi A. Light-driven surface patterning of supramolecular polymers with extremely low concentration of photoactive molecules. ACS Macro Lett. 2014;3: 1196–1200.
103. Kitamura I, Kato K, Berk RB, Nakai T, Hara M, Nagano S, et al. Photo-triggered large mass transport driven only by a photoresponsive surface skin layer. Sci Rep. 2020;10: 12664.
104. Bian S, Li L, Kumar J, Kim DY, Williams J, Tripathy SK. Single laser beam-induced surface deformation on azobenzene polymer films. Appl Phys Lett. 1998;73: 1817–1819.
105. Tsutsumi N, Fujihara A. Pulsed laser induced spontaneous gratings on a surface of azobenzene polymer. Appl Phys Lett. 2004;85: 4582–4584.

106. Baac H, Lee J-H, Seo J-M, Park TH, Chung H, Lee S-D, et al. Submicron-scale topographical control of cell growth using holographic surface relief grating. Mater Sci Eng C Mater Biol Appl. 2004;24: 209–212.
107. Rocha L, Păiuş C-M, Luca-Raicu A, Resmerita E, Rusu A, Moleavin I-A, et al. Azobenzene based polymers as photoactive supports and micellar structures for applications in biology. J Photochem Photobiol A Chem. 2014;291: 16–25.
108. Salvatore M, Oscurato SL, D'Albore M, Guarino V, Zeppetelli S, Maddalena P, et al. Quantitative study of morphological features of stem cells onto photopatterned azopolymer films. J Funct Biomater. 2020;11: 8.
109. Barillé R, Codron P, Mabilleau G, Manero F, Mallet R, Zielinska S, et al. Characterization of cells interactions with patterned azopolymer-based materials using SEM, AFM and video microscopy. Open Biomed Eng J. 2018;12: 92–100.
110. Rianna C, Calabuig A, Ventre M, Cavalli S, Pagliarulo V, Grilli S, et al. Reversible holographic patterns on azopolymers for guiding cell adhesion and orientation. ACS Appl Mater Interfaces. 2015;7: 16984–16991.
111. Pirani F, Angelini A, Frascella F, Rizzo R, Ricciardi S, Descrovi E. Light-driven reversible shaping of individual azopolymeric micro-pillars. Sci Rep. 2016;6. doi:10.1038/srep31702
112. Koçer G, ter Schiphorst J, Hendrikx M, Kassa HG, Leclère P, Schenning APHJ, et al. Light-responsive hierarchically structured liquid crystal polymer networks for harnessing cell adhesion and migration. Adv Mater. 2017;29: 1606407.
113. Hendrikx M, ter Schiphorst J, van Heeswijk EPA, Koçer G, Knie C, Bléger D, et al. Configurable multi-stable surface topographies: Re- and preconfigurable multistable visible light responsive surface topographies (small 50/2018). Small. 2018;14: 1870240.
114. Rossano L, Cimmino C, Cavalli S, Ventre M, Netti PA. Regulating fibroblast shape and mechanics through photoresponsive surfaces with concentric circular topographic patterns. Adv Mater Interfaces. 2018;5: 1800890.
115. De Martino S, Zhang W, Klausen L, Lou H-Y, Li X, Alfonso FS, et al. Dynamic manipulation of cell membrane curvature by light-driven reshaping of azopolymer. Nano Lett. 2020;20: 577–584.
116. Isomäki M, Fedele C, Kääriäinen L, Mäntylä E, Nymark S, Ihalainen TO, et al. Light-responsive bilayer cell culture platform for reversible cell guidance. Small Sci. 2022;2: 2100099.
117. Peussa H, Fedele C, Tran H, Fadjukov J, Mäntylä E, Priimägi A, et al. Light-induced nanoscale deformation in azobenzene thin film triggers rapid intracellular Ca^{2+}increase via mechanosensitive cation channels. bioRxiv. 2022. doi:10.1101/2022.09.27.509666

118. Rianna C, Rossano L, Kollarigowda RH, Formiggini F, Cavalli S, Ventre M, et al. Spatio-temporal control of dynamic topographic patterns on azopolymers for cell culture applications. Adv Funct Mater. 2016;26: 7572–7580.
119. Puliafito A, Ricciardi S, Pirani F, Čermochová V, Boarino L, De Leo N, et al. Driving cells with light-controlled topographies. Adv Sci (Weinh). 2019;6: 1801826.
120. Yang R, Jin W, Huang C, Liu Y. Azobenzene based photo-responsive hydrogel: Synthesis, self-assembly, and antimicrobial activity. Gels. 2022;8: 414.
121. Pennacchio FA, Fedele C, De Martino S, Cavalli S, Vecchione R, Netti PA. Three-dimensional microstructured azobenzene-containing gelatin as a photoactuable cell confining system. ACS Appl Mater Interfaces. 2018;10: 91–97.

Chapter 2

Photo-induced azopolymer surface reliefs formation

2.1. Introduction

Azobenzene-type materials are light-responsive systems in which the photo-isomerization of the azo-moiety at molecular level generates macroscopic variations in the chemical and physical properties of the hosting matrix [1]. In polymer containing azo molecules, the light-induced isomerization triggers a macroscopic surface mass displacement far below the polymer glass transition temperature Tg, which resulted in the formation of surface relief gratings (SRG). This event was observed for the first time in 1995 by Natansohn's [2] and Trypathy's [3] groups independently, which reported the formation of stable surface gratings optically induced on azopolymer film using the interference irradiation of two laser beams. The surface pattern formation was also stated in other azobenzene functionalized polymers such as amorphous polymers [4–6], side chain liquid crystalline polymers [7,8], supramolecular systems [9], amorphous molecular materials [10]. However, the mechanism underlying the light-driven mass movement of the overall polymer matrix is still unclear, though several theories were emerged in order to shed light on this interesting phenomenon [11–13]. Although the most common method to create surface relief gratings is the interference lithography in Lloyd's mirror configuration [2,3,14–18], other optical systems can be employed to induce the photo-patterning of the azopolymer surface, *e.g.*, one-beam irradiation and 1D Gaussian laser beam. A spontaneous arrangement of the flat azopolymer surface into ordered quasi hexagonal bumps by a one-beam irradiation was reported for the first time by Hubert *et al.* [19]. Even though these surface modulations showed structural

analogies with SRGs obtained by an interference pattern of light, they are commonly referred as spontaneous surface relief gratings (SSRG), whose self-organization mechanism is still under investigation. Furthermore, Bian *et al.* reported a single Gaussian beam-induced deformation on different azopolymer materials [20]. They demonstrated that the focused beam generates a hole in correspondence to the centre of the laser spot and the resulting surface deformation is dependent on the polarization and intensity of the laser beam. In particular, when the surface deformation is induced by a linearly polarized Gaussian beam a protrusion is formed in the centre, while the polymer chains move out from the central region and accumulate at the edges where the intensity is small. Conversely, if the light intensity is higher, a peak in the surface appeared in the centre of the exposed spot. In addition, when the surface deformation is induced by a circular polarization Gaussian beam, the polymer moves from the centre to the outside of the focused laser spot, thus forming a doughnut-shaped pattern. In recent years, the use of a gaussian beam of confocal microscope to impress photo-pattern on the surface of azo material has been vastly assessed [21,22]. For example, in our group, photo-pattern were embossed on the surface of poly(disperse red 1 methacrylate) (pDR1m) polymer by confocal microscope in order to realize innovative platforms for cellular behaviour investigation [23–27]. For example, De Martino *et al.* used it to obtain dynamic photo-switchable platforms capable of controlling cell fate [26]. Naturally, the employment of azopolymers substrates in biological applications as dynamic cell culture platforms able to guide and control cell functions, through the modulation of surface topography, required wet environmental conditions. However, when exposed to aqueous solutions, such as cell media, thin azopolymer films experience some instabilities, as previously reported [23,28]. In details, they observed the formation of "bubble-like" structures on the surface of the azopolymer, which can affect the efficacy of the photo-responsive properties of the material. Indeed, the presence of these protrusions hinders a precise control

over the geometrical features of the surface topography during light illumination, which is relevant for the transmission of the physical signal. Generally, thin polymer films can undergo several failures such as delamination, dewetting, or blistering. In our case, these "bubble-like" structures are blisters formed at azopolymer-substrate interface, as also stated by Audia *et al.* [29]. Different models are proposed to describe the mechanism underlying blister formation [30,31]. Berkelaar *et al.* studied experimentally as well as theoretically the process of blister formation in polystyrene films and suggested a quantitative model describing the blister growth [31]. In details, they proposed a mechanism based on water permeation through the polymer thin film driven by the high affinity of water molecules with the hydrophilic glass surface and caused by the presence of topological defects which act as nucleation sites. Once water permeated, small solute particles present at polymer-glass interface, *e.g.* residual contaminants or impurities left behind from fabrication procedures, start to diffuse into the water hollows, increasing the osmotic pressure, which lead to blister growth and coalescence, eventually provoking polymer detachment from the underneath substrate. Also, several methods were proposed to prevent blister formation, involving the use of hydrophobic layers which reduce the attraction between water and the substrate surface [29,31]. Although, the aforementioned model is described for polystyrene films, it can be applied also to other kinds of polymers and substrates. Indeed, this model well describes the mechanism of blister formation and growth in our pDR1m azobenzene-based polymer. In this chapter, a method to impress an anisotropic pattern in the form of parallel ridges and grooves on the surface of pDR1m, based on the use of 1D Gaussian beam of a confocal laser scanning microscope, was proposed. In particular, a relation between laser scanning parameters and topographical features was found, in order to finely control the shape of the embossed pattern. Also, azopolymer behaviour in wet conditions was characterized by optical microscope and Atomic Force Microscopy (AFM), shedding light on the formation of superficial "bubble-like"

structures, which resulted to be blisters formed at polymer-glass interface. Therefore, a procedure to prevent blister generation through glass surface silanization was presented.

2.2 Materials and Methods

Poly-Disperse Red 1-methacrylate (pDR1m), Trimethoxy[2-(7-oxabicyclo[4.1.0]hept-3-yl)ethyl]silane and all solvents were supplied by Sigma-Aldrich. Circular cover glasses were purchased from Thermo Scientific. MilliQ water was used in all the solutions and procedures.

2.2.1. Substrate Preparation

Poly-Disperse Red 1-methacrylate (pDR1m, Sigma-Aldrich) was dissolved in Chloroform (Sigma-Aldrich) at a concentration of 5% (w/v). 50 μL of the solution was spin-coated on 20 mm diameter circular cover glasses by using a spin coater (Laurell Technologies Corp.) at 2000 rpm, 2000 acceleration for 30 sec. A flat and homogenous polymer layer was obtained with a thickness of ≈ 300 nm, measured by Atomic Force Microscopy (Bruker Dimension Icon).

2.2.2. Pattern Inscription

Single photon confocal microscopy (Leica Microsystems, Germany) with an Argon laser and a 20× dry objective was used to impress precise and submicrometric patterns on pDR1m thin films. In details, laser source with a wavelength value of 514 nm was used to induce the continuous *trans-cis-trans* isomerization of disperse red 1 molecules, which resulted in surface mass migration and reliefs formation. Different laser intensities and scanning parameters (scan format and speeds) were examined.

2.2.3. Pattern Erasure

The pattern erasure was conducted by two different techniques. First, a confocal microscopy (Leica Microsystems, Germany), with an Argon laser (514 nm wavelength) and a 20× dry objective was used, exploiting the modulation of laser scan parameters (scan format and speeds). The second used the incoherent light of a mercury lamp (Leica Microsystems, Germany) with a Rhodamine filter, coupled to the confocal microscope, to randomly re-orient the disperse red 1 azo molecules with a time exposure of 2 min.

2.2.4. Azopolymer Surface Characterization

Surface characterization was performed by atomic force microscope (AFM). More specifically, Bruker Dimension Icon was used to examine the surface topography of pDR1m films. Silicon Nitride tips (SCANASYST-AIR, SCANASYST-FLUID, Bruker, USA) with a spring constant of 0.4 N/m were used in ScanAsyst mode, both in air and water at room temperature. Optical images were acquired by Single photon confocal microscopy (Leica Microsystems, Germany) with a 20× dry objective in transmitted mode at 633 nm wavelength, which was not able to induce photo-patterning, since the maximum absorption band of our polymer was in the range of 400-600 nm.

2.2.5. Hydrophobic Silanization of Glass Surface

The surface properties of glass substrates were altered by chemical modifications. In more details, glass substrates were firstly cleaned with a soap water solution, rinsed in water, sonicated in acetone (Sigma-Aldrich) for 15 min, then immersed in methanol (Sigma-Aldrich) for 5 min to remove further solvent residuals, thoroughly washed in water and lastly dried on a hot plate. Subsequently, the surface of cleaned glass substrates were activated with oxygen plasma (PFEIFFER VACUUM SingleGauge – CESAR RF Power Generator) for 1 min, after which they were immediately soaked into a Trimethoxy[2-(7-

oxabicyclo[4.1.0]hept-3-yl)ethyl]silane (Sigma-Aldrich) solution (2% in ET-OH/H_2O 95%/5% v/v) for 15 min at room temperature and then placed at 110°C for 20 min to boost the reaction. Finally, treated glass substrates were sonicated in ethanol for 15 min twice to remove the unbound molecules and then dried on hot plate prior to pDR1m spin-coating.

2.3. Results and Discussion

Azobenzene-based materials can be photo-activated by different light illumination techniques. In this work, the Gaussian beam of a Confocal Laser Scanning Microscope (CLSM) has been employed to realize topographical pattern on the surface of a pDR1m azopolymer film. A relation between laser scanning parameters and pattern geometrical features was found, which allowed to precisely control the morphology of the inscribing pattern. Moreover, since the light-induced material displacement of the azopolymer can be optically removed by exposing the surface to a non-polarized or a circularly polarized light, different light techniques able to remove the impressed pattern were investigated. In addition, because the photo-isomerization of the azo molecules can be induced several times without degrading the material or permanently changing the physic-chemical properties of the polymer, the "patterning-erasure" ability of the azo-materials was assessed in order to realize photo-switchable platforms for dynamic cell culture experiments. Lastly, the behaviour of the azo material in aqueous solutions was studied, demonstrating the formation of blisters. Therefore, a method to prevent their generation was proposed, based on glass surface chemical modifications through the use of silane molecules.

2.3.1. Pattern Inscription by Scanning Laser Beam

The high spatially focused 1D laser beam of a confocal microscope is exploited to precisely control the formation of well-defined reliefs on the azopolymer surface. Indeed, by changing the microscope parameters, such as laser intensity

and polarization, scan speed, format and direction, it is possible to control the amount of energy provided to the system in order to trigger the azopolymer mass transport, which in turn affects the geometrical features of the impressing pattern. Moreover, the confocal software allows to activate the laser illumination only inside specific regions-of-interest (ROI), thus accurately defining the areas where to inscribe the pattern. Also, by modulating the form of the ROIs (*e.g.*, circles, triangles, square and rectangular lines), topographies with different shapes and dimensions can be embossed, which makes this optical set-up extremely versatile. In order to evaluate the different laser scan parameters on the pattern geometry, a 20× objective (NA = 0.5) was used, which allowed to irradiate an area of 775 µm × 775 µm. An argon laser at 514 nm with intensity of 92 µW and a linear polarization orthogonal to the scan direction, was used to induce a continuous photo-isomerization of the disperse red 1 azo-molecules, which activates the surface mass displacement of the all polymer chains. Different laser scan formats (256 × 256, 512 × 512, 1024 × 1024) and speeds (10 Hz, 200 Hz and 400 Hz) were tested, corresponding to different pixels sizes and dwell times, respectively. As a result of the light illumination, a sinusoidal linear pattern in the form of parallel ridges/grooves was formed on the surface of the azo material, which recapitulates the scan lines of the laser. The effect of the combination of the two different microscope parameters (scan format and speed) on the pattern features was characterized in terms of ridges height and pitch. In the case of a 256 × 256 format, the pixel size was 3.01 µm, which resulted to be similar to the pitch of the pattern. Indeed, the light spot moves continuously along the x-direction, where the mass moves in the opposite direction according to the polarization direction, resulting in the presence of fringes on the peaks of the pattern, while the motion along the y-direction is dictated by the scan format, thus it moves from one pixel centre to the other defining the distance between the sinusoidal peaks (Fig. 2.1 A). Instead, the ridges height was shown to be affected also by the scan speed. More precisely, the height of the ridges resulted to increase by reducing the scan

speed. Indeed, if the format was maintained fixed, while the scan speed was varying, the height of the ridges reached values of 27.2 nm, 55.2 nm and 114.3 nm, for scan speed of 400 Hz, 200 Hz and 10 Hz, respectively. As expected, the reduction of the scan speed leaded to an increase of the dwell time, which means that the light remained longer on a single pixel, increasing the total energy provided to the system, thus enhancing the mass displacement. For 516 × 516 format the pattern pitch resulted equal to 1.5 µm (Fig. 2.1 B) with heights reaching 83.6 nm, 154.9 nm and 287.8 nm for the same scan speed values before evaluated.

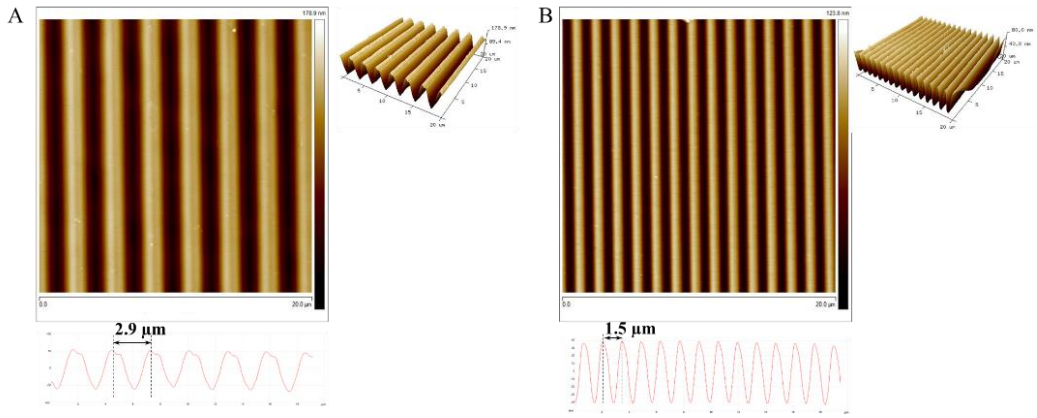

Figure 2.1. AFM images of sinusoidal pattern on pDR1m induced by laser illumination. Surface pattern obtained with A) 256 × 256 and B) 516 × 516 scan format.

These results showed a dependence of pattern heights on both scan parameters, with higher values observed for smaller pixel sizes and slower scan speeds (Fig. 2.2).

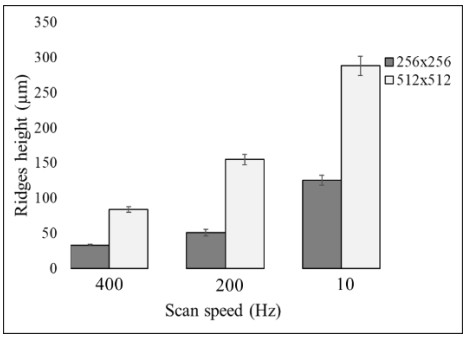

Figure 2.2. Mean values and standard deviation of ridges height evaluated with AFM for different laser scan parameters (format and speed).

Instead, for larger values of the format, no sinusoidal pattern formation could be observed. In this case the pixel dimension resulted to be coincident with (or be even smaller to) the lateral resolution of the microscope, which approximately is equivalent to the Full-width at half-maximum (FWHM) of the Gaussian beam, and equal to 685 nm in this particular condition, according to the Rayleigh criterion expressed by Eq. (1).

$$\text{Eq.(1)} \qquad r = 0.61\ \frac{\lambda}{NA},$$

where λ is the radiation wavelength and NA is the objective numerical aperture. Consequently, the laser line scans overlapped and irradiated the same regions several times, affecting the mass movement of the azo material which is then continuously wiped out by the repetitive passages of the light. Nevertheless, this can be exploited to realize topographies with different morphologies by activating the illumination only within ROIs of different shapes (Fig. 2.3 A). In addition, because the actuation of the material displacement induced by light is an energy dependent process, a reduction of the peaks heights was observed by half decreasing the intensity of the laser (Fig. 2.3 B). On the other hand, by increasing the number of iterations, *i.e.* the number of light passages along each scan line, the peaks height also increases (Fig. 2.3 C). Thus, depending on the application,

laser scanning parameters can be modulated in order to obtain the optimal geometrical features of the azopolymer surface topography.

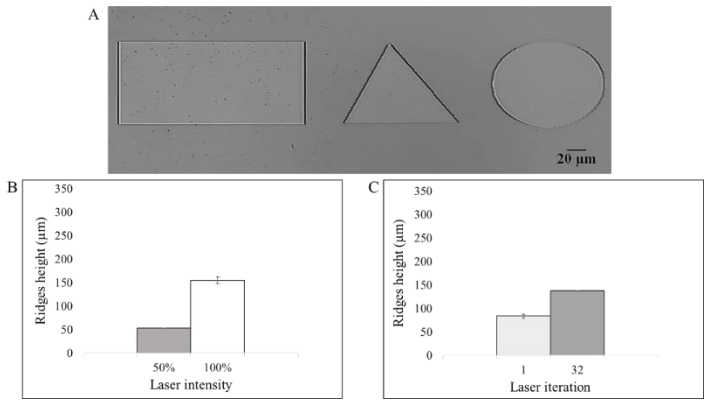

Figure 2.3 A) Confocal images in transmitted mode of surface topographies of different shapes obtained with 1024 × 1024 format. B) Laser intensity effect and C) iteration numbers on the ridges height.

2.3.2. Light-induced Erasure of the Surface Topography

The *trans-cis* photo-isomerization of the azobenzene molecules is a reversible process, since the initial random orientation of the azo-moieties can be restored by irradiating the material with a non-polarized or circularly polarized-light. Therefore, the impressed pattern on the azopolymer surface can be optically erased, enabling the realization of a dynamic photo-switchable substrate. In this work, two different methods were explored to remove the superficial pattern, *i.e.* the scanning of a focused laser beam of a confocal microscope and the incoherent light of a mercury lamp. The former exploits the scanning of a focused beam whose parameters can be regulated in order to eliminate rather than writing the pattern. Indeed, if the scan format and speed are selected in a way the laser spots overlap, the laser acts as a brush which wipes away the material, erasing the previous impressed pattern. On the other hand, the non-polarized light of a mercury lamp was used in order to randomly re-orient the azo-molecules, restoring the initial flat condition. In order to evaluate both methods, a linear pattern in the form of sinusoidal ridges/grooves was imprinted on the surface of

the azopolymer by using the laser of a confocal microscope, as previously described. The initial height and pitch of the pattern were 150 nm and 1.5 µm, respectively. In order to test the effects of scan parameters on the erasure process, different combinations were tested. A 20× objective (NA = 0.5) and an argon laser with 514 wavelength were used to trigger to mass displacement on the azopolymer surface. The scan format was chosen in order to overcome the limit of lateral resolution of the microscope, which is in this case 685 nm. Thus, the pixel size was set approximately equal or lower this value. Precisely, a 4096 × 4096 scan format was tested, which provided a pixel size of 189.26 nm. Scan speeds of 400 Hz, 200 Hz and 10 Hz were evaluated, while the intensity of the laser was maintained fixed and equal to 92 µW. In order to test the different parameters, laser illumination was activated in ROIs of different shape on the same initial pattern (Fig. 2.5 A). Results showed that fast scan speeds (400 Hz, 200 Hz) did not allow a complete removal of the pattern (Fig. 2.5 B, C), whereas a slow scan speed (10 Hz) leaded to a total reduction of the pattern peaks, leaving only surface roughness of small nanometres (Fig. 2.5 D).

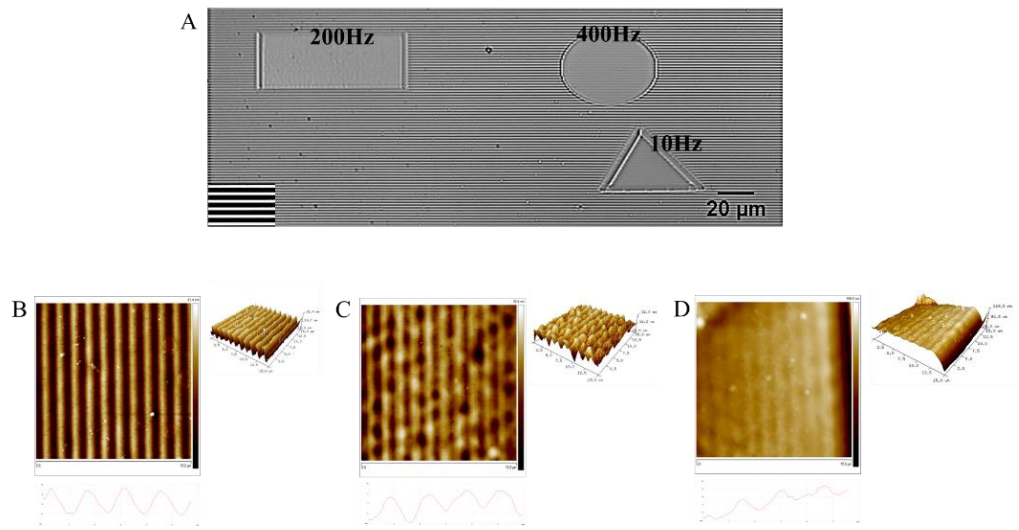

Figure 2.5. pDR1m surface characterization. A) Confocal image in transmitted mode of linear pattern erased in specific light illuminated ROIs by different laser scan speed. The insert in the left lower corner showed

the initial linear pattern, still present outside the illuminated regions. AFM bi-dimensional, 3D and cross section images of optically erased pattern by Gaussian laser beam with B) 400 Hz, C) 200 Hz and D) 10 Hz scan speed.

However, with this method a huge amount of energy was delivered to the azopolymer system, which could be damaged and undergoing chemical modifications that in turn could impair further photo-isomerization of the azo-moieties. Therefore, a different technique was tested to remove the superficial pattern, which exploits the milder non-polarized light of a mercury lamp. In details, the light coming from the lamp was not focused on a single pixel, but rather illuminated a wide region of the sample, thus providing lower energy/surface. Moreover, in our system, the mercury lamp was coupled to the confocal microscope allowing to define the region where illuminate the sample. A rhodamine filter with intensity of 27 mW was used to irradiate an area of 4.9 mm^2 on the azopolymer surface. After 2 min of illumination, a smoother surface was obtained (Fig. 2.6 A). Indeed, despite the periodicity of the pattern was still impressed, the initial depths were completely removed, resembling the roughness of a flat azopolymer surface not exposed to light illumination (Fig. 2.6 B).

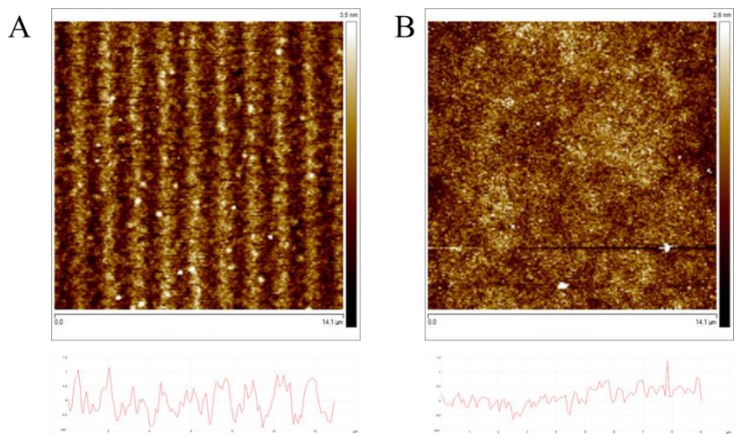

Figure 2.6. AFM bi-dimensional and cross section images of A) linear pattern erased by 2 min illumination of a mercury lamp and of B) a flat surface.

2.3.3. Patterning-Erasure cycles on Azopolymer Surface

The photo-switchable properties of azopolymers allow these materials to be used as dynamic platforms for several applications. Indeed, the reversible process of light-induced mass displacement permits to remove the superficial pattern, giving the possibility to re-write a new pattern on the same area. Moreover, since the isomerization of the azobenzene molecules can be light-activated thousands of times before chromophore photo-chemical modifications, several cyclic topographical variations can be optically realized on the surface of azo-molecules containing materials. In order to evaluate the efficacy of the patterning-erasing ability of the azopolymers, two different light techniques were employed to impress and remove the surface gratings. In more details, a sinusoidal linear pattern was imprinted by the Gaussian beam of a confocal laser scanning microscope, while the subsequent erasure was performed using a mercury lamp, as described above. The initial impressed pattern was characterized by a height and peak-to-peak distance of 150 nm and 1.5 μm, respectively. The azopolymer surface was stimulated up to 5 patterning-erasure consecutive cycles and the surface topography after the light-induced variations was characterized by atomic force microscopy in order to state the efficacy of the photo-switchable properties of the material. Results showed the capacity of the material to perfectly respond to the external stimuli even after several light illuminations, eventually recovering the initial flat surface, without presenting any degradation (Fig. 2.7). Therefore, the azopolymers can be potentially stimulated cyclically even more than 5 times, with a frequency that is limited only by the time needed to impress and remove the superficial pattern.

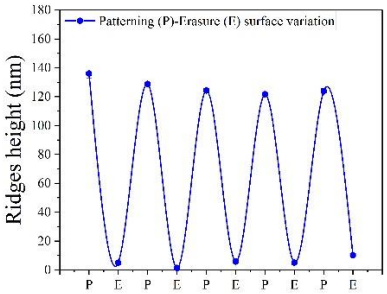

Figure 2.7. Representation of height ridges values evolution measured by AFM after each light-induced surface variation on pDR1m azopolymer film.

2.3.4. Azopolymer Blister Formation in Wet Conditions

Thin polymer films can undergo several modifications when exposed to aqueous environments. Glass coated azopolymers films, for example, can detach from the substrate in presence of water solutions due to the formation of blisters. In our case, the mechanism underlying blister development involve the generation of an osmotic pressure, as described by Berkelaar *et al.* [31]. The model describes blisters as cavities which form around a topological defect (TD), deposited at polymer-substrate interface, and therefore inducing the creation of an osmotic pressure that drives water towards the substrate surface, supported by the higher affinity of water molecules with the underneath substrate. Additionally, other small impurities present at substrate interface diffuse into the water bladder, increasing the osmotic pressure that lead to blister growth and eventually into polymer detachment. In our system, pDR1m azopolymer thin film of 300 nm thick was spin-coated onto glass substrate. When in contact with water, a quite instantaneous formation of "bubble-like" structures could be observed by optical microscope (Fig 2.7 A). In addition, surface topography was carried out in water condition by AFM in order to prove the presence of these structures (Fig 2.7 b). However, after air drying the surface, these blister deflates leaving indented holes

on the surface of the azo material of few nanometres deep, stating that blister formation induces plastic deformations on the azopolymer surface (Fig. 2.7 C).

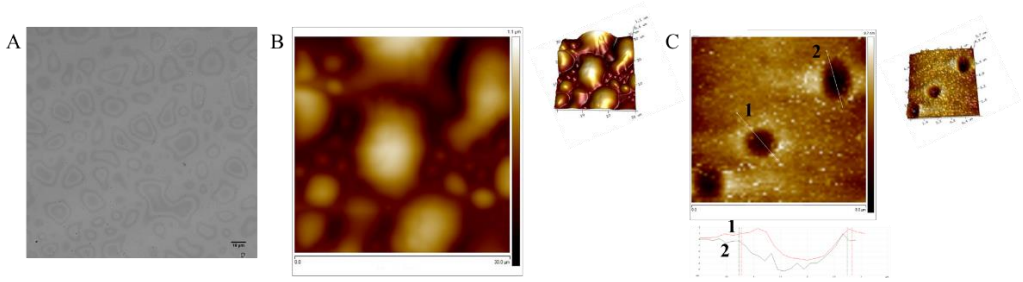

Figure 2.7. A) Optical images and B) AFM bi-dimensional and 3D images of blister formation on pDR1m surface in presence of water. The AFM was performed in ScanAsyst fluid mode. C) AFM of bi-dimensional and 3D images of air-dried pDR1m surface after contact with water showing the presence of plastically deformed holes left behind by previously formed blister cavities.

Moreover, if laser illumination was activated in order to emboss a topographical pattern on the surface, the azopolymer surface mass movement was not affected by the presence of the blister, instead the material arises over the relief, confirming that these structures were present under the polymer layer and they were not air bubbles formed on the surface. In details, the same structures were present on the surface before and after light-induced pattern formation, also preserving the same shape (Fig. 2.8 A). AFM of dried surfaces stated the permanent deformation generated by light on the blister holes (Fig. 2.8 B).

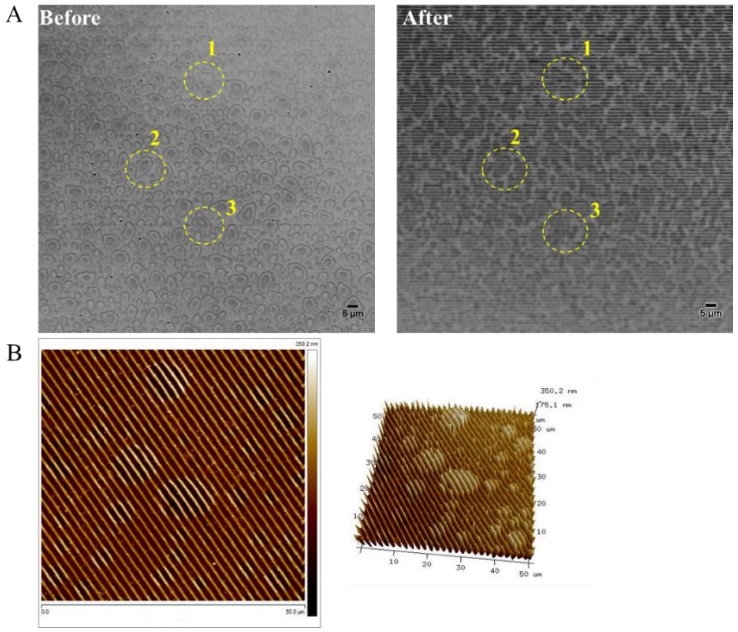

Figure 2.8. Blister characterization on pDR1m surface. A) Confocal images in transmitted mode of blister formed on the azopolymer surface before and after the pattern impression by laser. The structures are not affected by the material movement induced by light illumination, preserving their shape and position. B) AFM bi-dimensional and 3D images of linear pattern embossed in the presence of blister.

Instead, when the azopolymer surface was illuminated with a non-polarized light of a mercury lamp in presence of water, the light-induced mass displacement caused a reshape of blisters which deform and break into smaller structures (Fig. 2.8 A, B).

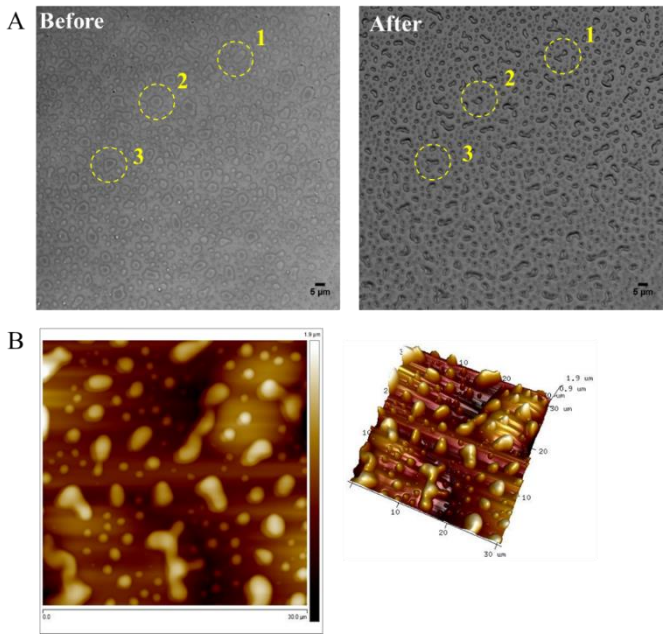

Figure 2.8. Blister characterization on pDR1m surface. A) Confocal images in transmitted mode of blister formed on the azopolymer surface before and after the light illumination from a mercury lamp. The reliefs are affected by the mass movement of the azopolymer, resulting in a deformation and rupture into smaller structures. B) AFM bi-dimensional and 3D images of deformed blister after mercury lamp irradiation.

2.3.4.1. Blister Prevention

The formation of blisters in wet environments at azopolymer-glass interface could be used to induce spontaneous patterning of the surface. However, in some applications where the topographical surface was intended to be precisely modulated in order to provide specific signals, such as in cell culture, this represent an undesired effect and should be surpassed. To this aim, different methods can be used to avoid the formations of blisters. For example, a deep cleaning of substrate surface with chemical detergents such as piranha solutions could be useful to dissolve dirty particles. Nevertheless, these washing procedures could in turn leave some crystal residues on the surface which favour the blister generation process [31]. Even so, a different method can be employed which consist of reducing the attraction of polar water molecules toward glass surface,

by placing an hydrophobic layer at the polymer-glass interface. Indeed, in this condition the osmotic pressure is balanced by the hydrophobic repulsive force which hampers the penetration of water at the interface. In this work, we propose the a modification of the glass surface properties by using a solution of Trimethoxy[2-(7-oxabicyclo[4.1.0]hept-3-yl)ethyl]silane [32]. In this process, the hydroxy groups of the silane molecules bind to the hydrophilic oxygen-activated glass surface, while the hydrophobic hydrocarbon tails were exposed at the polymer interface, thus lowering the interaction with the external aqueous solutions. Indeed, after the silane treatment, the surface of the glass coated pDR1m azopolymer showed no blister formation in presence of water (Fig. 2.9 A, B), allowing this platform to be used also in wet conditions, *e.g.* for cell culture experiments, where the cells have to be exposed to an aqueous environment, such that of the water-based cell medium.

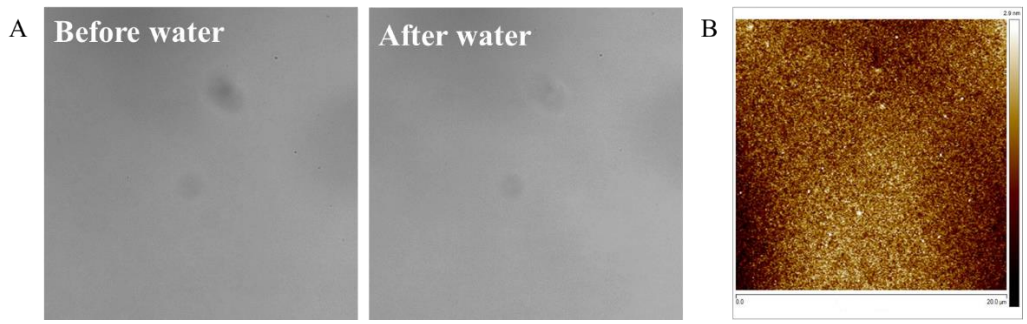

Figure 2.9. pDR1m surface characterization after silane treatment. A) Confocal images in transmitted mode of the same azopolymer surface region before and after water deposition and B) AFM bi-dimensional and 3D images of the pDR1m surface in water, stating no blister formation after the hydrophobic modification of the glass substrate.

2.4 Conclusion

Light responsive azo materials were powerful systems whose optical properties can be exploited in a large variety of applications. In particular, the ability of amorphous azopolymers to generate superficial gratings due to mass transport triggered by the *trans-cis* isomerization of the azo molecules as a consequence of

light absorption, have obtained great attention in the photonic and optical field [16,33–38], but also in biological applications as bioactive interfaces [39,40]. Moreover, the possibility to use different optical techniques and light sources to stimulate the formation of surface structures make these materials extremely versatile. Here, the Gaussian beam of a confocal laser scanning microscope was used in order to photo activate the mass displacement on the surface of pDR1m. In more details, a sinusoidal pattern in the form of ridges/groove was realized by using an Argon laser at 514 nm. Additionally, with the aim to control the geometrical features of the impressed pattern, different laser scanning parameters (intensity, scan speed and format) were tested. AFM surface characterization reported an implication of laser scan speed and format on ridges height and pitch. Also, the use of a confocal microscope laser and the incoherent light of a mercury lamp were separately examined as optical systems to erase the imprinted pattern. Eventually, the azopolymer behaviour in aqueous environments was analysed, stating the formation of cavities formed at polymer-substrate interface, called "blisters". Therefore, a method to prevent blister generation in azopolymer thin films was proposed, which was based on the use of silane molecules to realize an hydrophobic layer on the surface of the underneath glass substrate.

2.5 References

1. De Martino S, Mauro F, Netti PA. Photonic applications of azobenzene molecules embedded in amorphous polymer. Riv Nuovo Cimento. 2020;43: 599–629.
2. Paterson J, Natansohn A, Rochon P, Callender CL, Robitaille L. Optically inscribed surface relief diffraction gratings on azobenzene-containing polymers for coupling light into slab waveguides. Appl Phys Lett. 1996;69: 3318–3320.
3. Kim DY, Tripathy SK, Li L, Kumar J. Laser-induced holographic surface relief gratings on nonlinear optical polymer films. Appl Phys Lett. 1995;66: 1166–1168.
4. Barrett CJ, Natansohn AL, Rochon PL. Mechanism of optically inscribed high-efficiency diffraction gratings in azo polymer films. J Phys Chem. 1996;100: 8836–8842.

5. Viswanathan NK, Kim DY, Bian S, Williams J, Liu W, Li L, et al. Surface relief structures on azo polymer films. J Mater Chem. 1999;9: 1941–1955.
6. Yager KG, Barrett CJ. All-optical patterning of azo polymer films. Curr Opin Solid State Mater Sci. 2001;5: 487–494.
7. Zettsu N, Ogasawara T, Mizoshita N, Nagano S, Seki T. Photo-triggered surface relief grating formation in supramolecular liquid crystalline polymer systems with detachable azobenzene unit. Adv Mater. 2008;20: 516–521.
8. Isayama J, Nagano S, Seki T. Phototriggered mass migrating motions in liquid crystalline azobenzene polymer films with systematically varied thermal properties. Macromolecules. 2010;43: 4105–4112.
9. Koskela JE, Vapaavuori J, Ras RHA, Priimagi A. Light-driven surface patterning of supramolecular polymers with extremely low concentration of photoactive molecules. ACS Macro Lett. 2014;3: 1196–1200.
10. Kitamura I, Kato K, Berk RB, Nakai T, Hara M, Nagano S, et al. Photo-triggered large mass transport driven only by a photoresponsive surface skin layer. Sci Rep. 2020;10: 12664.
11. Sekkat Z, Wolfgang Knoll D, editors. Photoreactive Organic Thin Films. Academic Press; 2002.
12. Lee S, Kang HS, Park J-K. Photofluidization: Directional photofluidization lithography: Micro/nanostructural evolution by photofluidic motions of azobenzene materials (adv. Mater. 16/2012). Adv Mater. 2012;24: 2062–2062.
13. Mahimwalla Z, Yager KG, Mamiya J-I, Shishido A, Priimagi A, Barrett CJ. Azobenzene photomechanics: prospects and potential applications. Polym Bull (Berl). 2012;69: 967–1006.
14. Natansohn A, Rochon P. Photoinduced motions in azo-containing polymers. Chem Rev. 2002;102: 4139–4175.
15. Barrett CJ, Rochon PL, Natansohn AL. Model of laser-driven mass transport in thin films of dye-functionalized polymers. J Chem Phys. 1998;109: 1505–1516.
16. Priimagi A, Shevchenko A. Azopolymer-based micro- and nanopatterning for photonic applications. J Polym Sci B Polym Phys. 2014;52: 163–182.
17. Hurduc N, Donose BC, Macovei A, Paius C, Ibanescu C, Scutaru D, et al. Direct observation of athermal photofluidisation in azo-polymer films. Soft Matter. 2014;10: 4640–4647.
18. Rocha L, Dumarcher V, Denis C, Raimond P, Fiorini C, Nunzi J-M. Laser emission in periodically modulated polymer films. J Appl Phys. 2001;89: 3067–3069.
19. Hubert C, Fiorini-Debuisschert C, Raimond P, Nunzi J-M. Photoinduced spontaneous patterning of azopolymer films using light-controlled mass transport. In: Grote JG, Kaino T, editors. Organic Photonic Materials and Devices V. SPIE; 2003. doi:10.1117/12.475411

20. Bian S, Li L, Kumar J, Kim DY, Williams J, Tripathy SK. Single laser beam-induced surface deformation on azobenzene polymer films. Appl Phys Lett. 1998;73: 1817–1819.
21. Ambrosio A, Camposeo A, Carella A, Borbone F, Pisignano D, Roviello A, et al. Realization of submicrometer structures by a confocal system on azopolymer films containing photoluminescent chromophores. J Appl Phys. 2010;107: 083110.
22. Rianna C, Rossano L, Kollarigowda RH, Formiggini F, Cavalli S, Ventre M, et al. Dynamic cell substrates: Spatio-temporal control of dynamic topographic patterns on azopolymers for cell culture applications (adv. Funct. Mater. 42/2016). Adv Funct Mater. 2016;26: 7743–7743.
23. Rianna C, Rossano L, Kollarigowda RH, Formiggini F, Cavalli S, Ventre M, et al. Spatio-temporal control of dynamic topographic patterns on azopolymers for cell culture applications. Adv Funct Mater. 2016;26: 7572–7580.
24. Fedele C, De Gregorio M, Netti PA, Cavalli S, Attanasio C. Azopolymer photopatterning for directional control of angiogenesis. Acta Biomater. 2017;63: 317–325.
25. Rossano L, Cimmino C, Cavalli S, Ventre M, Netti PA. Regulating fibroblast shape and mechanics through photoresponsive surfaces with concentric circular topographic patterns. Adv Mater Interfaces. 2018;5: 1800890.
26. De Martino S, Cavalli S, Netti PA. Photoactive interfaces for spatio-temporal guidance of mesenchymal stem cell fate. Adv Healthc Mater. 2020;9: e2000470.
27. Cimmino C, Netti PA, Ventre M. A switchable light-responsive azopolymer conjugating protein micropatterns with topography for mechanobiological studies. Front Bioeng Biotechnol. 2022;10: 933410.
28. Rocha L, Păiuș C-M, Luca-Raicu A, Resmerita E, Rusu A, Moleavin I-A, et al. Azobenzene based polymers as photoactive supports and micellar structures for applications in biology. J Photochem Photobiol A Chem. 2014;291: 16–25.
29. Audia B, Fedele C, Tone CM, Cipparrone G, Priimagi A. Surface stability of azobenzene-based thin films in aqueous environment: Light-controllable underwater blistering. Adv Mater Interfaces. 2022;9: 2102125.
30. Jing B, Zhao J, Wang Y, Yi X, Duan H. Water-swelling-induced morphological instability of a supported polymethyl methacrylate thin film. Langmuir. 2010;26: 7651–7655.
31. Berkelaar RP, Bampoulis P, Dietrich E, Jansen HP, Zhang X, Kooij ES, et al. Water-induced blister formation in a thin film polymer. Langmuir. 2015;31: 1017–1025.
32. Uysal K, Firat IS, Creutz T, Aydin IC, Artmann GM, Teusch N, et al. A novel in vitro wound healing assay using free-standing, ultra-thin PDMS membranes. Membranes (Basel). 2022;13: 22.

33. Pang X, Lv J-A, Zhu C, Qin L, Yu Y. Photodeformable azobenzene-containing liquid crystal polymers and soft actuators. Adv Mater. 2019;31: e1904224.
34. Zheng Z-G, Lu Y-Q, Li Q. Photoprogrammable mesogenic soft helical architectures: A promising avenue toward future chiro-optics. Adv Mater. 2020;32: e1905318.
35. Albano G, Pescitelli G, Di Bari L. Chiroptical properties in thin films of π-conjugated systems. Chem Rev. 2020;120: 10145–10243.
36. Rekola H, Berdin A, Fedele C, Virkki M, Priimagi A. Digital holographic microscopy for real-time observation of surface-relief grating formation on azobenzene-containing films. Sci Rep. 2020;10: 19642.
37. Zhai Y, Cao L, Liu Y, Tan X. A review of polarization-sensitive materials for polarization holography. Materials (Basel). 2020;13: 5562.
38. Pilz da Cunha M, Debije MG, Schenning APHJ. Bioinspired light-driven soft robots based on liquid crystal polymers. Chem Soc Rev. 2020;49: 6568–6578.
39. Zhu C, Lu Y, Sun J, Yu Y. Dynamic interfacial regulation by photodeformable azobenzene-containing liquid crystal polymer micro/nanostructures. Langmuir. 2020;36: 6611–6625.
40. De Martino S, Netti PA. Dynamic azopolymeric interfaces for photoactive cell instruction. Biophys Rev (Melville). 2020;1: 011302.

Chapter 3

Dynamic Control of Cell Behaviour by *In-Situ* Photo-Patterning of Azopolymer Surface

3.1. Introduction

The external cellular environment (ECM) can regulate cell functions by the transmission of biochemical and biophysical signals, including biological, topographical and mechanical cues [1]. These stimuli are then transduced into biochemical e intracellular signalling through the process of mechanotransduction eventually affecting cell behaviour [2,3]. Several substrates and biomaterials were fabricated in the years in order to recapitulate the properties of the external matrix surrounding *in-vivo* context the cells [4–6]. In particular, novel technologies were implemented for the generation of biomaterials with microscale topographies to examine the influence of biophysical signals on cellular functions at the cell–substrate interface [7]. Indeed, numerous studies have shown the influence of substrate topography on cell adhesion, morphology, migration and differentiation mediated through the phenomenon of contact guidance [8]. For example, Charest *et al.* demonstrated that C2C12 myoblasts align along the direction of an array of ridges and grooves realized through optical lithographic patterning technique [9]. Moreover, topography was known to affect also nuclear size and organization. Indeed, the actin cytoskeleton is able to exert mechanical load on the cell nucleus, thus deforming its shape, eventually affecting chromatin arrangement and gene-expression [10–15]. Further, the external topographical constrains can even impact the genomic organization within the nucleus. Wang. Y *et al.* showed that chromosomes positioning within the nucleus can be regulated by cell geometry [16]. Although a wide range of studies focused

on the presentation of static topographical signals, the dynamicity is crucial when realizing platforms that reliably mimic the native extracellular environment. Thus, in recent years, several "smart" or "stimuli responsive" materials, able to provide time-varying topographical cues, were implemented to study cell behaviour [17,18]. These materials, through the realization of structured surfaces, are able to modify their morphology upon external stimuli, such as temperature, electric or magnetic field and light illumination. Among them, azopolymers materials gained great interest because of their biocompatibility and light responsiveness. Indeed, light illumination, at specific wavelengths, resulted less harmful to cells compared to all other external stimuli used to trigger material response [19]. Also, light allows a fine control over time of surface properties variation which can be activated by using a large variety of light illumination techniques. Therefore, they were even more employed as powerful dynamic platforms for cell cultures experiments [20]. In our group, a method for the fabrication of azopolymer-based devices was developed, capable of dynamically changing their topography upon illumination with a laser-based confocal microscope in presence of cells, in order to affect their morphology and functions [21–23]. As example, Fedele *et al.* exploited the versatility of this technique to study the effect of changes in topographical cues during early-stage angiogenesis through real-time azopolymer photopatterning, showing the influence of dynamic presentation of topographic signals on sprout formation and directionality [24]. In this work, topographic pattern relief, in the form of anisotropic parallel ridges and grooves was embossed *in-situ* on poly-disperse red1-methacrylate (pDR1m) functionalized surfaces in order to realize dynamic cell culture platforms with the aim to investigate cell behaviour in response to the surface topography variation. Thus, the effect of such topographic pattern inscription was evaluated on focal adhesions (FAs) morphology and assembly, cell shape and cytoskeleton organization of human breast epithelial cells (MCF10A). In addition, the impact of the light-induced topographic patterning on nuclear morphology and its inner structural

organization was also investigated in terms of nuclear deformation, chromosome arrangement and chromatin condensation state. Further, investigation on cell growth and proliferation rate induced by the nano topography was carried out. Lastly, since external topographical cues were shown to affect cell mechanics [25,26], cell and nuclear mechanical properties were evaluated by atomic force microscopy (AFM) upon azopolymer surface light-induced topographic patterning.

3.2. Materials and Methods

Poly-Disperse Red 1-methacrylate (pDR1m), Trimethoxy[2-(7-oxabicyclo[4.1.0]hept-3-yl)ethyl]silane and all solvents were supplied by Sigma-Aldrich. Circular cover glasses were purchased from Thermo Scientific. MilliQ water was used in all the solutions and procedures.

3.2.1. Sample Preparation

Surface of 20 mm diameter circular cover glasses were chemically modified by Trimethoxy[2-(7-oxabicyclo[4.1.0]hept-3-yl)ethyl]silane (Sigma-Aldrich) solution (2 % in ET-OH/H_2O 95 %/5 % v/v) following the protocol described in Chapter 2. Poly-Disperse Red 1-methacrylate (pDR1m, Sigma-Aldrich) was dissolved in Chloroform (Sigma-Aldrich) at a concentration of 5 % (w/v). 50 μL of the solution was spin-coated onto the silane-treated circular cover glasses by using a spin coater (Laurell Technologies Corp.) at 2000 rpm, 2000 acceleration for 30 sec. A flat and homogenous polymer layer was obtained with a thickness of ≈ 300 nm, measured by AFM (Bruker Dimension Icon).

3.2.2. Cell Culture

MCF10A cell line was cultured in Dulbecco's Modified Eagle Medium/Nutrient Ham's Mixture F-12 (DMEM/F-12) (Sigma-Aldrich) supplemented with 5 % horse serum, 0.1 % human Epidermal Growth Factor (hEGF), 0.1 % insulin, 0.1 % hydrocortisone, 1 % penicillinstreptomycin, 1 % L-glutamine at 37 °C in a

humidified atmosphere of 95 % air and 5 % CO_2. Cells were seeded onto the planar polymeric substrates using a density of 1.000 cells/cm^2. Prior to cell seeding, pDR1m substrates were sterilized under UV light for 30 min and incubated for 1 h at room temperature with 50 μg/ml fibronectin (Sigma-Aldrich).

3.2.3. Pattern Inscription and Characterization

MCF10A cells were cultivated on pDR1m coated glass substrates for 24 h. Then, light-induced topographic surface patterning was performed *in-situ* on living cells by using single photon confocal microscopy (Leica Microsystems, Germany) with an Argon laser (514 nm) and a 20× dry objective. The technique used to impress linear pattern on pDR1m surfaces was described in Chapter 2. For experiments with living cells, the optical set-up was implemented with an incubator for the maintenance of physiological temperature (37 °C) and CO_2 (5 %) conditions. Surface characterization was carried out by AFM and scanning electron microscope (SEM). For AFM, a Bruker Dimension Icon was employed, using Silicon Nitride tips (SCANASYST-AIR, Bruker, USA) with a spring constant of 0.4 N/m were used in ScanAsyst mode, in air at room temperature. SEM images were acquired with Ultra Plus FESEM scanning electron microscope (Zeiss, Germany). Light-induced patterned pDR1m samples were mounted on microscope stubs and sputter coated with gold (approximately 10 nm thickness).

3.2.4. Immunofluorescence and Live Staining

Cells were fixed at specific time points with 4% paraformaldehyde for 15 min, permeabilized in 0.1% Triton X-100 in PBS for 10 min and then blocked with 3% bovine serum albumin (BSA) for 1 h. Focal adhesions (FAs) were stained with anti-paxillin monoclonal antibody solution (1:200 dilution, Ab32084) for 1 h in 3% BSA in PBS. Heterochromatin was assessed with anti-human Tri-Methyl Histone K27-H3K27me3 (clone C36B11, Cell Signalling, 1:400 dilution) or Tri-Methyl-Histone H3 (Lys9) H3K9me3 antibody (9754, Cell Signaling, 1:100

dilution) for 1 h in 3% BSA in PBS. After incubation, substrates were washed 3 times with PBS (3 min x wash) and then incubated with antibody conjugated to Alexa Fluor 488 (dilution 1:1000; Molecular Probes) for 1 h in a humid chamber. Actin filaments were stained by incubating samples with Alexa Fluor 555-phalloidin (1:200 dilution) for 1h in a humid chamber. Nuclei were stained by incubating samples with DAPI (dilution 1:1000; Sigma) for 15 min at 37 °C. Then, samples were mounted in Vectashield. For live staining, cells were incubated in SiR-DNA (SC007, Spirochrome) (dilution 1:1000) for 30 min at 37 °C.

3.2.5. Sample Preparation for FIBSEM

Samples were fixed in 2.5 % glutaraldehyde (Electron Microscopy Sciences) in 0.1 M sodium cacodylate buffer (pH 7.3, Electron Microscopy Sciences) at 4 °C overnight and washed 3 times in the same buffer before quenching in 20 mM glycine (Sigma Aldrich) for 20 min at 4 °C. After rinsing with buffer (3 × 5 min at 4 °C), samples were post-fixed in an aqueous solution of 2 % osmium tetroxide (Electron Microscopy Sciences) and 1 % potassium ferrocyanide (Electron Microscopy Sciences) and incubated for 1 h on ice in the dark. After washing (3 × 5 min) with buffer on ice, samples were washed in distilled water and left until room temperature was reached. After this time, specimens were incubated with 1 % thiocarbohydrazide (TCH_Electron Microscopy Sciences) at room temperature for 20 min in the dark and washed (3 × 5 min) in distilled water. The TCH solution was freshly prepared (powder dissolved in water and melt in the oven at 60 °C for 1 h) and filtered before using. Substrate with cells were post fixed in 2 % osmium tetroxide (aqueous solution) for 1 h at room temperature in the dark, washed 3 times in distilled water and in-bloc stained with 1 % aqueous uranyl acetate (Electron Microscopy Sciences) overnight at 4 °C. After rinsing with chilled deionized water, specimens were treated with 0.15% tannic acid aqueous solution for 3 min and again rinsed (3 × 5 min) with water. Samples were dehydrated in

increasing concentration of 2-PrOH (10 %, 30 %, 50 %, 70 %, 90 %, 100 %, Sigma-Aldrich) for 10 min each step on ice, except for the last step in 100 % 2-PrOH that was performed 3 times at room temperature. Substrates with cells were infiltrated with a mixture of increasing concentration of Spurr's low viscosity embedding resin (Electron Microscopy Sciences) in 2-PrOH, at room temperature in a sealed container, using these ratios: 1:3 for 2 h, 1:1 (overnight), 2:1 for 2 h. The mixture was replaced with freshly 100% Spurr resin and the resin infiltration was carried out at room temperature overnight. To remove the excess of resin, each sample was mounted vertically for 2 h and washed with 2PrOH, then put in the oven at 70 °C for the resin polymerization. Before FIBSEM imaging specimens were mounted with colloidal silver paste (RS components) to aluminium pin stub (Ted Pella) and sputtered with a 20 nm layer of Gold by using the HR208 Cressington sputter coating.

3.2.6. SEM Imaging and FIB Cross-sectioning

For SEM imaging and FIB cross sectioning**,** samples were loaded in to the Focus Ion Beam Scanning Electron Microscope chamber (Helios CX 5_Thermofisher Company) and secondary imaging has been performed with ETD detector (Everhart Thomley Detector) with a voltage of 3 kV. The region of interest located on the sample has been covered with a 1 µm thick layer of platinum deposited via ion beam-assisted deposition. After trenching out and polishing the cross section imaging has been performed with TDL detector (Through Lens Detector) in immersion mode with a backscattered acquisition with a voltage between 2-3 kV and a current between 0.17-0.34 nA. The milling serial sections of overall nucleus of each sample were acquired in automated mode by using the auto Slice & View software (Thermifisher) at 30 kV with a current in a range of 0.43-0.79 nA. Images were then post-processed with Fiji (ImageJ, NIH) and Imod software (open source_University of Colorado). FIB cross-sectioning was performed orthogonally to the pattern direction.

3.2.7. Chromosome Painting

Chromosome territories were labelled by fluorescence *in situ* hybridization (FISH), following protocol described by Nastali P. *et al.* [27]. Briefly, after immunostaining, cells were newly fixed with 4% paraformaldehyde for 10 minutes. Afterwards, samples were firstly incubated in 20% glycerol/PBS for 1h and then exposed to three freeze-thawing cycles in liquid nitrogen. Subsequently, cells were permeabilized in 0.07% Triton-X/PBS/0.1 M HCl for 10 min and DNA was denaturated in 50% Formamide/2xSSC (pH = 7.4) for 10 min Finally, chromosome painting probes (Metasystems, Xcyting Chromosome Paints) were added to the samples, denaturated for 3 min. at 75 °C, and hybridized for 24 h at 37 °C in hybridization chamber. Then, cells were washed for 10 min in 2xSSC and 0.1 SSC buffers. Lastly, nuclei were stained with DAPI (1:1000 solution) and the samples were mounted in Vectashield Antifade Mounting Medium (Vector Laboratories, Cat. H-1000-10)

3.2.8. Cell Live Imaging

MCA10A cell nuclei images acquisition was performed by using Single photon confocal microscopy (Leica Microsystems, Germany), implemented with an incubator at 37 °C and 5 % CO_2. A 20× objective (NA = 0.5) was used. Nuclei were stained with SiR-DNA dye (λ_{abs}=652 nm) prior to topography linear pattern inscription. Nuclei of cells on the flat surface were acquired with 633 nm laser. Then, a light-induced linear topography patterning was performed by using the same optical system, in order to preserve samples positions. Afterwards, a time-lapse acquisition was conducted every 30 min until 24 h post pattern inscription in order to monitor the nuclear deformation during time of the same cells.

3.2.9. Image Analysis

FAs, cell and nucleus morphometry measurements were performed by using Fiji. Immunofluorescence images were acquired using LSM-700 confocal microscope

(Zeiss), 63× oil objective (NA = 1.4). Cell elongation was measured by phalloidin-stained cells using the MomentMacroJ version 1.3 script (hopkinsmedicine.org/fae/mmacro.htm). More precisely, cell elongation index was defined as the ratio of the principal moments (Imax/Imin). High values of Imax/Imin identify elongated cells. Cell orientation was defined as the angle that the principal axis of inertia forms with a reference axis. The reference axis was considered as the x-axis. Nuclear and chromosome volumes were evaluated from confocal z-stack images by Imaris software, which provided a measure of 3D surface reconstruction. Also, H3K27me3 and H3K9me3 fluorescence intensity mean values were measured within the obtained volumes and represented as ratio with respect to DAPI fluorescence integrated intensity values. Distance between chromosomes and inter-distance between heterochromatin domains were measured on confocal z-stack images by using Imaris spot function, which provides a procedure to detect point-like structures. Specifically, for chromosomes, the distance was evaluated by positioning a single 1 μm diameter sphere within the 3D reconstruction of the chromosomal structure. The dimension of the sphere was chosen in order not to overcome the z-resolution of the confocal microscope. Then, the distance between the spots located within the two homologous chromosomes was calculated. For heterochromatin domains, the spheres were placed automatically by the software within images of H3K27me3/H3K9me3 stained nuclei. More precisely, they were positioned automatically by the software in regions with a local fluorescence contrast based on absolute intensity. Average distance between neighbouring spots was then calculated. Statistical significance was assessed through Kruskall-Wallis or ANOVA test (Origin).

3.2.10. Cell Proliferation Rate

Cell number counting was carried out on 10 different field of views on both flat and patterned surfaces by using single photon confocal microscopy (Leica

Microsystems, Germany), implemented with an incubator at 37 °C and 5 % CO_2. A 20× objective (NA = 0.5) was used. A time-lapse acquisition was conducted every 30 min until 48 h post pattern inscription in order to monitor the number of proliferating cells.

3.2.11. Cell Mechanical Properties

JPK NanoWizard II AFM was used to measure mechanical properties of living cells. An optical microscope was combined to the AFM to control tips and samples. Soft cantilevers (SAA-SPH-1UM, nominal spring constant 0.25 N/m) were used to investigate cell mechanical properties. The AFM was operated in force spectroscopy mode. A total of 64 force curves were measured over a cell area of 2 × 2 μm^2. Mechanical properties of cells, in terms of Young modulus values were estimated from each force curve within a force map. Evaluation of the Young modulus was performed with JPKSPM data processing software. The Hertzian model was used to calculate Young's modulus for every force curve, thus generating 64 values for each force map, following relation in eq. 1, which expressed the relation between the indentation δ and the loading force F in the case of an infinitely hard sphere of radius R (AFM tip) touching a soft planar surface

$$\text{Eq. (1)} \qquad F = \frac{4}{3}\frac{E}{1-\nu}\sqrt{r}\delta^{3/2}$$

where E is Young's modulus and ν is the Poisson ratio, assumed equal to 0.5. Results showed the average value calculated from each force curve as a representative modulus of each force measured. Statistical significance was assessed through Kruskall-Wallis or ANOVA test (Origin).

3.3. Results and Discussion

Dynamic cell stimulation by means of surface topographic cues could represent an effective strategy to precisely modulate cellular function and fate [28,29].

More precisely, linear patterning such as micro/nano ridges/grooves reliefs proved to affect cell alignment and elongation due to a process known as contact guidance that occurs at cell-material interface [30]. Also, the nature and properties of the cell-material interface such as nanoscale features could impact the intensity and the spatial distribution of cytoskeletal generated forces acting on nuclear envelope. Therefore, mechanical stresses and strains deforming nuclear shape are transmitted deep within the nuclear matter, ultimately modifying chromatin organization and gene-expression [31,32]. Thus, the precise presentation of such of topographic stimuli could represent an efficient strategy for the dynamic and controlled deformation of cell nuclei via cytoskeleton contractility and for the activation of specific genetic pathway. To this aim, in this work, the effect of azopolymer surface dynamic photo-patterning on human breast epithelial cells (MCF10A) was investigated both at cell-material interface along with inner nuclear organization levels. In details, a linear pattern was realized on the surface of pDR1m azopolymer on living cells by the Gaussian beam of a confocal microscope, as described in the previous chapter. Then, confocal microscopy along with image analysis were performed in order to fully characterize cell-material interaction processes (FAs and cytoskeleton) along with nuclear internal structure reorganization (chromosomal territories and chromatin organization). Lastly, both cell and nucleus mechanical properties after pattern inscription were assessed by means of AFM.

3.3.1. Light-Induced Topography Patterning

The surface of pDR1m thin film was *in-situ* modulated in order to control cell behaviour. More precisely, a linear pattern in the form of parallel ridges/grooves was embossed on living cells by using the Gaussian beam of a Confocal Laser Scanning Microscope (CLSM). An Argon laser was employed in order to trigger the continuous *trans-cis-trans* isomerization of disperse red 1 molecules (DR1), thus inducing a surface mass migration of azo-material according to the light

polarization. Although the maximum absorption of the pDR1m was 467 nm, a 514 nm wavelength was chosen in order not to affect cell viability, since visible light in the green/red-shifted band was known to be less harmful to cells. Confocal parameters (intensity, scan speed, format and iterations) were finely tuned in order to generate a topographic pattern in the form of sinusoidal ridges/grooves on the top of the culturing surface able to modulate cellular adhesion processes [30,33–35]. The depth and pitch of the sinusoidal linear pattern were 200 nm and 1.5 µm, respectively, with 1:1 ridge/groove ratio, as stated by SEM and AFM surface characterization (Fig.3.1)

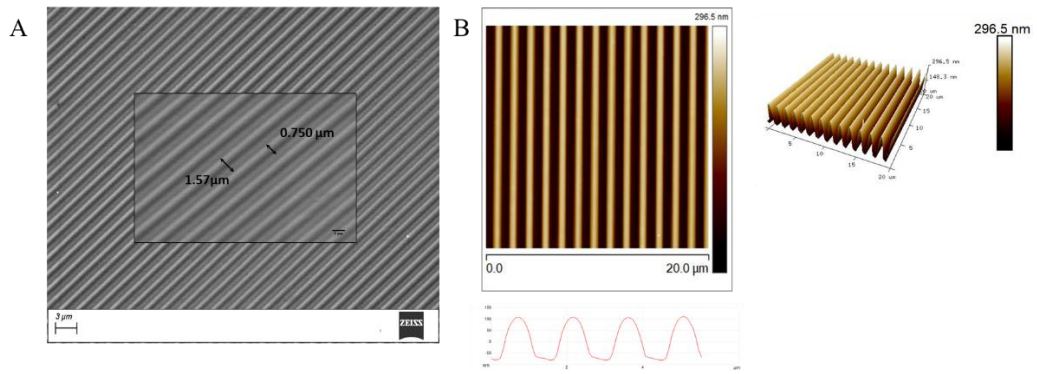

Figure 3.1. A) SEM and B) AFM bi-dimensional, cross-section and 3D images of optically linear gratings realized on pDR1m surface.

3.3.2. Cell Focal Adhesions and Cytoskeleton Organization

Cell-material interaction is a process mediated by FAs, subcellular structure acting as cell's anchoring points on the top of culturing substrate. Then, the recognition of external environmental cues is directly mediated by these subcellular structures, which re-organize themselves accordingly [36]. Thus, we firstly investigated how FAs morphology changes in response the exposure to topographical signals. More precisely, after culturing MCF10A cells for 24 h on pDR1m-fibronectin coated surfaces, we illuminated culturing surfaces in order to create sinusoidal/linear topographic pattern reliefs and FAs morphological

arrangement was evaluated by means of immunofluorescence staining of paxillin proteins both at early and late culturing time after pattern inscription. FAs resulted oriented and aligned along the pattern direction already 3 h post pattern inscription, while they showed a random orientation on flat surfaces (Fig. 3.2 A, B). Moreover, FAs formed on patterned surfaces resulted smaller in length and area if compared to those formed on flat surfaces (Fig. 3.2 D, E). We hypothesized that such phenomenon was most probably a consequence of a dynamic re-organization of the adhesion plaques after disassembly process due to pattern impression. On the other hand, FAs aspect ratio (AR) appeared bigger on the pattern, stating the ability of the linear topography to impair FAs lateral growth (Fig. 3.2 F).

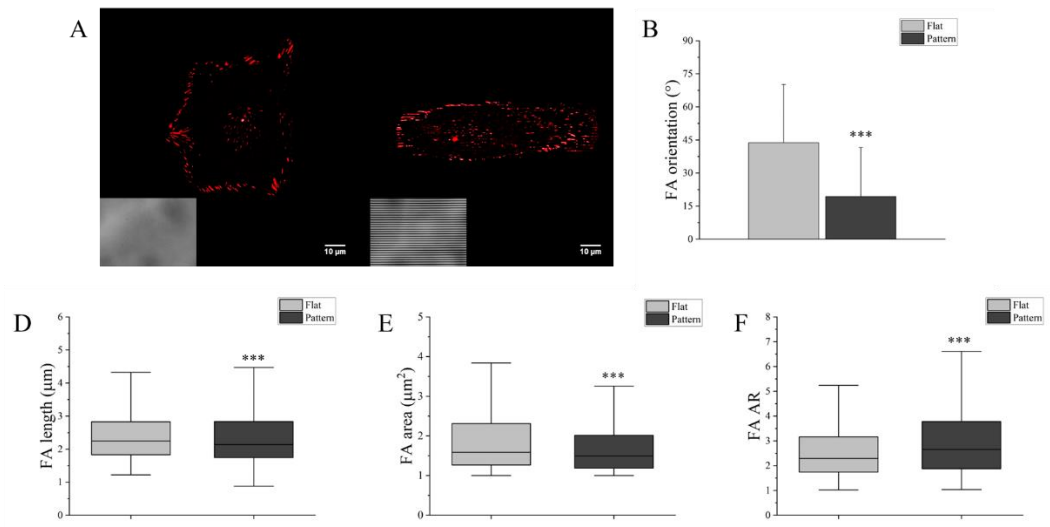

Figure 3.2. A) Confocal images of MCF10A focal adhesions (paxillin, red) on flat (left) and pattern (right) surface. The insert in the left lower corner represented images of flat and pattern surfaces in transmitted mode (the pattern was shown with horizontally oriented parallel lines). B) FAs orientation on flat and pattern surface. Angles were evaluated with respect to pattern direction and with respect to the horizontal axis for patterned and flat surfaces, respectively (~ 45° was considered as random orientation). Data are represented as mean values and standard deviations. Results of FAs C) length, D) area and F) aspect ratio (AR) on flat and pattern surfaces, represented as box plots with their median values. Analyses were performed on the same sample on patterned and flat areas, at the same culturing time and after 3h from pattern inscription.

Only mature focal adhesion (area > 1 μm²) were considered in the analyses (*** $p < 0.005$, not significant if not shown).

The biophysical signals generated by the external extracellular environments are transmitted through focal adhesions to the cell cytoskeleton. Changes in positioning and orientation of FAs can induce an extensive reorganization of actin cytoskeleton structure. Thus, confocal images of phalloidin-stained MCF10A cells were acquired at different time points and cellular response to linear pattern inscription was investigated at cell-scale levels in terms of cell orientation, elongation and spreading area. After 3 h post pattern inscription cells resulted oriented along the pattern direction, while cells on the flat surface appeared randomly oriented (Fig. 3.3 A, B). Also, actin fibres analyses on angle distribution stated that they were oriented and aligned along the pattern, while they showed a flatter distribution on the planar surface (Fig. 3.3 C, D). In addition, cells resulted more elongated with a larger spreading area on the pattern compared to flat surfaces (Fig. 3.3 E, F). These results demonstrated that linear light-induced pattern was able induce cytoskeleton actin fibres alignment along a preferential direction dictated by the underlying pattern affecting cell morphology.

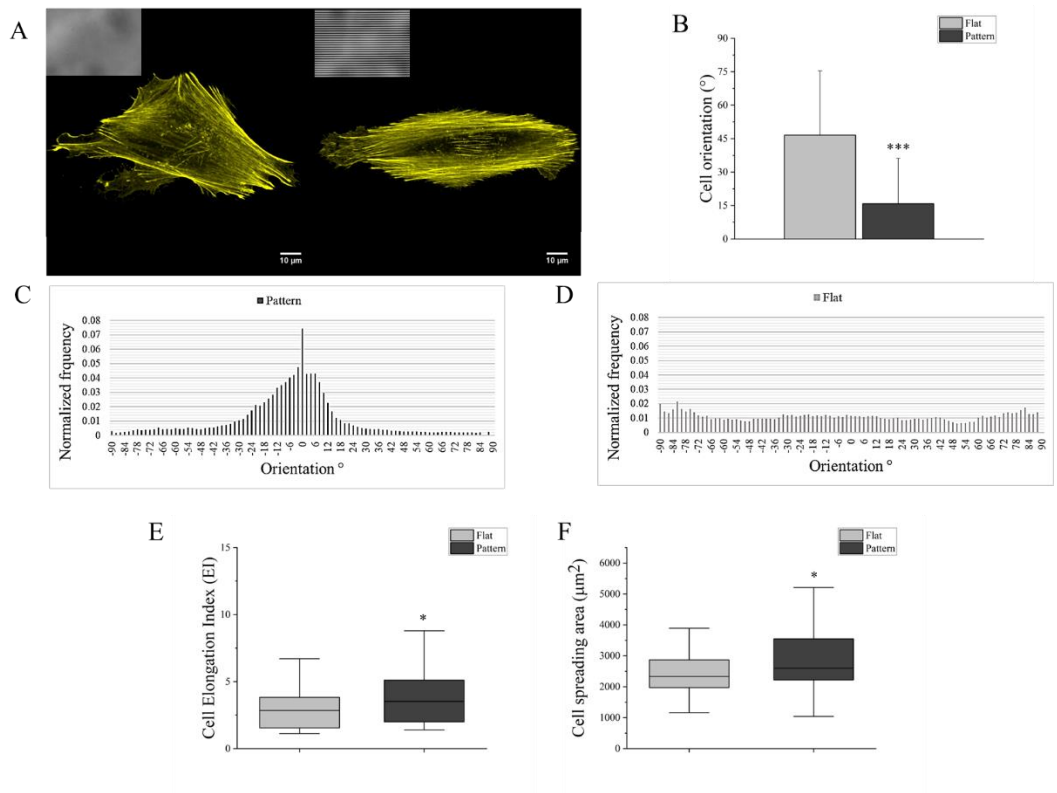

Figure 3.3. A) Confocal images of MCF10A cells labelled with phalloidin (yellow, cytoskeleton) on flat (left) and pattern (right) surface. The insert in the left upper corner represented images of flat and pattern surfaces in transmitted mode (the pattern was shown with horizontally oriented parallel lines). B) Cell orientation on flat and pattern surface. Angles were evaluated with respect to pattern direction and with respect to the horizontal axis for patterned and flat surfaces, respectively (~ 45° was considered as random orientation). Data are represented as mean values and standard deviations. Actin fibres orientation distribution on C) pattern and D) flat surfaces (Fibres were normalized with respect to the total number). Results of cell C) elongation index (EI) D) area and F) aspect ratio (AR) on flat and pattern surfaces, represented as box plots with their median values Analyses were performed on the same sample on patterned and flat areas, at the same culturing time and after 3h from pattern inscription (*** $p < 0.005$, * $p < 0.05$, not significant if not shown).

These results showed that cells react to the emerging topography already few hours after stimuli transmission. The re-organization of cell structure mediated by the actin cytoskeleton alignment, is likely controlled by a coordinated process of disassembly and new formation of adhesions along the pattern direction, which occurs in a relatively fast manner (3 h post pattern inscription). However, the

complete maturation of these cellular substructures resulted to be not finalized in the same time frame, manifesting the need of a longer time to stably adapt to the new environmental conditions. For this reason, the same analyses were also performed at longer time following the pattern inscription. Our results showed an increase of the percentage of FAs aligned along the pattern directions after 24 h from the surface topography variation (Fig. 3.4 A). Conversely, FAs area did not showed any substantial changes 24 h after pattern inscription (Fig. 3.4 B), while aspect ratio and length resulted to attain higher values at longer time (Fig. 3.4 C, D). These data confirmed the hypothesis that an initial re-arrangement of the adhesion plaques during the first hours of the signal presentation occurred and this signal triggers events leading to the elongation of FAs plaques along the top of pattern ridges (Fig. 3.4 E).

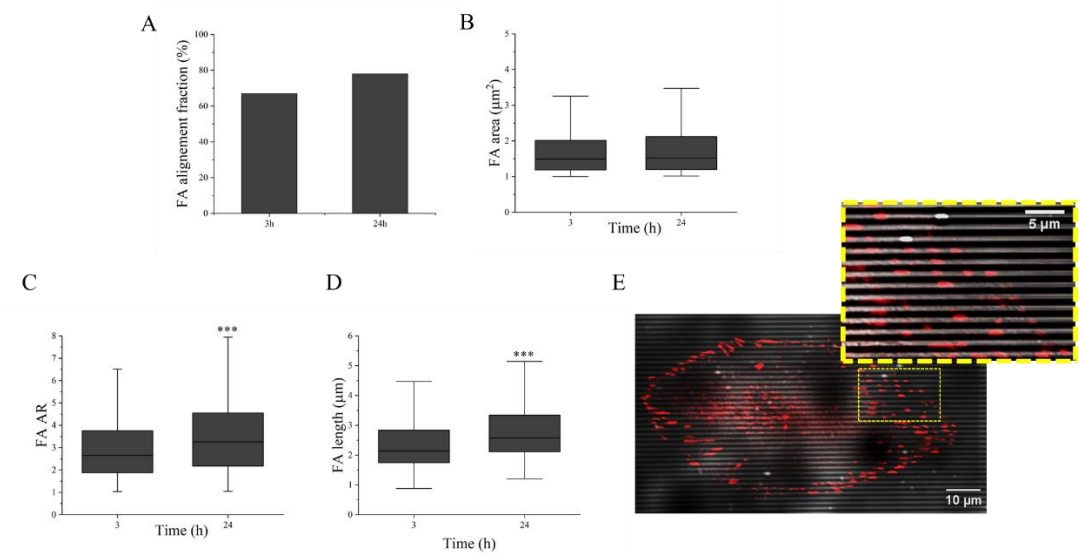

Figure 3.4. Analyses of MCF10A focal adhesions after 3 h and 24 h from pattern inscription. A) Percentage of focal adhesions (FAs) aligned along pattern direction ($0° < \theta < 20°$). Results of FAs C) length, D) area and F) aspect ratio (AR), represented as box plots with their median values. E) Representative confocal images of focal adhesions (paxillin, red) grown on top of pattern ridges after 24 h from pattern realization. The insert showed a zoom of the yellow dot-dashed delimited area on the image. Only mature focal adhesion (area > 1 μm²) were considered in the analyses (*** $p < 0.005$, not significant if not shown).

Moreover, cell cytoskeleton also showed a dynamic evolution on the linear light-induced pattern. Indeed, after 24 h post pattern inscription, the percentage of oriented cells increased (Fig. 3.4 A), appearing more elongated, compared to early time (Fig. 3.4 B). However, cells spreading area resulted not dependent on manifestation of the signal for longer time (Fig. 3.4 C). These results, along with focal adhesions assessment, stated that cells need time to adapt their subcellular structures to the new environmental conditions.

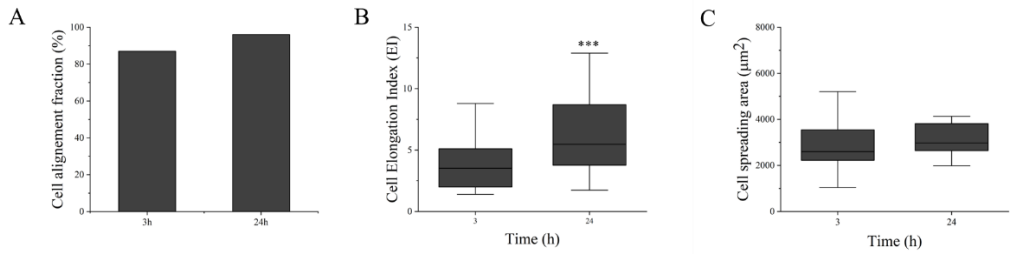

Figure 3.4. Analyses of MCF10A cell morphology after 3 h and 24 h from pattern inscription. A) Percentage of cells oriented along the pattern direction. Results of cell B) elongation index (EI) and C) spreading area represented as box plots with their median values (*** $p < 0.005$, not significant if not shown).

3.3.3. The Impact of Light-induced Topographic Pattern on Nucleus Morphology

Nucleus is the largest and stiffest organelle in eukaryotic cells [37] and it is known that changes in actin cytoskeleton network alter the forces acting on the nuclear envelope, ultimately affecting its morphology, state and mechanics [10,11]. Indeed, external physical signals, such as topographical cues, can be transmitted to the nucleus through cytoskeleton-nucleus linking complexes, deforming its shape and influencing gene-expression [31,38,39]. To this aim, nucleus morphology upon linear pattern inscription on pDR1m-fibronectin coated surfaces was evaluated and compared to flat control at both early and long culturing time points. More precisely, nuclear orientation, area, aspect ratio (AR), volume and height were measured after 3, 24 and 48 h from pattern impression in

order to completely characterize the time-evolving nuclear deformation induced by the nano-topographical signal inscription. Our analyses showed that nuclei oriented along pattern direction after 3 h from pattern formation (Fig. 3.5 A). Instead, nuclear projected area was measured from slices projection of z-stack confocal images, resulting not affected by the inscription of the topographical signal at early time. However, after 24 h of culturing, the area of nuclei of MCF10A cells cultured on the light-induced patterned regions were larger than those grown on flat regions. In addition, investigating the variation induced by the nano-topography during time, nucleus area appeared to significantly increase after 24 h with respect to early time. After 48 h from pattern inscription, nuclear area was shown to be smaller compared to flat control, although bigger than nuclei after 24 h (Fig. 3.5 B). Moreover, nuclear aspect ratio, which provided a measure of nuclear elongation, was shown larger than flat control only after 24 h from pattern inscription and even if progressively increased until 48 h on pattern surfaces, it resulted not different to the nuclei of MCF10A cells cultured on flat surfaces (Fig. 3.5 C).

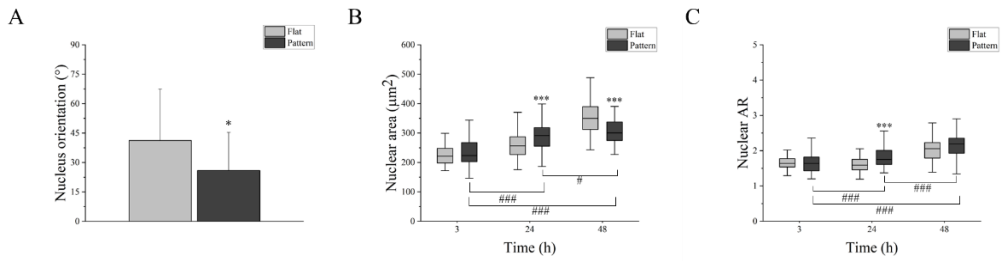

Figure 3.5. A) MCF10A nucleus orientation on pattern and flat surface after 3 h from pattern realization. Results of nuclear B) area and C) AR represented as box plots with their median values. Upper asterisks represented significant differences with respect to flat condition, while lower hashes represented significant differences induced by nano-topography during time progression (***, ### $p < 0.005$, *, # $p < 0.05$, not significant if not shown).

In addition, nuclear volume, calculated from 3D reconstruction of z-stack confocal images, also showed a temporal evolution similar to nuclear projected

area. However, a significant increase of nuclear volume was already appreciable after 3 h post topographic pattern inscription. Additionally, nuclear volume of MCF10A cells cultured for 48 h post pattern inscription resulted smaller if compared to those cultured on flat surfaces. Nevertheless, both experimental groups attained higher values with respect to early culturing times (Fig. 3.6 A). These results stated a different impact of the topographical signal on the nuclear volume at early and long culturing time. Indeed, at 3 h post pattern inscription, nuclear volume increase is due to nuclear height growth, as shown by nuclear thickness measurements. Basically, nuclear height resulted to increase with respect to flat control at 3 h post pattern inscription, probably as a consequence of cell re-organization on the surface modulations. However, at 24 h post pattern inscription, nuclear height flattened to values comparable with those of cell nuclei cultured on flat control surfaces. Finally, at 48 h post pattern inscription, nuclear height reached a stationary value if compared to values attained at 24 h, while it resulted smaller if compared with nuclei of cell cultured than control surfaces (Fig. 3.6 B, C). This could be probably due to the presence of stiffer actin fibres which organize upon the nucleus in response to the nano-topography inscription and impair nuclear growth along the z direction.

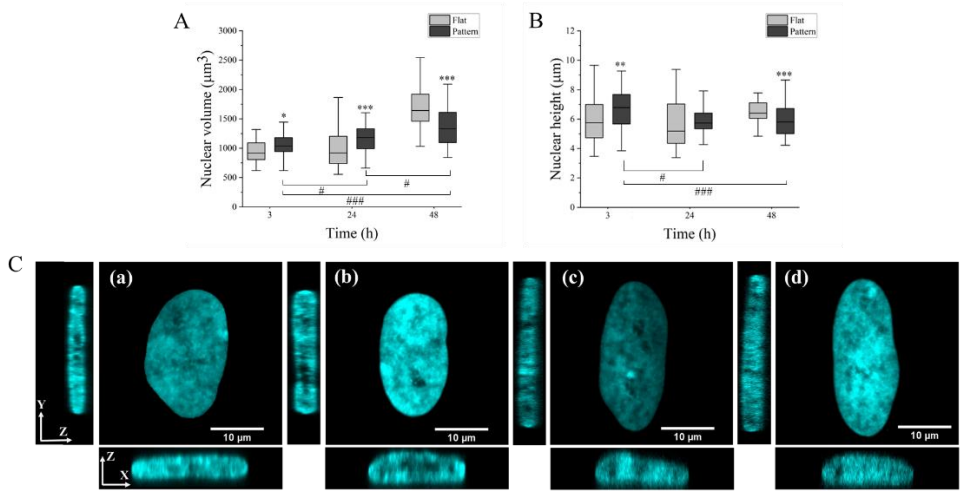

Figure 3.6. Results of MCF10A nuclear A) volume and B) height represented as box plots with their median values. Upper asterisks represented significant differences with respect to flat condition, while lower hashes represented significant differences induced by nano-topography during time progression (***, ### $p < 0.005$, ** $p < 0.01$, *,# $p < 0.05$, not significant if not shown). C) Confocal images and orthogonal view of DAPI stained nuclei (cyan) on (a) flat surface and linear pattern after (b) 3 h, (c) 24 h and (d) 48 h.

Additionally, in order to verify the nuclear morphology variation upon linear light-induced topography patterning on pDR1m surface, evaluation of nuclear volume was performed by analysing confocal z-stack images of live nuclei. Specifically, MCF10A cell nuclei were live stained with SiR-DNA dye in order to monitor the evolution of the same cell nuclei before and after the pattern inscription until 24 h from pattern inscription. Our results confirmed the trends observed for distinct populations of cells (Fig. 3.7 A).

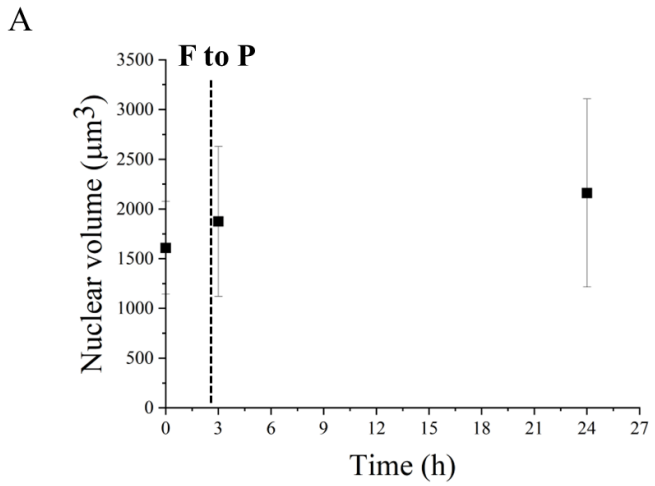

Figure 3.7. A) Nuclear volume time evolution of the same SiR-DNA live stained nuclei from initial flat condition to 24 h post light-induced topography patterning. Results were showed with median values and standard deviation.

Then, FIBSEM cross-section imaging was carried out in order to further qualitatively validate fluorescence confocal image analyses of nuclei morphology. Indeed, orthogonal view of nuclei on flat and pattern surfaces confirmed the z-variation of the nuclear thickness upon pattern impression observed from confocal images analyses, with cell nuclei at 3 h post pattern inscription appearing bigger than nuclei on both flat control and nuclei exposed to light-induced patterning after 24 h (Fig. 3.8 A). Thus, at longer times the growth of nuclear volume following the pattern formation was rather caused by an increment of nuclear area, as reported in Fig. 3.5 B, as a consequence of the stretching force generated by cell cytoskeleton actin fibres aligned parallel to the pattern direction.

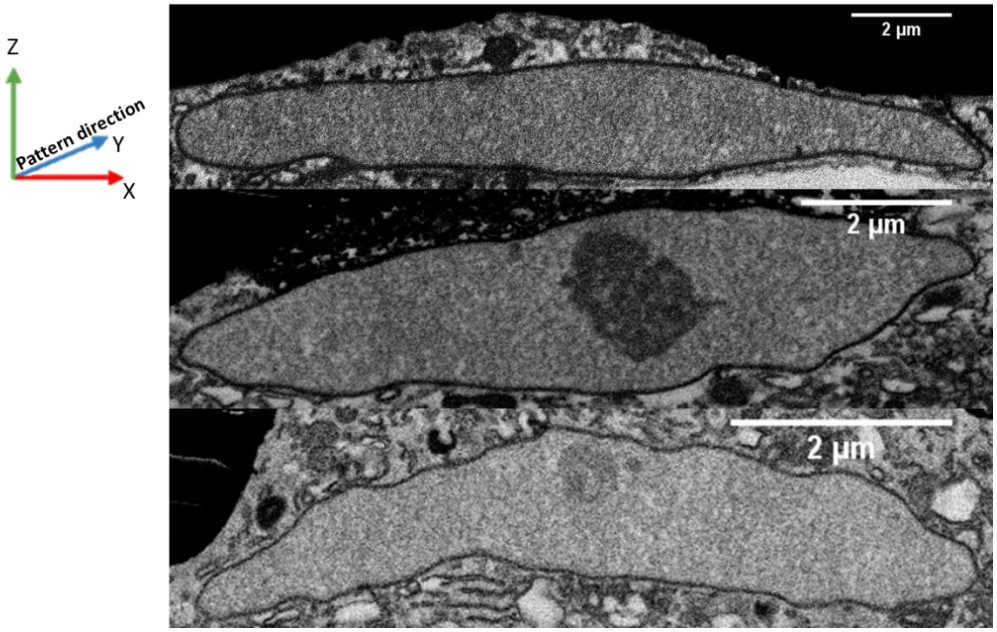

Figure 3.8. A) FIB cross-sectional images of MCF10A cells nuclei cultured on (a) flat, (b) 3 h and (c) 24 h post pattern inscription surfaces. Images were acquired orthogonally to the linear pattern direction, showing nuclear lowest dimension along x-axis in the x-y plane.

Additionally, the results on analyses on cell and nuclear morphology pointed out a correlation between cell spreading area and nuclear volume growth during time (Fig 3.9 A).

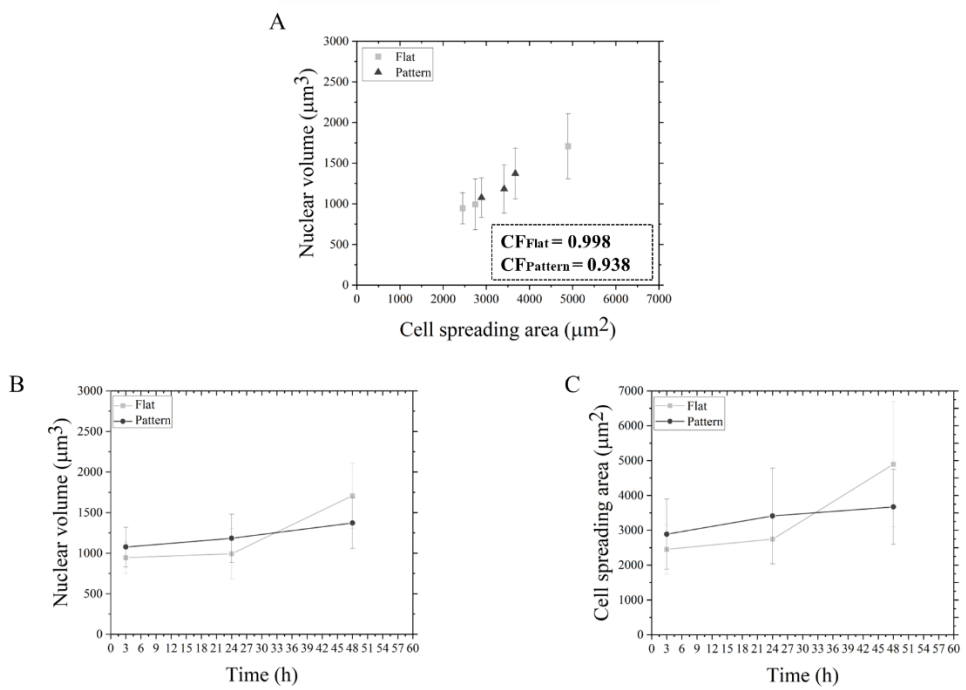

Figure 3.9. A) Graphical representation of MCF10A nuclear volume evolution along with cell spreading area for both flat and pattern surfaces. The graph showed the Pearson Correlation Factor (CF) values between the two morphological parameters. B) Nuclear volume and C) Cell spreading area temporal evolution on flat and pattern surfaces. Results were represented with median values and SD.

Therefore, these results indicated that cell and nuclear growth exhibited a similar temporal evolution on flat and pattern surfaces, though showing a different rate not only along the cell time culture course but also in the presence of nano-topography (Fig. 3.9 B, C). Thus, since Cadart C. *et al*. demonstrated that cell volume-specific growth rate depends also on cell cycle phase [40], the linear pattern impressed on azopolymer surface could have an implication also on cell cycle duration and proliferation rate.

3.3.4. Nano-Topography Effect on Cell Proliferation

Several studies reported the effect of topography on cellular proliferation rate [41–45]. Chaudhuri. P *et al.*, demonstrated that anisotropic micro-gratings could reduce proliferation of MCF-10A cells through the activation of Rho-ROCK-

Myosin signalling which induce a Mechanically-Induced Dormancy (MID) effect on the cells [46]. Also, Wu. C *et al.* reported that C2C12 myoblasts cells grown on polymer based substrates with nanogrooves exhibited a lowered proliferation rate as much as ~29% [47]. Thus, we examined the impact of azopolymer linear pattern inscription on the cell growth and proliferation. In details, a time lapse confocal acquisition of 10 selected fields of view in transmitted mode was performed after 3, 24 and 48 h from the presentation of the topographical signal. Results revealed that cells proliferated faster on the flat surface, whereas all the cells exposed to the nano-topography surface variation grew slowly (Fig. 3.10 A). Specifically, cell growth rate (gr) was calculated by using the following exponential equation

$$N_t = N_0 \cdot e^{(gr \cdot t)} \quad [68]$$

where N_t is the cell number at time t, N_0 is the initial number of cells and t is the observation time from culture. Then, growth rates values were evaluated from the exponential fitting-curves, resulting equal to 0.0165 and 0.0141 h^{-1} for flat and pattern surfaces, respectively. Furthermore, cell growth rates appeared to increase between 24 h and 48 h from culture time on both flat and pattern surfaces, although with lower values on the patterned ones (Fig. 3.10 B).

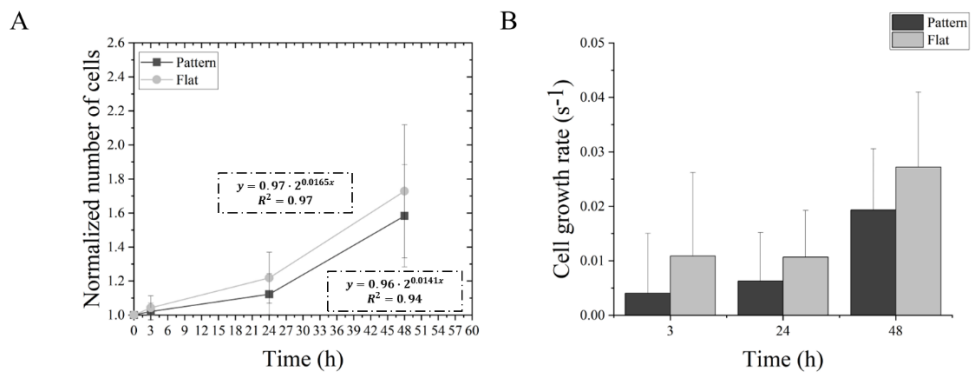

Figure 3.10. Graphs of cell proliferation rate. B) Normalized total number of cells counted on flat and pattern surfaces during time culture progression. The graphs showed the curve fitting equations and R^2 values. B)

Growth rates values after 3 h, 24 h and 48 h from pattern impression on flat and patterned regions. Results were showed with their mean values and standard deviation.

These results suggested an impact of the nano-topography on the cell cycle progression, which in turn resulted in a difference of cell growth and proliferation rate between the two conditions. Indeed, other studies demonstrated that cell adhesion signalling is able to feed into cell-cycle checkpoints and in case of abnormal adhesion signalling, cells can alter cell-cycle dynamics [43].

3.3.5. Alterations of Chromosome Territories Architecture in Response to Topography Variation

Genomes are organized into discrete chromosome territories (CT) inside the interphase nucleus of eukaryotic cells [48]. Variations of chromosome positions can affect their accessibility to transcription factors thus altering gene expression [49]. Indeed, Penelope M. *et al.* demonstrated that nano-topography can trigger changes in nuclear organisation associated with deregulated gene expression and a concomitant positioning modification inside the nucleus of hMSC cells [50]. Further, Wang. Y *et al.* showed that cell geometry can modulate 3D chromosome arrangement, modifying their positioning and orientation within the nucleus [16]. Therefore, in this work chromosome territories (CTs) organization changes in response to light-induced linear pattern on azopolymer surface were evaluated. More specifically, CT 12 volume and relative inter-distances between the two homologous chromosomes were measured by using fluorescence *in situ* hybridization (FISH). CTs 12 volume was calculated from 3D surface reconstruction of z-stack confocal images. Out results showed that CTs 12 volumes increased at 3 h post pattern inscription compared to flat control and they resulted even bigger at 24 h post pattern inscription (Fig. 3.11 A, B). Additionally, inter-distances between the two homologous chromosomes also appeared higher at both 3 h and 24 h post pattern inscription compared to those on flat surfaces (Fig. 3.11 C, D).

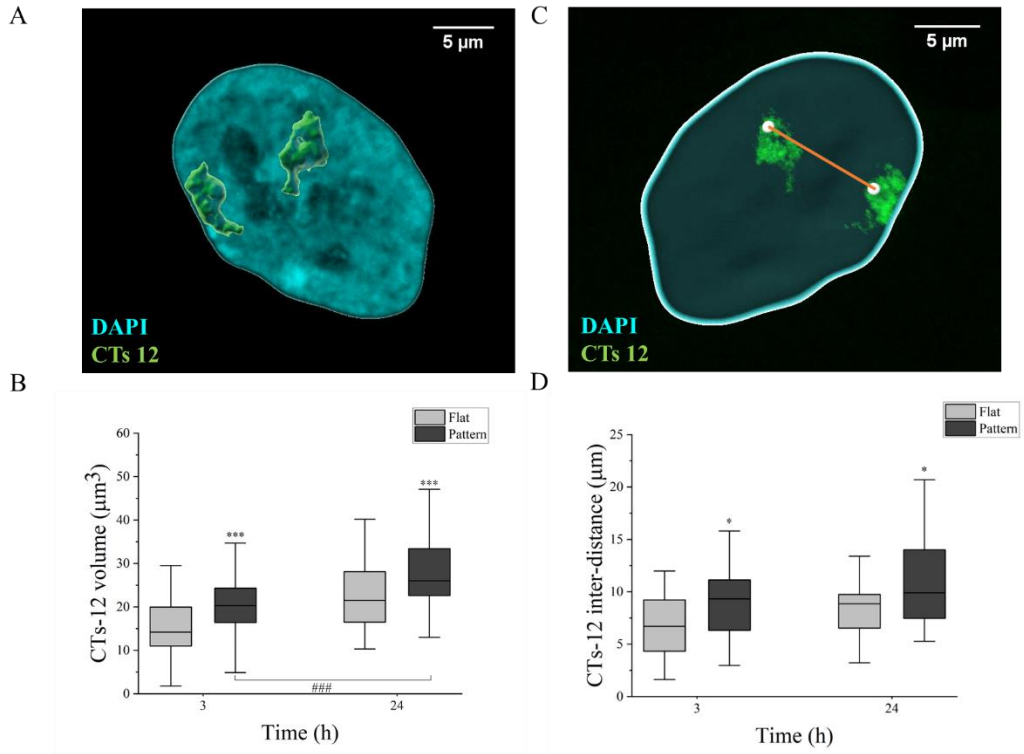

Figure 3.11. A) Representative 3D volume reconstruction of CTs 12 from z-stack confocal images of FISH and DAPI (cyan) stained MCF10A cells nuclei. B) Results of CTs 12 volume variation at 3 h and 24 h post pattern inscription, compared to flat control. C) Inter-distance calculation between the two homologous CTs 12 represented as spots and D) the valuated inter-distances variation at 3 h and 24 h post pattern inscription, compared to flat control. Results were showed as box plots with their median value (***, ### $p < 0.005$, * $p < 0.05$, not significant if not shown).

These results were in accordance with the nucleus volume growth, meaning that both chromosomes volumes and inter-distances increased as a consequence of nuclear expansion.

3.3.6. Chromatin Organization and Condensation

In eukaryotic cells, the genetic material is arranged into a protein complex called chromatin, where DNA are wrapped around two copies of histone proteins [51], forming the nucleosome structure. This basic unit can incur into several variations including DNA methylation and histone post-translational modifications [52],

which in turn can impact the chromatin condensation state and DNA processes including replication, transcription, and repair [53,54]. It is well known that the transmission of physical cues from cell-material interaction can regulate nucleus organization and chromatin condensation [55,56]. Here, the effect of nano-topography on heterochromatin state and arrangement within the nucleus of MCF10A cells was investigated. More precisely, fluorescence intensity of H3K9me3 and H3K27me3 markers was evaluated in response to linear pattern inscription to examine the condensation levels of both constitutive and facultative heterochromatin, respectively. In addition, analyses of the average inter-distance between heterochromatin domains (HCDs) were carried out in order to explore the possibility of macroscopic nuclear deformation to propagate into its inner structure up to chromatin level. From the analyses of H3K27me3 intensity it was showed that its levels within nuclei of cells exposed to the pattern inscription remained equal to those within nuclei of cells on flat controls at early time post pattern inscription, whereas they decreased in nuclei of cells after 24 h from pattern inscription, indicating a reduction of chromatin condensation, which state the ability of the topographical signal to induce an opening of the chromatin structure (Fig. 3.12 A, B). However, H3K27me3 domains inter-distances exhibited a variation between cells on flat and patterned surfaces already 3 h post pattern inscription. Indeed, after 3 h and 24 h post pattern inscription, chromatin domains distances resulted to be higher with respect to those calculated for flat control (Fig 3.12 C). These results were in accordance with the analyses on nuclear volume. Indeed, comparing flat and patterned surfaces, HCDs inter-distances increased in correspondence of a volumetric growth, stating that as the nucleus increases in response to the linear pattern formation, also HCDs moved away from each other. In order to exclude a measurement bias on the distances analyses, due to reduced fluorescence intensity values, which could have affected the identification of fluorescent domains, the number of spots for each nucleus was calculated at both early and long culturing time. Likely, the number of spots

between flat and patterned surfaces were not different, stating that HCDs distancing was effectively due to a volume expansion (Fig 3.12 D).

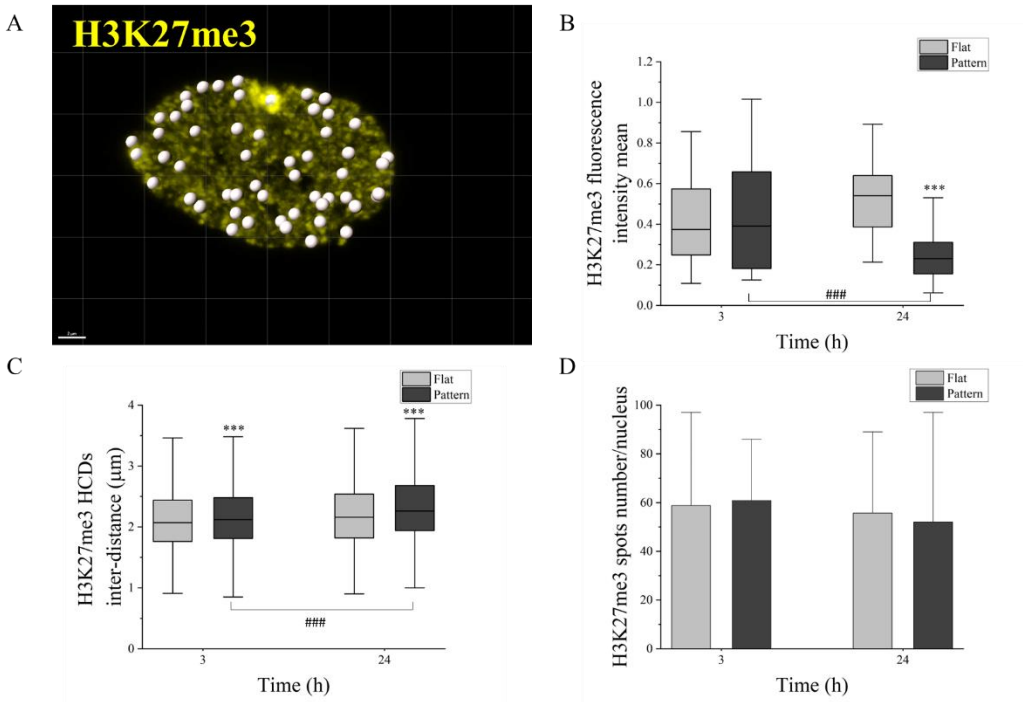

Figure 3.12. A) Representative image of 3D spots reconstruction (1 µm diameter spheres) on confocal image of MCF10A nuclei stained for H3K27me3 (yellow). Spots were placed automatically by the software on regions with varying fluorescence intensity grades. Box plots showing mean value of H3K27me3 B) intensity fluorescence mean measured within nuclear volume, C) HCDs inter-distance and D) normalized spots number calculated for each nucleus, for both flat and patterned surfaces during culturing time (*** $p < 0.005$, not significant if not shown). Scale bar is 2 µm.

In addition, similar results were obtained for H3K9me3 analyses of fluorescence intensity and HCDs inter-distances. Indeed, fluorescence intensity mean values resulted equal to flat control 3 h post pattern inscription, while they appeared lower than flat controls 24 h post pattern inscription (Fig. 3.13 A, B). However, H3K9me3 HCDs inter-distances showed the same time-evolution obtained from H3K27me3 HCDs inter-distances evaluation, with HCDs distances that resulted

to increase at both 3 h and 24 h following pattern inscription compared to flat control, (Fig. 3.13 A, C), as for H3K27me3 HCDs.

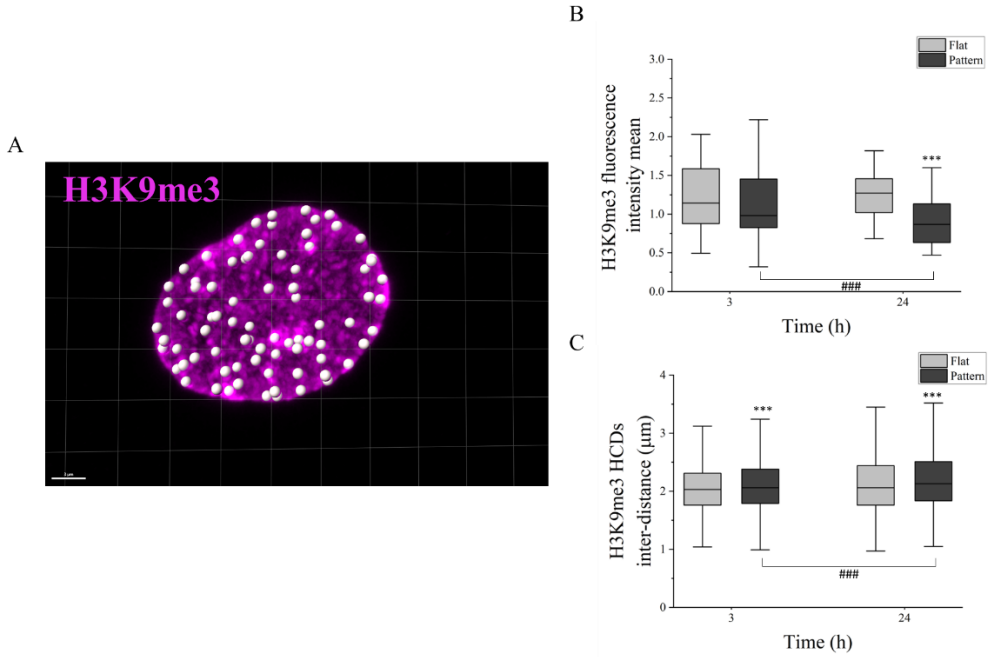

Figure 3.13. A)) Representative image of 3D spots reconstruction (1 µm diameter spheres) on confocal image of MCF10A nuclei stained for H3K9me3 (magenta). Spots were placed automatically by the software on regions with varying fluorescence intensity grades. Box plots showing mean value of H3K9me3 B) intensity fluorescence mean measured within nuclear volume, C) HCDs inter-distance on flat and patterned surfaces during culturing time (***, ### $p < 0.005$, not significant if not shown). Scale bar is 3 µm.

3.3.7. Cell and Nuclear Mechanics

Cell interactions with the external environment can influence cell adhesion and cytoskeleton organization, thus also affecting cell mechanics. Indeed, cytoskeletal filaments both produce and resist mechanical loads, allowing cells to resist shape deformation [60]. In addition, the force generated at cell-material interface are sensed by FAs and transmitted by the cytoskeleton to the nucleus [37,61–63], altering also its mechanical properties [64,65]. In this work, cell tensional state was evaluated by AFM, which is a widely employed powerful technique used to characterize an extensive range of biological and synthetic interfaces [66]. In

details, since cytoskeletal and nuclear mechanics are the principal contributors to overall cell mechanics [67], both cell and nucleus Young's Modulus were measured on living cells in order to examine the effect of topography variation upon the surface of pDR1m on their mechanical properties. A force mapping with 64 curves over an area of 2 × 2 μm^2 was performed on each cell, on two different regions, covering cell body (Fig. 3.14 A , region A) and cell perinuclear area (Fig. 3.14 A, region B), which were supposed to provide elasticity of cell cytoplasm and nucleus, respectively. Results showed that after 3h from linear pattern impression, Young's modulus of both oriented cells and nuclei was higher than cell grown on flat surfaces, with nuclei exhibiting lower values (Fig. 3.14 B, C). As expected, tensional state of cells increased in response to the force generated by the linear nano-topography to orient and align them along the pattern direction. In addition, mechanical properties were also evaluated at longer time after pattern realization. Precisely, after 24h both Young's moduli appeared to increase compared to early time (Fig. 3.14 D, E), stating the time-varying cell mechanics response to the topographical signal.

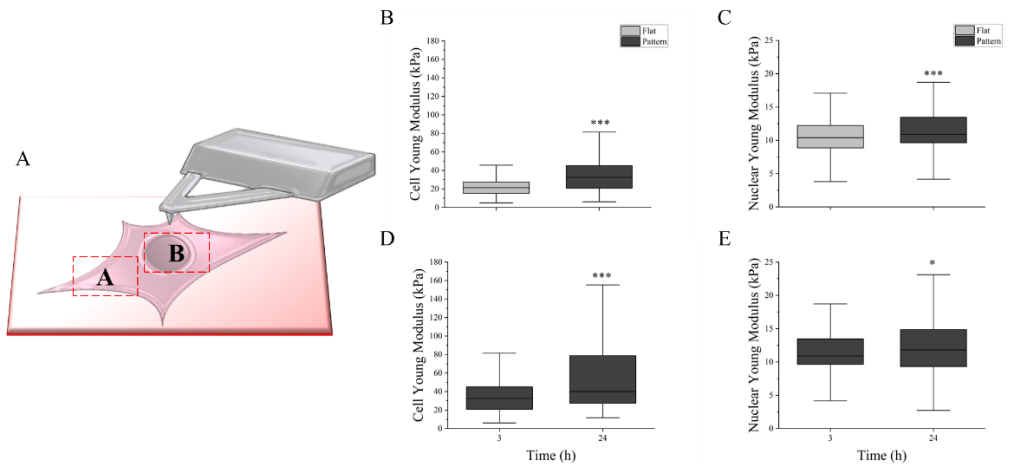

Figure 3.14. A) Graphical representation of AFM measurement on cell body (A) and nuclear region (B). Young modulus of B) cell cytoplasm and C) nucleus after 3h from pattern inscription compared to flat surface. Comparison of elastic moduli of D) cell cytoplasm and nucleus D) at early and long time after pattern

realization. Results were showed as box plots with their median values. (*** P < 0.005, * p <0.05, not significant if not shown).

3.4. Conclusion

Azopolymer substrates were used in order to realize photo-responsive platforms for cell behaviour investigation. Linear pattern were embossed *in-situ* on the surface of the azo material in presence of MCF10A cells by means of a confocal laser microscopy set-up. Then, cell response to the underneath topography variation was evaluated in terms of FAs assembly, cytoskeleton orientation and alignment, nucleus morphology and chromatin organization. Results reported that cell subcellular structures were able to sense the topographical signal already after 3 h from the transmission of the stimulus. Nevertheless, analyses at longer time stated that cells showed a dynamic adaptation behaviour, with increasing spreading area and elongation, meaning that they required time to accommodate the new external environment. Additionally, measures on nuclear volume revealed that the optical impressed linear pattern induced a volumetric growth which exhibited a time evolution different from cells grown on planar surfaces. This result suggested an impact of nano-topography on cell cycle, resulting in a reduced proliferation rate of cells. Moreover, the morphology variation of nucleus caused by the topographical cues was reflected also within its internal structure, stating that macroscopic deformation generated from the force applied by the cell cytoskeleton, could be transmitted to its inside up to chromatin level. Indeed, the nuclear expansion dictated by the linear pattern was followed by homologous chromosomes volume and distance increase. Furthermore, analyses on chromatin scale revealed that levels of both facultative, expressed by H3K27me3 marker, and constitutive, expressed by H3K9me3 marker, chromatin reduced 24 h post pattern inscription, stating the efficacy of the topographical signal to induce a reduction of the chromatin condensation state, thus rendering the genetic material more accessible to transcription factors. Additionally, also heterochromatin

domains inter-distances increased in response to pattern formation. Lastly, Atomic Force Microscopy measurements of cell mechanics showed that the alignment of cytoskeleton actin fibres along the pattern direction produced a cell stiffening resulting in higher cells and nuclei Young modulus values.

3.5. References

1. Doyle AD, Nazari SS, Yamada KM. Cell-extracellular matrix dynamics. Phys Biol. 2022;19: 021002.
2. Eyckmans J, Boudou T, Yu X, Chen CS. A hitchhiker's guide to mechanobiology. Dev Cell. 2011;21: 35–47.
3. DuFort CC, Paszek MJ, Weaver VM. Balancing forces: architectural control of mechanotransduction. Nat Rev Mol Cell Biol. 2011;12: 308–319.
4. Wade RJ, Burdick JA. Engineering ECM signals into biomaterials. Mater Today (Kidlington). 2012;15: 454–459.
5. Custódio CA, Reis RL, Mano JF. Engineering biomolecular microenvironments for cell instructive biomaterials. Adv Healthc Mater. 2014;3: 797–810.
6. Guimarães CF, Marques AP, Reis RL. Pushing the natural frontier: Progress on the integration of biomaterial cues toward combinatorial biofabrication and tissue engineering. Adv Mater. 2022;34: e2105645.
7. Nikkhah M, Edalat F, Manoucheri S, Khademhosseini A. Engineering microscale topographies to control the cell-substrate interface. Biomaterials. 2012;33: 5230–5246.
8. Seonwoo H, Bae W-G, Park S, Kim H-N, Choi KS, Lim KT, et al. Hierarchically micro- and nanopatterned topographical cues for modulation of cellular structure and function. IEEE Trans Nanobioscience. 2016;15: 835–842.
9. Charest JL, García AJ, King WP. Myoblast alignment and differentiation on cell culture substrates with microscale topography and model chemistries. Biomaterials. 2007;28: 2202–2210.
10. Jean RP, Gray DS, Spector AA, Chen CS. Characterization of the nuclear deformation caused by changes in endothelial cell shape. J Biomech Eng. 2004;126: 552–558.
11. Khatau SB, Hale CM, Stewart-Hutchinson PJ, Patel MS, Stewart CL, Searson PC, et al. A perinuclear actin cap regulates nuclear shape. Proc Natl Acad Sci U S A. 2009;106: 19017–19022.
12. Jain N, Iyer KV, Kumar A, Shivashankar GV. Cell geometric constraints induce modular gene-expression patterns via redistribution of HDAC3 regulated by actomyosin contractility. Proc Natl Acad Sci U S A. 2013;110: 11349–11354.

13. Vishavkarma R, Raghavan S, Kuyyamudi C, Majumder A, Dhawan J, Pullarkat PA. Role of actin filaments in correlating nuclear shape and cell spreading. PLoS One. 2014;9: e107895.
14. Bhattacharjee P, Cavanagh BL, Ahearne M. Effect of substrate topography on the regulation of human corneal stromal cells. Colloids Surf B Biointerfaces. 2020;190: 110971.
15. Song Y, Soto J, Chen B, Hoffman T, Zhao W, Zhu N, et al. Transient nuclear deformation primes epigenetic state and promotes cell reprogramming. Nat Mater. 2022;21: 1191–1199.
16. Wang Y, Nagarajan M, Uhler C, Shivashankar GV. Orientation and repositioning of chromosomes correlate with cell geometry-dependent gene expression. Mol Biol Cell. 2017;28: 1997–2009.
17. Kirschner CM, Anseth KS. In situ control of cell substrate microtopographies using photolabile hydrogels. Small. 2013;9: 578–584.
18. Uto K, Tsui JH, DeForest CA, Kim D-H. Dynamically tunable cell culture platforms for tissue engineering and mechanobiology. Prog Polym Sci. 2017;65: 53–82.
19. Lee HP, Gaharwar AK. Light-responsive inorganic biomaterials for biomedical applications. Adv Sci (Weinh). 2020;7: 2000863.
20. De Martino S, Netti PA. Dynamic azopolymeric interfaces for photoactive cell instruction. Biophys Rev (Melville). 2020;1: 011302.
21. Rianna C, Rossano L, Kollarigowda RH, Formiggini F, Cavalli S, Ventre M, et al. Spatio-temporal control of dynamic topographic patterns on azopolymers for cell culture applications. Adv Funct Mater. 2016;26: 7572–7580.
22. Rossano L, Cimmino C, Cavalli S, Ventre M, Netti PA. Regulating fibroblast shape and mechanics through photoresponsive surfaces with concentric circular topographic patterns. Adv Mater Interfaces. 2018;5: 1800890.
23. Cimmino C, Netti PA, Ventre M. A switchable light-responsive azopolymer conjugating protein micropatterns with topography for mechanobiological studies. Front Bioeng Biotechnol. 2022;10: 933410.
24. Fedele C, De Gregorio M, Netti PA, Cavalli S, Attanasio C. Azopolymer photopatterning for directional control of angiogenesis. Acta Biomater. 2017;63: 317–325.
25. Yim EKF, Darling EM, Kulangara K, Guilak F, Leong KW. Nanotopography-induced changes in focal adhesions, cytoskeletal organization, and mechanical properties of human mesenchymal stem cells. Biomaterials. 2010;31: 1299–1306.
26. Rianna C, Ventre M, Cavalli S, Radmacher M, Netti PA. Micropatterned azopolymer surfaces modulate cell mechanics and cytoskeleton structure. ACS Appl Mater Interfaces. 2015;7: 21503–21510.
27. Nastały P, Maiuri P. Preparing map of chromosome territory distribution frequency. Methods Mol Biol. 2021;2157: 213–219.

28. Cimmino C, Rossano L, Netti PA, Ventre M. Spatio-temporal control of cell adhesion: Toward programmable platforms to manipulate cell functions and fate. Front Bioeng Biotechnol. 2018;6: 190.
29. Ventre M, Netti PA. Engineering cell instructive materials to control cell fate and functions through material cues and surface patterning. ACS Appl Mater Interfaces. 2016;8: 14896–14908.
30. Leclech C, Villard C. Cellular and subcellular contact guidance on microfabricated substrates. Front Bioeng Biotechnol. 2020;8: 551505.
31. Teo BKK, Ankam S, Chan LY, Yim EKF. Nanotopography/mechanical induction of stem-cell differentiation. Methods Cell Biol. 2010;98: 241–294.
32. Newman P, Galenano-Niño JL, Graney P, Razal JM, Minett AI, Ribas J, et al. Relationship between nanotopographical alignment and stem cell fate with live imaging and shape analysis. Sci Rep. 2016;6. doi:10.1038/srep37909
33. Crouch AS, Miller D, Luebke KJ, Hu W. Correlation of anisotropic cell behaviors with topographic aspect ratio. Biomaterials. 2009;30: 1560–1567.
34. Lamers E, van Horssen R, te Riet J, van Delft FC, Luttge R, Walboomers XF, et al. The influence of nanoscale topographical cues on initial osteoblast morphology and migration. Eur Cell Mater. 2010;20: 329–343.
35. Wong ST, Teo S-K, Park S, Chiam K-H, Yim EKF. Anisotropic rigidity sensing on grating topography directs human mesenchymal stem cell elongation. Biomech Model Mechanobiol. 2014;13: 27–39.
36. Zuidema A, Wang W, Sonnenberg A. Crosstalk between cell adhesion complexes in regulation of mechanotransduction. Bioessays. 2020;42: e2000119.
37. Kirby TJ, Lammerding J. Emerging views of the nucleus as a cellular mechanosensor. Nat Cell Biol. 2018;20: 373–381.
38. Chalut KJ, Kulangara K, Giacomelli MG, Wax A, Leong KW. Deformation of stem cell nuclei by nanotopographical cues. Soft Matter. 2010;6: 1675–1681.
39. Cutiongco MFA, Jensen BS, Reynolds PM, Gadegaard N. Predicting gene expression using morphological cell responses to nanotopography. Nat Commun. 2020;11: 1384.
40. Cadart C, Venkova L, Piel M, Cosentino Lagomarsino M. Volume growth in animal cells is cell cycle dependent and shows additive fluctuations. Elife. 2022;11. doi:10.7554/eLife.70816
41. Liliensiek SJ, Campbell S, Nealey PF, Murphy CJ. The scale of substratum topographic features modulates proliferation of corneal epithelial cells and corneal fibroblasts. J Biomed Mater Res A. 2006;79: 185–192.
42. Kulangara K, Yang J, Chellappan M, Yang Y, Leong KW. Nanotopography alters nuclear protein expression, proliferation and differentiation of human mesenchymal stem/stromal cells. PLoS One. 2014;9: e114698.

43. Jones MC, Zha J, Humphries MJ. Connections between the cell cycle, cell adhesion and the cytoskeleton. Philos Trans R Soc Lond B Biol Sci. 2019;374: 20180227.
44. Beijer NRM, Nauryzgaliyeva ZM, Arteaga EM, Pieuchot L, Anselme K, van de Peppel J, et al. Dynamic adaptation of mesenchymal stem cell physiology upon exposure to surface micropatterns. Sci Rep. 2019;9: 9099.
45. Gao C, Tang L, Hong J, Liang C, Tan LP, Li H. Effect of laser induced topography with moderate stiffness on human mesenchymal stem cell behavior. JPhys Mater. 2019;2: 034006.
46. Chaudhuri PK, Pan CQ, Low BC, Lim CT. Topography induces differential sensitivity on cancer cell proliferation via Rho-ROCK-Myosin contractility. Sci Rep. 2016;6: 19672.
47. Wu C, Chin CSM, Huang Q, Chan H-Y, Yu X, Roy VAL, et al. Rapid nanomolding of nanotopography on flexible substrates to control muscle cell growth with enhanced maturation. Microsyst Nanoeng. 2021;7: 89.
48. Turner L-A, J Dalby M. Nanotopography - potential relevance in the stem cell niche. Biomater Sci. 2014;2: 1574–1594.
49. Iyer KV, Maharana S, Gupta S, Libchaber A, Tlusty T, Shivashankar GV. Modeling and experimental methods to probe the link between global transcription and spatial organization of chromosomes. PLoS One. 2012;7: e46628.
50. Tsimbouri PM, Murawski K, Hamilton G, Herzyk P, Oreffo ROC, Gadegaard N, et al. A genomics approach in determining nanotopographical effects on MSC phenotype. Biomaterials. 2013;34: 2177–2184.
51. Rivera C, Gurard-Levin ZA, Almouzni G, Loyola A. Histone lysine methylation and chromatin replication. Biochim Biophys Acta. 2014;1839: 1433–1439.
52. Campos EI, Reinberg D. Histones: annotating chromatin. Annu Rev Genet. 2009;43: 559–599.
53. Misteli T, Soutoglou E. The emerging role of nuclear architecture in DNA repair and genome maintenance. Nat Rev Mol Cell Biol. 2009;10: 243–254.
54. Li B, Carey M, Workman JL. The role of chromatin during transcription. Cell. 2007;128: 707–719.
55. Keeling MC, Flores LR, Dodhy AH, Murray ER, Gavara N. Actomyosin and vimentin cytoskeletal networks regulate nuclear shape, mechanics and chromatin organization. Sci Rep. 2017;7: 5219.
56. Damodaran K, Venkatachalapathy S, Alisafaei F, Radhakrishnan AV, Sharma Jokhun D, Shenoy VB, et al. Compressive force induces reversible chromatin condensation and cell geometry-dependent transcriptional response. Mol Biol Cell. 2018;29: 3039–3051.
57. Alexandrow MG, Hamlin JL. Chromatin decondensation in S-phase involves recruitment of Cdk2 by Cdc45 and histone H1 phosphorylation. J Cell Biol. 2005;168: 875–886.

58. Leman AR, Noguchi E. The replication fork: understanding the eukaryotic replication machinery and the challenges to genome duplication. Genes (Basel). 2013;4: 1–32.
59. Fidorra J, Mielke T, Booz J, Feinendegen LE. Cellular and nuclear volume of human cells during the cell cycle. Radiat Environ Biophys. 1981;19: 205–214.
60. Ingber DE. Tensegrity I. Cell structure and hierarchical systems biology. J Cell Sci. 2003;116: 1157–1173.
61. Makhija E, Jokhun DS, Shivashankar GV. Nuclear deformability and telomere dynamics are regulated by cell geometric constraints. Proc Natl Acad Sci U S A. 2016;113: E32-40.
62. Haase K, Macadangdang JKL, Edrington CH, Cuerrier CM, Hadjiantoniou S, Harden JL, et al. Extracellular forces cause the nucleus to deform in a highly controlled anisotropic manner. Sci Rep. 2016;6: 21300.
63. Pennacchio FA, Nastały P, Poli A, Maiuri P. Tailoring cellular function: The contribution of the nucleus in mechanotransduction. Front Bioeng Biotechnol. 2020;8: 596746.
64. Guilluy C, Osborne LD, Van Landeghem L, Sharek L, Superfine R, Garcia-Mata R, et al. Isolated nuclei adapt to force and reveal a mechanotransduction pathway in the nucleus. Nat Cell Biol. 2014;16: 376–381.
65. Newberg J, Schimpf J, Woods K, Loisate S, Davis PH, Uzer G. Isolated nuclei stiffen in response to low intensity vibration. J Biomech. 2020;111: 110012.
66. Alsteens D, Gaub HE, Newton R, Pfreundschuh M, Gerber C, Müller DJ. Atomic force microscopy-based characterization and design of biointerfaces. Nat Rev Mater. 2017;2: 17008.
67. Fischer T, Hayn A, Mierke CT. Effect of nuclear stiffness on cell mechanics and migration of human breast cancer cells. Front Cell Dev Biol. 2020;8: 393.
68. Sherley JL, Stadler PB, Stadler JS. A quantitative method for the analysis of mammalian cell proliferation in culture in terms of dividing and non-dividing cells. Cell Prolif. 1995;28: 137–144.

Chapter 4

Cyclic Topography Modulation of Azopolymer Surface to Spatio-Temporally Control Cell Functions

4.1. Introduction

The ECM is a dynamic environment which undergoes remodelling processes during growth, diseases, regeneration and wound healing [1–3]. For example, over production or reduced turnover of ECM are hallmarks of tissue fibrosis of many organs [4]. Moreover, the interplay between cells and their microenvironment is a mechanism regulated both in space and time, with stresses continuously generated at different length scales [5]. Thus, the ECM provides to cells both biochemical and biophysical cues which change in a spatiotemporal manner, influencing their functions. Additionally, many soft tissues, such as the heart, blood vessels, lungs and cartilage often are subjected to cyclic strains. Indeed, the endothelial cells (ECs) that are present in the inner layer of blood vessels, are constantly exposed to multiple dynamic mechanical stimuli, including hemodynamic shear stress, pulsatile stretch, and passive signalling cues, generated by the ECM [6]. Therefore, the realization of culturing platform capable to change "on-demand" their physiochemical properties represents a strategy to mimic cellular micro environment thus allowing to investigate cellular behaviour in condition that can better recapitulate the complexity of their native context. In the last years, several "smart" or "stimuli responsive" biomaterials were fabricated, which were capable of modulate their properties in response to

external stimuli, such as pH, heat, electric or magnetic field, mechanical stretching and light [7–9]. For tissue engineering applications, the realization of smart materials able to mimic the dynamic physical, chemical and biological aspects of the native ECM is extremely challenging. In 2D, Mao T. *et al.* designed and fabricated a two-layer microfluidic chip to allow the cyclic stretching of the elastic polymer PDMS, for studying the behaviour of human mesenchymal stem cells (hMSCs) to a series of frequencies from 0.00003 to 2 Hz and varied amplitudes of 2%, 5%, or 10% [10]. Cui Y. *et al*. also demonstrated that stretched soft pillar arrays, with, 1–5% cyclic stretching over a frequency range of 0.01–10 Hz affected cellular spreading and the assembly of actin stress fibre of primary mouse embryonic fibroblasts (PMEFs) [11]. Further, numerous devices for cyclical cellular mechano-stimulation were engineered to investigate cellular response also in a 3D environment [12–15]. On the contrary, only few studies which provided a spatio-temporal control of the topographical signal in a reversible and cyclic manner were conducted [16]. Lam *et al.* first developed a micro topographical platform for cell culture consisting of reversible wave-like microfeatures on PDMS. They demonstrated that C2C12 cells were able to align, unalign, and realign repeatedly in response to the formation and removal of the microfeatures [17]. Also, Kiang et *al.* used a soft polyacrylamide hydrogel with nickel microwires embedded within the top surface, which induced cyclic surface roughness variation. They showed that wavy micropattern influenced spindle factor and area of vascular smooth muscle cells after 1 h in culture [18]. Moreover, several works focused on the employment of shape memory polymers (SMPs), which rely on polymer transition temperature to trigger topography modulation from a temporary to a permanent shape. Le D.M. *et al.* showed that hMSC morphology could be switched from highly aligned to stellate shape in response to a surface variation from a 3 μm × 5 μm channel array to a flat surface [19]. Nevertheless, SMPs provide only a single one way direction surface topography switching, hindering the possibility to apply cyclic stimuli. Azobenzene-based

materials well achieve this aim. Indeed, the photo-isomerization of the azo molecule represents a powerful mechanism for the realization of switchable biomaterials able to regulate cell-material cross-talk in a dynamic way [20]. More precisely, the possibility to realize and remove structural reliefs on the surface of azopolymers allowed these materials to deliver cyclic topographical signal to cells in a spatiotemporally controlled manner. For example, Isomaki M. *et al.* developed a bi-layer system composed of thin layer of Disperse Red 1-containing molecular glass covered by protective film of PDMS where the imprinted SRG were subsequentially removed during cell growth, reorienting the focal adhesions of epithelial cells [21]. Here, the photo-switching properties of pDR1m azopolymer were exploited in order to control both in space and time the presentation of topographical cues to human breast epithelial cells (MCF10A). In more details, anisotropic light-induced topographic pattern were embossed by laser light illumination on pDR1m azopolymer coated surface in presence of living cells at specific time after seeding. Then, after giving cells the time to adapt to the new environmental conditions, the underlying pattern was removed by irradiating the surface with the incoherent light of a mercury lamp. The effect of the cyclic stimulation on cell behaviour was investigated in terms of FAs, cellular and nucleus morphology and organization at early time after the inscription and the removal of the topographic cues. Moreover, after light-induced patterning and erasure cycles, cellular and nucleus mechanical properties after light-induced patterning and erasure cycles were evaluated by means of AFM. Finally, we reported some original preliminary yet striking results based on application of multiple cycle of inscription/erasure surface patterning evaluating their impact on supracellular organization along with nuclear ones.

4.2. Materials and Methods

4.2.1. Sample Preparation

The materials and methods used for samples preparation was already described in paragraph 3.2.1 of Chapter 3.

4.2.2. Cell Culture

The materials used for cell cultures were already described in paragraph 3.2.2 of Chapter 3.

4.2.3. Pattern Inscription and Erasure

The techniques used to impress and remove the linear pattern on pDR1m surfaces were described in Chapter 2. Method of pattern inscription in presence of living cells was already described in paragraph 3.2.3 of Chapter 3. Surface characterization was carried out by Atomic Force Microscopy (AFM) along with scanning electron microscope (SEM). For AFM, a Bruker Dimension Icon was employed, using Silicon Nitride tips (SCANASYST-AIR, Bruker, USA) with a spring constant of 0.4 N/m were used in ScanAsyst mode, in air at room temperature. SEM images were acquired with Ultra Plus FESEM scanning electron microscope (Zeiss, Germany). Photo-patterned pDR1m samples were mounted on microscope stubs and sputter coated with gold (approximately 10 nm thickness). The switching of surface topography was performed in presence of living cells. In details, cells were seeded on the flat surface of pDR1m for 24 h, after which they were exposed to a single or double cycle of light-induced patterning-erasure (P-E), meaning that they were firstly illuminated in order to inscribe the linear pattern, which was subsequently removed. For single cycle experiments, a faster topography surface photo-switching frequency (the inverse of period time occurring between the patterning and the erasure) was used (T = 3 h), while for investigating cell behaviour in response to a double P-E cycle, a slower frequency (T = 12 h) was used to avoid the delivering to cells of a high energy amount in a short time interval.

4.2.4. Immunofluorescence and Live Staining

Cells were fixed at specific time points (3 h post pattern inscription and 3 h post pattern erasure) with 4% paraformaldehyde for 15 min, permeabilized in 0.1% Triton X-100 in PBS for 10 min and then blocked with 3% bovine serum albumin (BSA) for 1 h. Focal adhesions (FAs) were stained with anti-paxillin monoclonal antibody solution (1:200 dilution, Ab32084) for 1 h in 3% BSA in PBS. Heterochromatin was assessed with anti-human Tri-Methyl Histone K27-H3K27me3 antibody (clone C36B11, Cell Signalling, 1:400 dilution) for 1 h in 3% BSA in PBS. After incubation, substrates were washed 3 times with PBS (3 min per wash) and then incubated with anti-rabbit secondary antibody conjugated to Alexa Fluor 488 (dilution 1:1000; Molecular Probes) for 1 h in a humid chamber. Actin filaments were stained by incubating samples with Alexa Fluor 555-phalloidin (1:200 dilution) for 1h in a humid chamber. Nuclei were stained by incubating samples with DAPI (dilution 1:1000; Sigma) for 15 min at 37 °C. Then, samples were mounted in Vectashield Antifade Mounting Medium (Vector Laboratories, Cat. H-1000-10). For live staining, cells were incubated in SiR-DNA (SC007, Spirochrome) (dilution 1:1000) for 30 min at 37 °C.

4.2.5. Cell Live Imaging

MCA10A cell nuclei images acquisition was performed by using Single photon confocal microscopy (Leica Microsystems, Germany), implemented with an incubator at 37 °C and 5 % CO_2. A 20 x objective (NA = 0.5) was used. Nuclei were stained with SiR-DNA dye (λ_{abs}=652 nm) prior to topography linear pattern inscription. Nuclei of cells on the flat surface were acquired with 633 nm laser. Then, P-E surface topography photo-switching was performed by using the same optical system, in order to preserve samples positions. Afterwards, a time-lapse acquisition was conducted every 30 min until 3 h post pattern inscription and 3h post pattern erasure in order to monitor the nuclear deformation during time of the same cells.

4.2.6. Image Analysis

FAs, cell and nucleus morphological measurements were performed by using Fiji. Immunofluorescence images were acquired using a LSM-700 confocal microscope (Zeiss), 63× oil objective (NA=1.4). Cell elongation was measured by phalloidin-stained cells using the MomentMacroJ version 1.3 script (hopkinsmedicine.org/fae/mmacro.htm). More precisely, cell elongation index was defined as the ratio of the principal moments (Imax/Imin). High values of Imax/Imin identify elongated cells. Cell orientation was defined as the angle that the principal axis of inertia forms with a reference axis. The reference axis was considered as the x-axis. Nuclear volumes were evaluated from confocal z-stack images by Imaris software, which provided a measure of 3D surface reconstruction. Also, fluorescence intensity mean values were measured within the obtained volumes. For live staining, cells were incubated in SiR-DNA (SC007, Spirochrome) (dilution 1:1000) for 30 min at 37 °C. Inter-distance between heterochromatin domains were measured on confocal z-stack images by using Imaris spot function, which provide a procedure to detect point-like structures. The dimension of the spheres was chosen in order not to overcome the z-resolution of the confocal microscope. For heterochromatin domains, the spheres were placed automatically by the software within immunofluorescent images of H3K27me3 stained nuclei. More precisely, they were positioned automatically by the software in regions with a local fluorescence contrast based on absolute intensity. Average distance between neighbours spots was then calculated. Statistical significance was assessed through Kruskall-Wallis or ANOVA test (Origin).

4.2.7. Cell Mechanical Properties

JPK NanoWizard II AFM was used to measure mechanical properties of living cells. An optical microscope was combined to the AFM to control tips and samples. Soft cantilevers (SAA-SPH-1UM, nominal spring constant 0.25 N/m)

were used to investigate cell mechanical properties. The AFM was operated in contact mode at a scan rate of 1 Hz. A total of 64 force curves were measured over a cell area of $2 \times 2\ \mu m^2$. Mechanical properties of cells, in terms of Young's modulus values were estimated from each force curve within a force map. Evaluation of the Young modulus was performed with JPKSPM data processing software. The Hertzian model was used to calculate Young's modulus for every force curve, thus generating 64 values for each force map. Results showed the median calculated from these values as a representative modulus of each force measured. Statistical significance was assessed through Kruskall-Wallis or ANOVA test (Origin).

4.3. Results and Discussion

The reciprocal communication between cells and ECM occurs in a dynamic environment, with the ECM continuously undergoing remodelling processes thus presenting pattern of biochemical and biophysical signals at cell-matrix interface, which evolve during tissue growth and diseases [1]. Therefore, the development of materials able to recapitulate the dynamic cell-ECM interplay is of great relevance to study cell behaviour changes in response to time-varying stimuli. To this aim, we realized a photo-switchable platform by exploiting the optical properties of pDR1m azopolymer thin films, which allowed to precisely present/remove specific topographical signals to cells. In particular, the possibility to inscribe and subsequently remove the topographical pattern on the azopolymer surface provided a means to control and guide cell functions throughout the transmission of cyclic topographic cues. Therefore, human breast epithelial cells (MCF10A) behaviour upon topographic photo-switching was investigated in terms of FAs and cell cytoskeleton re-organization few hours after inscription/erasure cycle. In addition, nuclear morphology and inner structures organization were investigated after surface photo-switching in order to test the efficacy of the platform to reverse nuclear deformations induced by the

topographical cues, up to chromatin level. Finally, analyses of cell mechanics were carried out to examine the possibility to regulate also cell tensional state by finely tuning both in space and time the presentation of external topographical signals.

4.3.1. Light-Induced Topographic Patterning and Erasure

Linear pattern was impressed on the surface of pDR1m by using confocal microscope set-up described previously. Although, the characterization of the light-induced topographic pattern was already presented in Chapter 3, here erased surface was also characterized by means of SEM and AFM (Fig. 4.1 A, B).

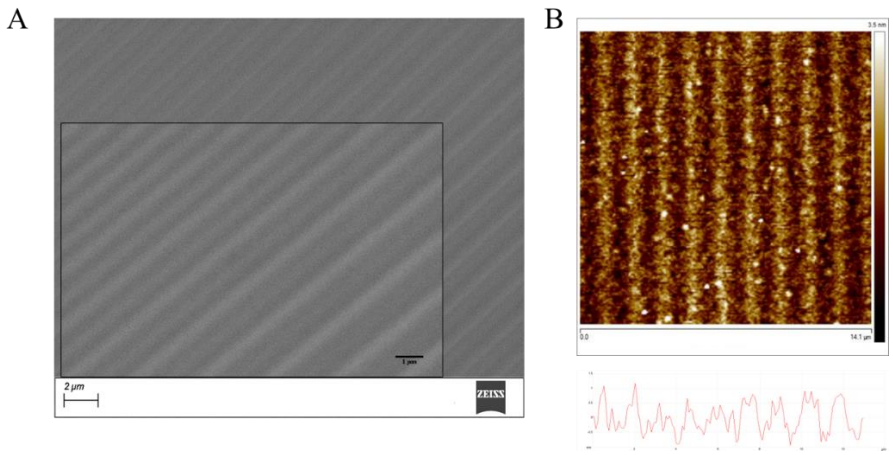

Figure 4.1. A) SEM and B) AFM bi-dimensional and cross-section of optically erased linear gratings realized on pDR1m surface.

The surface analyses reported that the procedure was not able to totally remove the inscribed pattern, still presenting on the surface as wavy periodic structures after 2 min illumination. However, the depths were enormously reduced to few nanometres (2-5 nm), which were comparable to the roughness of flat non illuminated regions of azopolymer surface, as previously showed (Fig 2.6).

4.3.2. Cell Focal Adhesions and Cytoskeleton Re-organization on the Photo-Switching Platform

FAs constitute the mechanical link between the extracellular material substrate and the intracellular cytoskeleton, through which external physical signals were transmitted to cell internal structures. For this reason, cell response to topography photo-switching was firstly examined in terms of FAs re-organization. As discussed in the previous chapter, pattern inscription induced a fast reorganization of FAs plaques, thus changing their morphological features already after 3 h of culturing. However, we asked if such fast FAs reorganization occurs also after the removal of the topographical cues. To this aim, we chose to perform topography surface photo-switching from patterned to erased surfaces after 3 h of culturing and FAs re-arrangement was investigated after a single patterning-erasure (P-E) cycle. More precisely, cells seeded on the planar surface were initially exposed to *in-situ* light-induced topographic patterning and then, after giving cells the time to adapt to the new environmental conditions, the underlying pattern was removed by illuminating the sample with a mercury lamp. Thus, cells subjected to P-E cycle experienced flat-to-pattern-to-erased topographic surface variation as schematically illustrated in Figure 4.2 A.

A

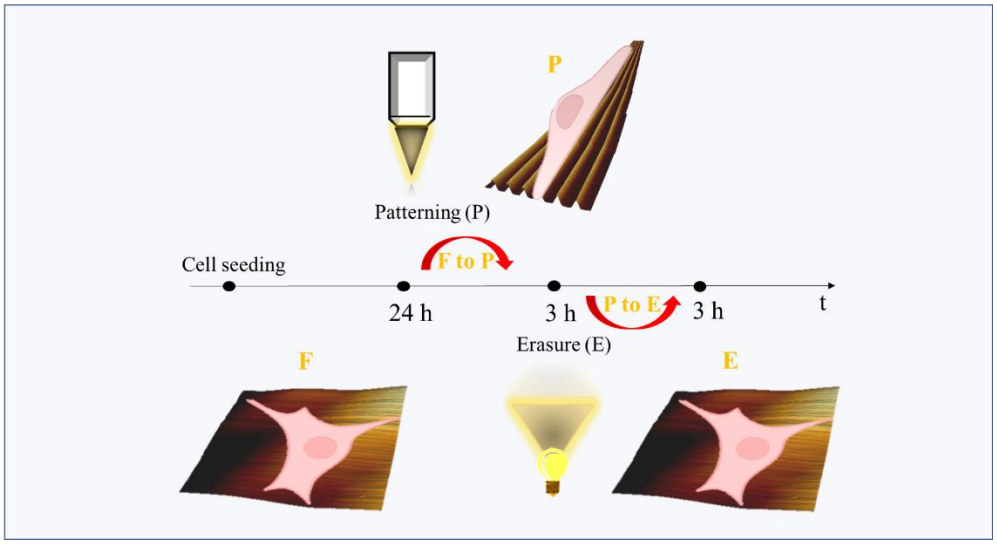

Figure 4.2. Graphical representation of the topography photo-switching process during the P-E cycle on the pDR1m surface in presence of cells.

More in details, the impact of the azopolymer platform photo-switching was assessed by means of immunofluorescence staining of MCF10A FAs plaques (paxillin) after one P-E cycle on the erased surfaces (E) and compared to cells grown on flat regions (F) and cells exposed to *in-situ* light-induced topographic patterning (P) at the same culturing time. Results showed that, similarly to FAs on flat controls, FAs were randomly oriented on the erased surfaces after the P-E cycle, while FAs maintained exposed to the topographic pattern, *i.e.* not subjected to the pattern erasure, appeared oriented along the pattern direction after the same culturing time (Fig. 4.3, A, B). Also, FAs length and aspect ratio after the P-E cycle reached values comparable to FAs grown on flat regions, differently to FAs assembled in the presence of pattern, which resulted more elongated (Fig. 4.3 C, D). Lastly, FAs area of cell cultured after the P-E cycle also attained values comparable to those cultured on flat control surfaces, conversely from those formed on patterned surfaces that retained smaller values (Fig. 4.3 D).

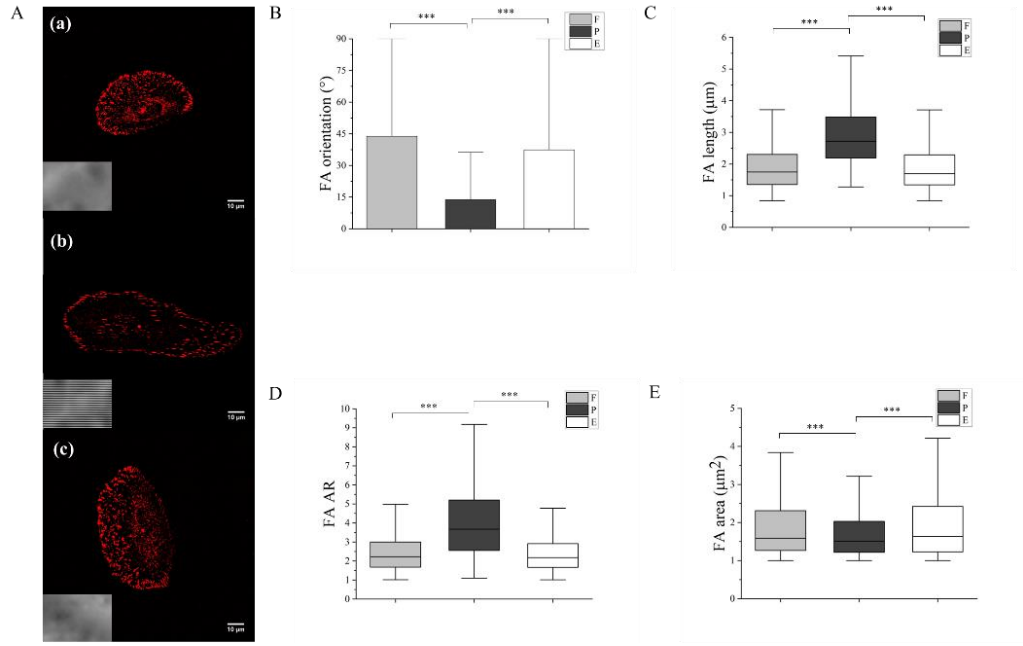

Figure 4.3. A) Confocal images of MCF10A focal adhesions (paxillin, red) on flat (la), light-induced topographic patterned (b) and erased (c) surface. The insert in the left lower corner represented images of flat, patterned and erased surfaces in transmitted mode (the pattern was shown with horizontally oriented parallel lines). B) FAs orientation on flat (F), patterned (P) and erased (E) surfaces. Angles were evaluated with respect to pattern direction for patterned surface and with respect to the horizontal axis for flat and erased surfaces (~ 45° was considered as random orientation). Data are represented as mean values and standard deviations. Results of FAs C) length, D) aspect ratio (AR) and F) area on flat, patterned and erased surfaces, represented as box plots with their median values. Analyses were performed on cells exposed to flat, light-induced topographic patterning and P-E cycle surfaces of diverse regions within the same sample, in order to reduce variability due to different substrates. Only mature focal adhesions (area > 1 µm²) were considered in the analyses (*** $p < 0.005$, not significative if not shown).

Along these lines, AFM topography scanning over MCF10A cells exposed to the light induced and erased topography pattern shaded light onto the mechanism by which the loss of topographical cues sensing occurs after the erasure of the topographic pattern. In fact, in MCF10A cells cultured on nanograted patterned surfaces revealed that cells filopodia protrusions were assembled on top of the pattern ridges, thus favouring focal adhesion growth and elongation along the direction of the pattern (Fig. 4.4 A). However, on the erased surface, filopodia are

able to overcome the residual periodical structure (Fig. 4.4 B), stating that the roughness obtained with these light illumination parameters could be perceived by the cells as that present on the flat surface.

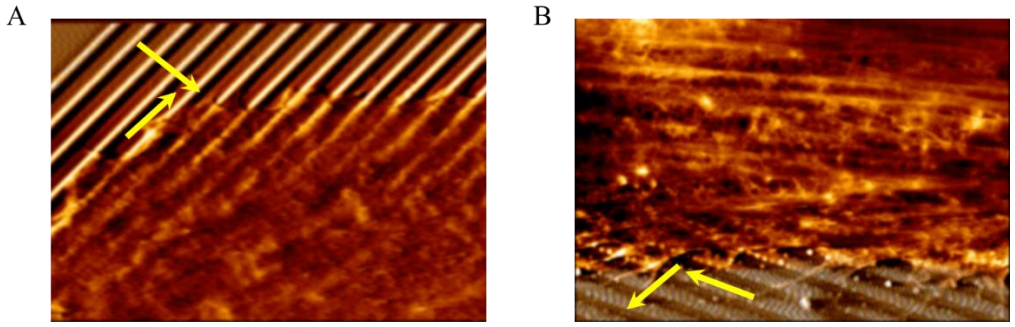

Figure 4.4. AFM 2D topography images of MCF10A cell filopodia on the A) patterned and B) erased pDR1m surfaces. Graphs showed that filopodia on the light-induced pattern assembled on top of pattern ridges, while after the pattern erasure they were able to laterally bulge out, surpassing the residual pattern.

These results stated the ability of the pDR1m azopolymer engineered platform to deviate and revert FAs arrangement by removing "on-demand" the underneath topographic signal. Additionally, since FAs organization can influence cell morphology through the transmission of the topographical signals to cell cytoskeleton, as also shown in the previous chapter, analyses on confocal phalloidin-stained MCF10A cells were performed in order to examine the effect of the photo-switching platform at different cellular length scale. Thus, cell orientation, elongation and spreading area were evaluated after the P-E cycle on the erased surface (E), which were compared to flat control (F) and cells displayed to the light-induced topographic pattern (P). Results showed that cells on the erased surface appeared to recover a random orientation, comparable to cells grown on flat surfaces, while at the same culturing time, cells not exposed to the pattern erasure, *i.e.* cells remained on the patterned surfaces, resulted oriented along the pattern direction (P) (Fig. 4.5 A, B). Also cell elongation index (EI) and cellular spreading area of MCF10A cells subjected to P-E cycle exhibited values similar to those of the cells cultured on the flat surface. Conversely, MCF10A

cells cultured on the patterned surfaces attained a higher elongation and bigger area values (Fig. 4.5 C, D). These results stated the efficacy of the photo-switching platform to control cell shape in a way that cells restored, following the topographical signal removal, a morphological organization that shared several similitudes with those that have never been exposed to any topographical cues.

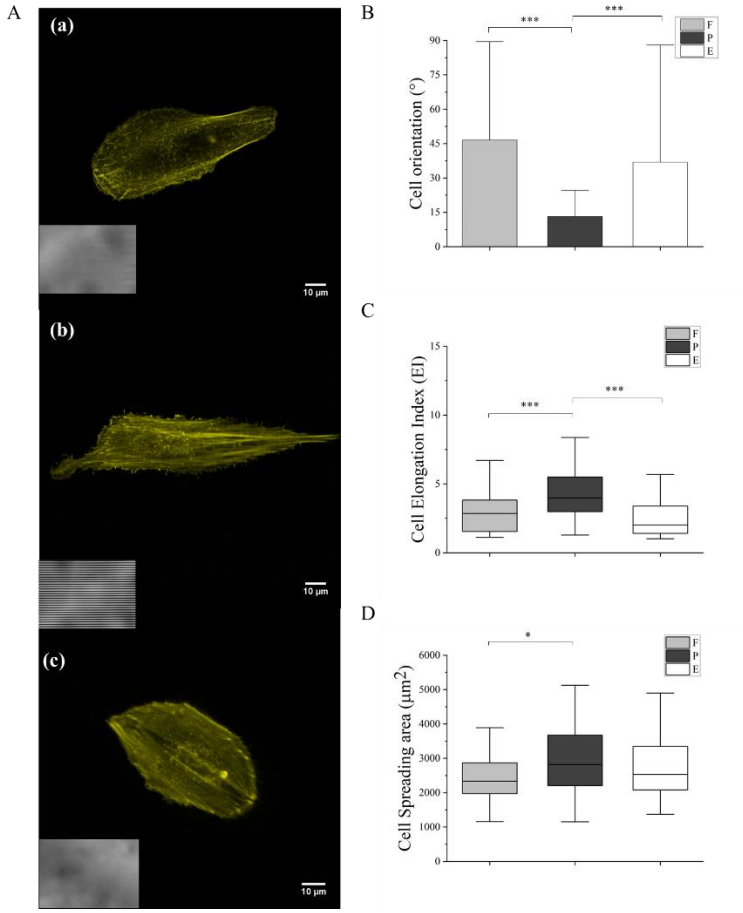

Figure 4.5. A) Confocal images of MCF10A cells labelled with phalloidin (yellow, cytoskeleton) on flat (a), patterned (b) and erased (c) surfaces. The insert in the left lower corner represented images of flat, patterned and erased surfaces in transmitted mode (the pattern was shown with horizontally oriented parallel lines). B) Cell orientation on flat (F), patterned (P) and erased (E) surfaces. Angles were evaluated with respect to pattern direction for patterned surface and with respect to the horizontal axis for flat and erased surfaces (~ 45° was considered as random orientation). Data are represented as mean values and standard deviations. Results of cell C) elongation index (EI) and D) area on flat, patterned and erased surfaces, represented as box plots with their median values. Analyses were performed on cells exposed to flat, light-induced topographic

patterning and W-E cycle surfaces of diverse regions within the same sample, in order to reduce variability due to different substrates (*** $p < 0.005$, * $p < 0.05$, not significative if not shown).

4.3.3. Analyses of Cell Nuclei Morphology on the Photo-Switching Platform

It is known that topographical cues can be transmitted from adhesions to the nucleus throughout cell cytoskeleton, inducing nuclear morphology deformations eventually affecting gene-expression [22,23]. De Martino *et al.* reported the possibility to induce cyclic cellular and nuclear stretches to reroute otherwise committed human mesenchymal stem cells (hMSC) to osteoblastic lineage by dynamically changing the surface of azopolymer thin film from ordered parallel lines to grid shaped surfaces [24]. Here, the photo-switchable properties of pDR1m thin films were exploited to evaluate the feasibility of the dynamic platform to transmit cyclic topographic stimuli to human breast epithelial cells (MCF10A) capable to reverse nuclear deformations. More specifically, nuclear morphology and organization in terms of orientation, aspect ratio (AR), area and volume were investigated firstly on fixed samples after a single patterning-erasure (P-E) cycle. The topography photo-switching from patterned to erased surfaces was performed after 3 h from pattern inscription, as for the experiments described in the previous paragraph. Nuclear morphological parameters of cells experienced P-E cycle were measured 3 h after pattern erasure and compared to those of cells grown on flat regions and cells exposed to light-induced topography pattern, *i.e.* without pattern erasure, at the same culturing time. Analyses on nuclei orientation showed that the nuclei on the erased surface (E) after the P-E cycle recover a random orientation similar to nuclei of cells cultured on flat surfaces (F), while nuclei on the pattern (P) resulted oriented along the pattern direction (Fig. 4.6 A). However, as already investigated in the previous chapter, nuclei AR and projected area appeared not influenced by the topographical signal at early time from its transmission (Fig. 3.5 A, B, Chapter 3), thus after the P-E cycle nuclei showed

values equal to both flat and patterned surfaces, as expected (Fig. 4.6 B, C). Nevertheless, nuclear volume and height of cells exposed to the P-E cycle showed values similar to flat condition, diversely to cells nuclei displayed to the pattern which exhibited both bigger volume and height as a consequence of the topographical stimulus presentation (Fig. 4.6 D, E), demonstrating the ability of the dynamic platform to restore initial nuclear morphological organization.

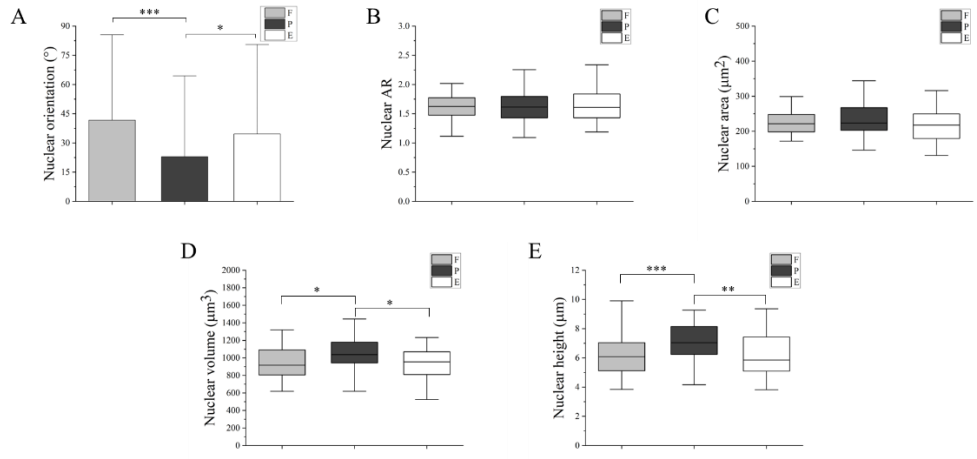

Figure 4.6 A) MCF10A nucleus orientation on flat (F), patterned (P) and erased (E) surfaces. Results of nuclear B) AR, C) area, D) volume and E) height represented as box plots with their median values. Analyses were performed on cells exposed to flat, light-induced topographic patterning and P-E cycle surfaces of diverse regions within the same sample, in order to reduce variability due to different substrates (*** $p < 0.005$, ** $p < 0.01$, * $p < 0.05$, not significative if not shown).

Additionally, in order to verify the nuclear morphology variation upon topography photo-switching on pDR1m surface, evaluation of nuclear orientation and volume was performed by analysing confocal z-stack images of nuclei of living cells. In more details, MCF10A cell nuclei were live stained with SiR-DNA dye in order to monitor the evolution of the same cell nuclei before and after the F-to-P and P- to-E surface photo-switching. Specifically, confocal images of nuclei of living cells were acquired on flat surfaces, 3 h after F-to-P and 3 h after P-to-E photo-switching. Results confirmed the trends observed for distinct

populations of cells for both nuclear orientation and volume, suggesting that a fast cellular response occurred at different supracellular levels (Fig. 4.7 A, B).

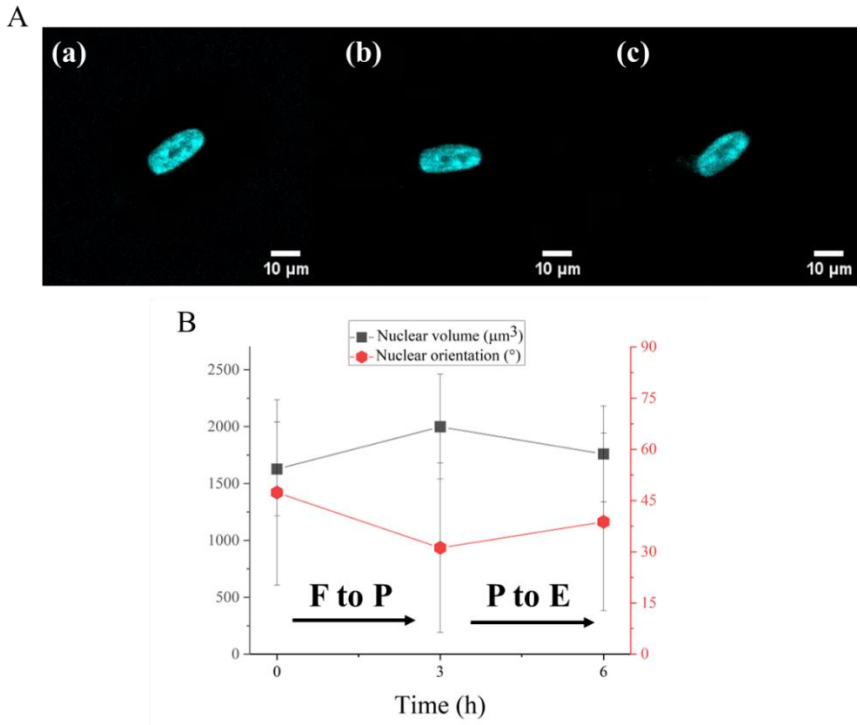

Figure 4.7. A) Representative confocal images of the same MCF10A cell nucleus (SiR-DNA, cyan) undergoing flat (a) to pattern (b) and pattern to erased (c) photo-switching during cell culture. B) Evolution of nuclear orientation and volume analyses performed on living SiR-DNA stained cells subjected to the surface photo switching. Results were showed as mean values and standard deviations.

4.3.4. Chromatin Organization and Condensation

External physical signals can be transmitted to the nucleus influencing its internal structure organization ultimately affecting chromatin condensation state and gene-expression [25]. Thus, in order to examine the effect of surface topography photo-switching on heterochromatin condensation state and arrangement within the nucleus of MCF10A cells, fluorescence intensity of H3K27me3 marker, which allowed to measure the condensation levels of facultative heterochromatin, was evaluated after performing a single P-E cycle. In addition, analyses of the average inter-distance between heterochromatin domains (HCDs) were also

performed. Previous analyses on H3K27me3 marker (paragraph 3.3.6, Chapter 3) revealed that the light-induced topography pattern did not produce a change in the fluorescence intensity mean values between cells exposed to flat and patterned surface, stating that the level of facultative heterochromatin was not influenced by the presence of the topographical cues. Therefore, we did not expect a variation upon photo-switching from F-to-P and from P-to-E surfaces. Indeed, analyses on confocal images of H3K27me3 stained nuclei exposed to P-E cycle reported similar values to flat and patterned controls (Fig. 4.8 A). However, the analyses of inter-distances between the heterochromatin domains (HCDs) showed that the photo-switching platform was able to affect the distance between HCDs after the P-E cycle, reducing them to values similar to the distance of HCDs of nuclei on flat surfaces, both exhibiting lower values than HCDs of nuclei exposed to the topographical signal (Fig. 4.8 B). These results were in accordance with previous analyses, which demonstrated that a nuclear volume expansion was followed by an increase of the distance between HCDs. Here, after the P-E cycle, the nuclear volume of MCF10A cells appeared to return to initial lower values, which corresponded also to a recovering of the initial HCDs inter-distances.

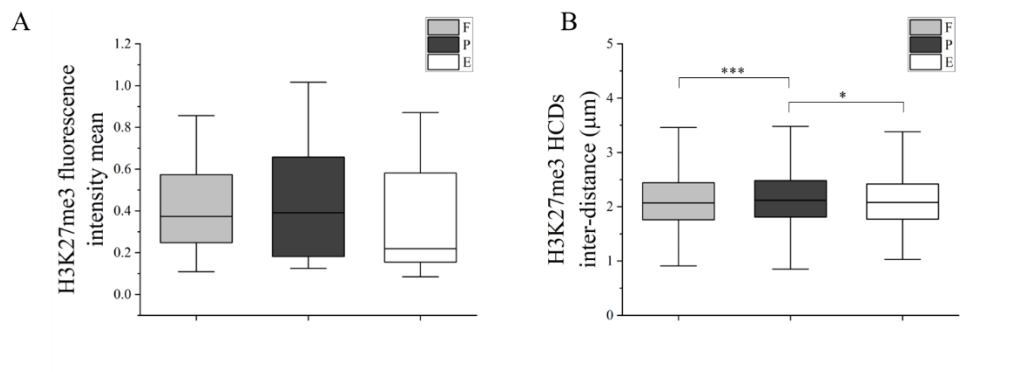

Figure 4.8. Box plots showing mean value of H3K27me3 A) intensity fluorescence mean measured within nuclear volume and C) HCDs inter-distance for both flat (F), patterned (P) and erased (E) surfaces (*** $p < 0.005$, * $p < 0.05$, not significative if not shown).

Therefore, these results showed the potentiality of the dynamic platform to also control also the internal structure organization of the cell nucleus, in terms of heterochromatin domains inter-distances, by regulating the presentation and removal of the topographical signal during cell culture.

4.3.5. Reversed Cell Tensional State after Topography Surface Photo-Switching

Cell mechanical properties can be considered as an indicator of cell tensional state, which can be influenced by external factors. The impression of a topographical linear pattern on the pDR1m surface has proven to increase both cell and nuclear Young's modulus (paragraph 3.3.7 ,Chapter 3), as a consequence of cytoskeleton actin fibres alignment and elongation along the pattern. Additionally, analyses on cell and nuclear morphology revealed that cells were able to recover their initial organization after the removal of the topographical signal. In particular, cell re-organize their cytoskeleton actin fibres, which were previously aligned along a preferential direction dictated by the topographical signal, in a random conformation. Thus, we measured cell and nuclear mechanical properties after a single P-E cycle to find out if cells were able to release the topography-induced mechanical stress upon pattern erasure. Topography erasure was performed after 3 h from pattern inscription. Atomic Force Microscopy (AFM) was used to evaluate Young's modulus of living cells on the flat surface (F), after 3 h from pattern inscription and 3 h after pattern erasure (E). A force mapping with 64 curves over an area of $2 \times 2\ \mu m^2$ was performed on each cell, on two different regions, covering cell body (Fig. 4.9 A, region A) and cell perinuclear area (Fig. 4.9 A, region B), which were supposed to provide elasticity of cell cytoplasm and nucleus, respectively. Results showed that after 3 h from pattern erasure, both cell and nuclear Young's moduli returned to values similar to initial flat condition, which were lower than moduli of cells exposed to the

topographical signal (Fig. 4.9 B, C), meaning that cells can revert their tensional state in response to surface topographic pattern withdraw.

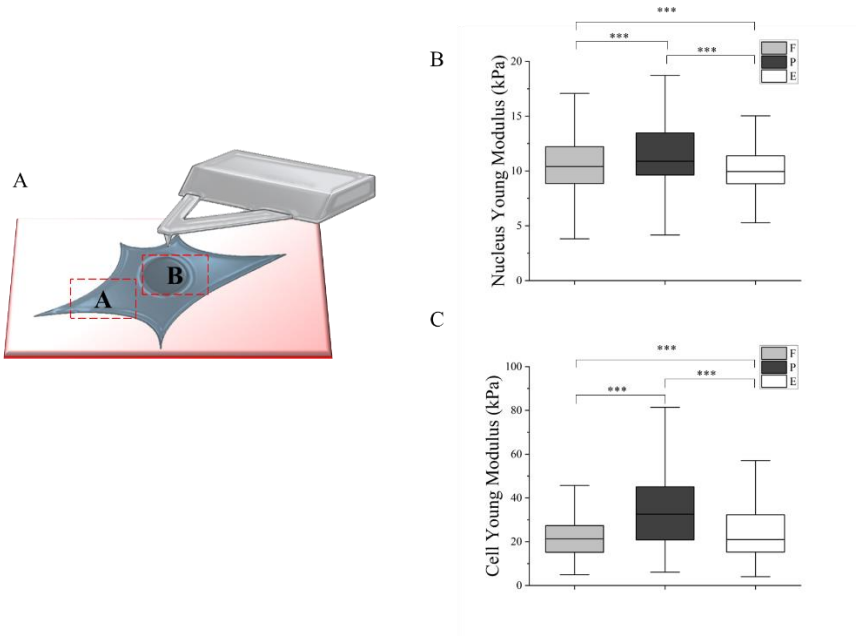

Figure 4.9. Graphical representation of AFM measurement on cell body (A) and nuclear region (B). Young modulus of B) cell cytoplasm and C) nucleus on flat, after 3 h form pattern inscription and after 3 h from pattern erasure. Results were showed as box plots with their median values. (*** $P < 0.005$).

4.3.6. The Effect of Multiple Patterning-Erasure Cycles on Cell and Nuclear Morphology

Several tissues and organs in their natural environment were exposed to multiple dynamic mechanical stimuli, such as heart and blood vessels [26]. Thus, in recent years numerous studies focused on the fabrication of engineered biomaterials able to recreate the highly dynamic nature of the environment surrounding the cells [27]. To this aim, azobenzene-based materials are good candidates since their photo-switching optical properties allowed to realize platforms able to cyclically stimulate cells by continuously presenting/removing surface topographical cues. Here, in order to investigate cell response to multiple topographical stimulation, the surface of pDR1m was exposed to a double patterning-erasure (P-E) cycle,

given that it can be illuminated several times without showing material degradation or photochemical modifications of molecules as shown in the Chapter 2. In more details, cells seeded for 24 h on the flat pDR1m surface (F) were exposed to the light-induced topography patterning which generated an anisotropic linear pattern (P) that was subsequently erased (E) by means of a mercury lamp, after cell adaptation to the physical cues. This P-E cycle of azopolymer topographic features was performed twice on the living cells during the cell culturing time on the pDR1m substrate. The surface photo-switching was executed every 12 h to both allow cells to adapt to the new environmental conditions and provide a larger temporal window in which cells were exposed to a huge amount of light-energy, thus reducing photo-toxic effect (Fig. 4.10 A).

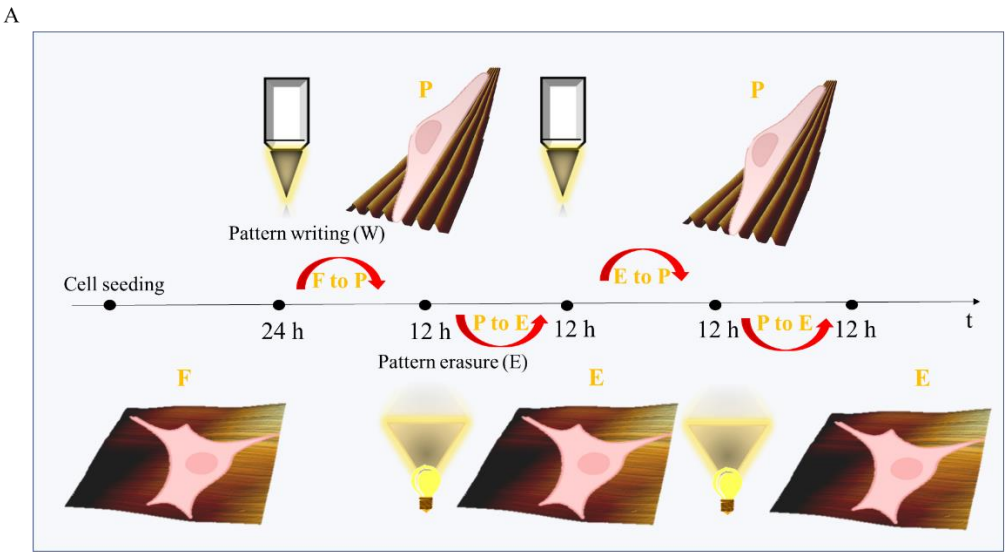

Figure 4.10 A) Graphical representation of the topography photo-switching process during the double P-E cycle on the pDR1m surface in presence of cells.

Validation of cell morphology adjustment upon changes in surface topography was made by optical microscopy observations. In details, confocal microscopy images of MCF10A cells exposed to the double P-E cycle were acquired in transmitted mode on flat surface and after 12 h post each surface topography

photo-switching in order to state cell responsiveness, in terms of morphological qualitative features, to the underlying surface variation, thus also affirming that the multiple light illuminations performed on living cells did not perturb cell viability (Fig. 4.11 A). Then, confocal images phalloidin-stained MCF10A cells were acquired at the end of the double P-E cycle on the erased surface and compared to cells cultured on both flat and cells exposed to light- induced patterned, *i.e.* without pattern erasure, surfaces at the same culturing time (Fig. 4.11 B). Analyses reported that MCF10A cells were able to restore a random orientation and a less elongated shape as a proof of the topographical signal removal (Fig. 4.11 C).

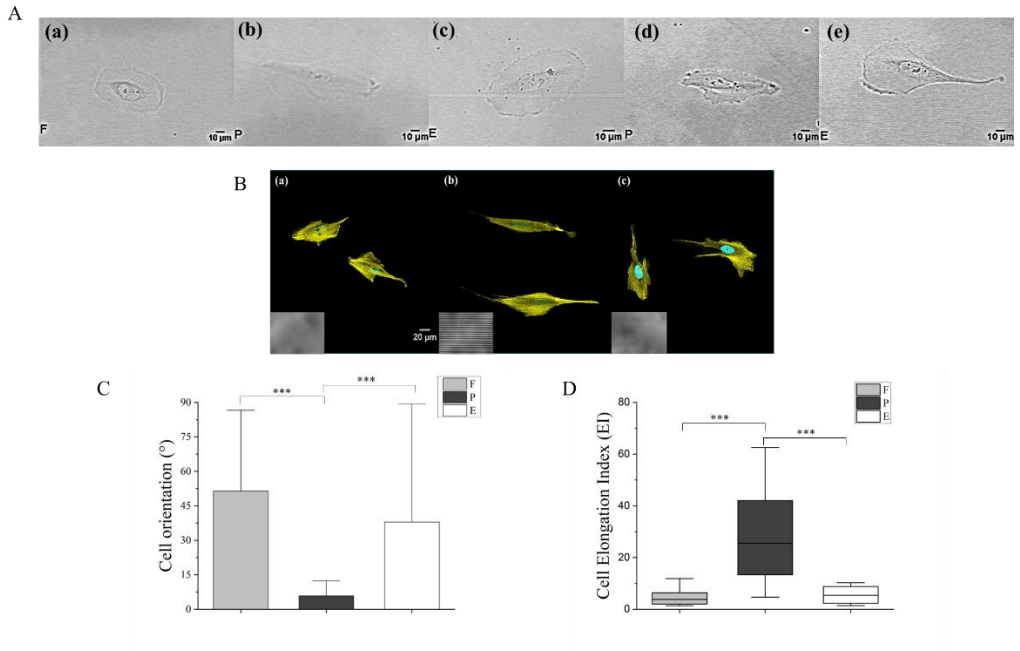

Figure 4.11. Bright field images of MCF10A cells seeded on pdR1m (a) flat surface, (b) 12 h post first pattern inscription, (c) 12 h post first pattern erasure, (d) 12 h post second pattern inscription and (e) 12 h post second pattern erasure. B) Confocal images of phalloidin-stained MCF10A cells (cytoskeleton, yellow) and DAPI stained nuclei (cyan). C) Results of cell orientation on flat, patterned and erased, after the double P-E cycle, surfaces represented as mean values and standard deviation. D) Results of cell elongation index (EI) on flat, patterned and erased, after the double P-E cycle, surfaces represented as box plots with their median values. (*** $p < 0.005$, not significant if not shown).

Since we are interested to investigate the effect of cyclic topographic stimulation on nuclear organization, cell response upon the double P-E cycle was observed also in terms of nuclear morphology, which was shown in the previous chapter to be impacted by the transmission of light-induced topography pattern. In particular, nuclear orientation, aspect ratio (AR) and volume variation on the erased surface (E) after the two P-E surface photo switching was calculated from z-stack confocal images of DAPI stained nuclei and compared to nuclei of cells exposed to flat (F) surfaces and patterned (P), *i.e.* not subjected to pattern erasure, surfaces at the same cell culturing time. The analyses showed cell nuclei on the erased surface restored the random orientation exhibiting also elongation values, (aspect ratio) equal to those of nuclei cultivated on the flat surface (Fig. 4.12 A, B). Additionally, analyses on nuclear height and volume showed that both nuclear morphological parameters of cells on the erased surface assumed values similar with respect to nuclei of cells on the flat surfaces, resulting higher than nuclear height and volume of cells maintained exposed to the topographic pattern for 48 h (Fig. 4.12 C, D). These results demonstrated that even after two topography photo switching cells were able to re-organize their subcellular structures, recovering the configuration they assumed in the absence of topographical stimulus.

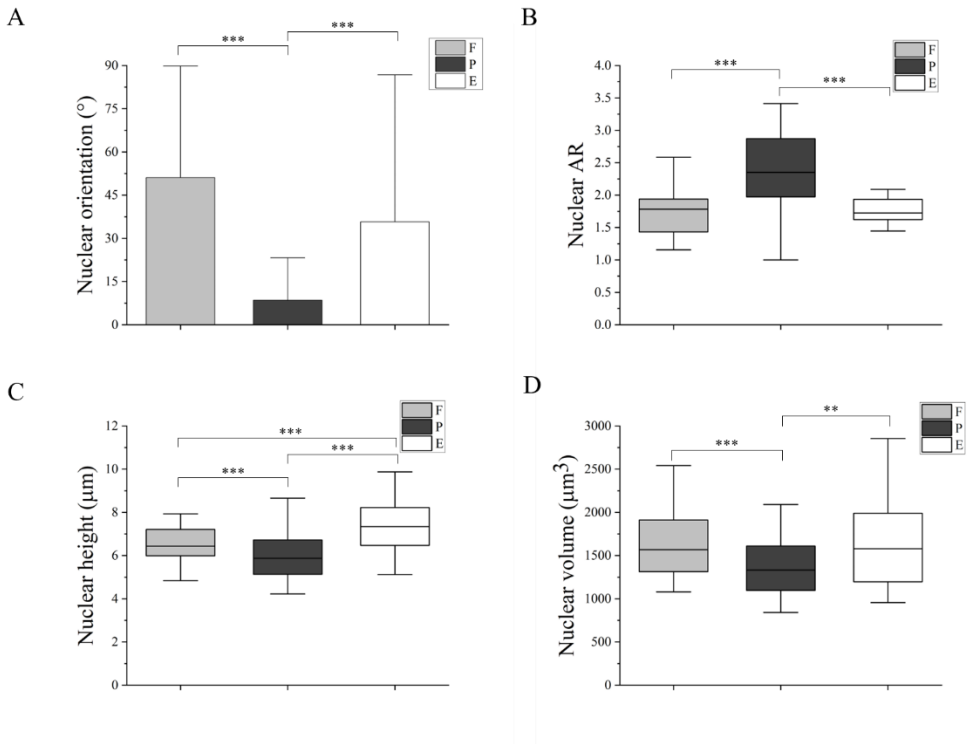

Figure 4.12. A) Results of MCF10A nuclear orientation showed as mean values and standard deviation. Results of MCF10A nuclear B) aspect ratio (AR), C) height and D) volume. Analyses were performed on cells exposed to flat, light-induced topographic patterning and double P-E cycle surfaces of diverse regions within the same sample, in order to reduce variability due to different substrates (*** $p < 0.005$, not significative if not shown).

4.4. Conclusion

The photo-switching properties of pDR1m were exploited in order to realize dynamic platform able to spatiotemporally control the transmission of specific topographic signals to MCF10A cells. Indeed, the possibility to induce multiple surface topography variations allowed to present and remove a topographic signal at precise time instants of cell growth in order to control and guide cell behaviour and functions. Here, we showed that light-induced topography patterning and erasure (P-E) cycles were capable to induce a reversible cell response in terms of FAs, cell and nuclear morphology. Also, chromatin organization within the nucleus appeared to be affected by the cyclic stimulation, with heterochromatin

domains reducing their inter-distances following nuclear volume reduction in response to pattern erasure after the P-E cycle. Moreover, evaluation of cell and nuclear mechanics, measured after every surface topography photo-switching, revealed that cells can revert also their tensional state as a consequence of cell cytoskeleton re-organization from a topography-induced stretched configuration to more relaxed arrangement. Furthermore, MCF10A cells showed a reversible response to both rapid and a slow topography photo-switching frequencies (T = 3 h and T = 12 h) used in a single or double P-E cycle, respectively, validating the potential of the dynamic platform to provide also multiple topography stimuli in response to which cells proved to return to the initial conformational state they assumed on the flat surface before surface light-induced patterning. In conclusion, this dynamic platform represented a means to control cell functions both in space and in time, which can be exploited also as a way to guide stem cell final fate for tissue growth and regeneration applications.

4.5. References

1. Gattazzo F, Urciuolo A, Bonaldo P. Extracellular matrix: a dynamic microenvironment for stem cell niche. Biochim Biophys Acta. 2014;1840: 2506–2519.
2. Rozario T, DeSimone DW. The extracellular matrix in development and morphogenesis: a dynamic view. Dev Biol. 2010;341: 126–140.
3. Lu P, Weaver VM, Werb Z. The extracellular matrix: A dynamic niche in cancer progression. J Exp Med. 2012;209: i1–i1.
4. Lu P, Takai K, Weaver VM, Werb Z. Extracellular matrix degradation and remodeling in development and disease. Cold Spring Harb Perspect Biol. 2011;3: a005058–a005058.
5. Özkale B, Sakar MS, Mooney DJ. Active biomaterials for mechanobiology. Biomaterials. 2021;267: 120497.
6. Charbonier FW, Zamani M, Huang NF. Endothelial cell mechanotransduction in the dynamic vascular environment. Adv Biosyst. 2019;3: e1800252.
7. Khan F, Tanaka M. Designing smart biomaterials for tissue engineering. Int J Mol Sci. 2017;19. doi:10.3390/ijms19010017
8. Cai P, Hu B, Leow WR, Wang X, Loh XJ, Wu Y-L, et al. Biomechano-interactive materials and interfaces. Adv Mater. 2018;30: 1800572.

9. Mohamed MA, Fallahi A, El-Sokkary AMA, Salehi S, Akl MA, Jafari A, et al. Stimuli-responsive hydrogels for manipulation of cell microenvironment: From chemistry to biofabrication technology. Prog Polym Sci. 2019;98: 101147.
10. Mao T, He Y, Gu Y, Yang Y, Yu Y, Wang X, et al. Critical frequency and critical stretching rate for reorientation of cells on a cyclically stretched polymer in a microfluidic chip. ACS Appl Mater Interfaces. 2021;13: 13934–13948.
11. Cui Y, Hameed FM, Yang B, Lee K, Pan CQ, Park S, et al. Cyclic stretching of soft substrates induces spreading and growth. Nat Commun. 2015;6: 6333.
12. Liu H, Usprech J, Sun Y, Simmons CA. A microfabricated platform with hydrogel arrays for 3D mechanical stimulation of cells. Acta Biomater. 2016;34: 113–124.
13. Chandorkar Y, Castro Nava A, Schweizerhof S, Van Dongen M, Haraszti T, Köhler J, et al. Cellular responses to beating hydrogels to investigate mechanotransduction. Nat Commun. 2019;10: 4027.
14. Liu H, MacQueen LA, Usprech JF, Maleki H, Sider KL, Doyle MG, et al. Microdevice arrays with strain sensors for 3D mechanical stimulation and monitoring of engineered tissues. Biomaterials. 2018;172: 30–40.
15. Chen Y-W, Wang K, Ho C-C, Kao C-T, Ng HY, Shie M-Y. Cyclic tensile stimulation enrichment of Schwann cell-laden auxetic hydrogel scaffolds towards peripheral nerve tissue engineering. Mater Des. 2020;195: 108982.
16. Fumasi FM, Stephanopoulos N, Holloway JL. Reversible control of biomaterial properties for dynamically tuning cell behavior. J Appl Polym Sci. 2020;137: 49058.
17. Lam MT, Clem WC, Takayama S. Reversible on-demand cell alignment using reconfigurable microtopography. Biomaterials. 2008;29: 1705–1712.
18. Kiang JD, Wen JH, del Álamo JC, Engler AJ. Dynamic and reversible surface topography influences cell morphology. J Biomed Mater Res A. 2013;101: 2313–2321.
19. Dynamic Topographical Control of Mesenchymal Stem Cells by Culture on Responsive Poly(ϵ-caprolactone) Surfaces.
20. Wu K, Sun J, Ma Y, Wei D, Lee O, Luo H, et al. Spatiotemporal regulation of dynamic cell microenvironment signals based on an azobenzene photoswitch. J Mater Chem B Mater Biol Med. 2020;8: 9212–9226.
21. Isomäki M, Fedele C, Kääriäinen L, Mäntylä E, Nymark S, Ihalainen TO, et al. Light-responsive bilayer cell culture platform for reversible cell guidance. Small Sci. 2022;2: 2100099.
22. Chalut KJ, Kulangara K, Giacomelli MG, Wax A, Leong KW. Deformation of stem cell nuclei by nanotopographical cues. Soft Matter. 2010;6: 1675–1681.

23. Cutiongco MFA, Jensen BS, Reynolds PM, Gadegaard N. Predicting gene expression using morphological cell responses to nanotopography. Nat Commun. 2020;11: 1384.
24. De Martino S, Cavalli S, Netti PA. Photoactive interfaces for spatio-temporal guidance of mesenchymal stem cell fate. Adv Healthc Mater. 2020;9: e2000470.
25. Damodaran K, Venkatachalapathy S, Alisafaei F, Radhakrishnan AV, Sharma Jokhun D, Shenoy VB, et al. Compressive force induces reversible chromatin condensation and cell geometry-dependent transcriptional response. Mol Biol Cell. 2018;29: 3039–3051.
26. Shyu K-G. Cellular and molecular effects of mechanical stretch on vascular cells and cardiac myocytes. Clin Sci (Lond). 2009;116: 377–389.
27. Castro N, Ribeiro S, Fernandes MM, Ribeiro C, Cardoso V, Correia V, et al. Physically active bioreactors for tissue engineering applications. Adv Biosyst. 2020;4: e2000125.

Conclusion and Future Perspectives

In this work, an azopolymer thin film based dynamic platform is proposed with the aim to investigate cell behaviour in response to light-induced surface topography variation. Indeed, in recent years the introduction of "on-demand" time-varying material properties into engineered substrates for the study of cell behaviour has resulted to be a requirement in order to reliably mimic the highly dynamic native extracellular microenvironment. Several works has been reported where cell-material interactions were studied at the interface, showing the influence of micro-nano topography on cell functions, even though the majority of these works were conducted in static conditions. However, the emerging of active materials, able to change their properties in response to external triggers, provide the possibility to control both in space and in time the presentation of physical signals to cells. Nevertheless, a limited number of cell culturing substrates capable of transmitting cyclic topographical signals to cells have been developed. Here, an intensive study and characterization of azopolymer material properties was conducted with the aim to realize a dynamic platform able to control both in space and in time the presentation of light-induced topographical signals to cells. In more details, in **Chapter 1** an overview of cell−material interaction with the mechanism of physical signal transmission from focal adhesions to the nucleus was discussed together with azopolymers optical properties and their biological applications. In **Chapter 2** a detailed description of confocal microscope set-up used to imprint linear pattern in the form of parallel ridges/grooves on the azopolymer surface was given as well as the relation between topographical pattern geometrical features and laser scanning parameters, allowing to finely control the shape of the sinusoidal imprinted pattern in terms of height and pitch. Moreover, two different methods of topography erasure were proposed based on azopolymer surface light illumination of either the Gaussian beam of a confocal microscope or the incoherent light of a

mercury lamp. Lastly, a method to prevent blister formation at azopolymer film/glass substrate interface in presence of water solutions through glass surface silanization was proposed in order to enhance azopolymer adequacy for cell culture experiments. In **Chapter 3**, azopolymer substrates were used in order to realize photo-responsive platforms for cell behaviour investigation. More specifically, a linear pattern was embossed *in-situ* on the surface of the azo material in presence of human breast epithelial cells (MCF10A) by means of a confocal laser microscopy set-up. Then, cell response to the underneath topography variation was evaluated during time in terms of focal adhesion assembly, cytoskeleton orientation and alignment, nucleus morphology and chromatin organization. Results showed that cell subcellular structures were able to sense the topographical signal already after 3 h from the transmission of the signal. Also, analyses at longer time reported that cells showed a dynamic adaptation behaviour, with increasing spreading area and elongation, meaning that they required time to accommodate the new external environment. Additionally, measures on nuclear volume revealed that the light-induced linear pattern causes a volumetric growth which exhibited a time evolution different from cells grown on planar surfaces. This result suggested an impact of nano-topography on cell cycle, resulting in a reduced proliferation rate of cells. Moreover, the morphology variation of nucleus caused by the topographical cues was reflected also within its internal structure, stating that macroscopic deformation generated from the force applied by the cell cytoskeleton, could be transmitted to its inside up to chromatin level. Indeed, the nuclear expansion dictated by the linear pattern was followed by homologous chromosomes volume and distance increase. Furthermore, analyses on chromatin scale revealed that its levels reduced 24 h post pattern inscription stating the ability of the dynamic platform to open the chromatin structure, thus rendering genomic materials more accessible to transcription factors. Additionally, heterochromatin domains inter-distances resulted to increase in response to pattern formation, demonstrating a

re-organization of the inner nuclear structure following pattern inscription. Lastly, Atomic Force Microscopy measurements of cell mechanics showed that the alignment of cytoskeleton actin fibres along the pattern direction produced a cell stiffening resulting in higher cells and nuclei Young modulus values. In **Chapter 4**, the photo-switching properties of azopolymer were exploited in order to realize dynamic platform able to spatiotemporally control the transmission of specific topographic signals to MCF10A cells. Indeed, the possibility to induce multiple surface topography variations allowed to present and remove a topographic signal at precise time instants of cell growth in order to control and guide cell behaviour and functions. Here, we showed that light-induced topography patterning and erasure (P-E) cycles were capable to induce a reversible cell response in terms of focal adhesions, cell and nuclear morphology. Also, chromatin organization within the nucleus appeared to be affected by the cyclic stimulation, with heterochromatin domains reducing their inter-distances following nuclear volume reduction in response to pattern erasure after the P-E cycle. Moreover, evaluation of cell mechanics revealed that both cell and nuclear Young modulus, measured after every surface topography photo-switching, showed that cells can revert also their tensional state as a consequence of cell cytoskeleton re-organization from a topography-induced stretched configuration to more relaxed arrangement. Furthermore, MCF10A cells showed a reversible response to both rapid and a slow topography photo-switching frequencies (T = 3 h and T = 12 h) used in a single or double P-E cycle, respectively, validating the potential of the dynamic platform to provide also multiple topography stimuli in response to which cells proved to return to the initial conformational state they assumed on the flat surface before surface light-induced patterning.

In conclusion, we developed a dynamic platform for cell behaviour investigation which is able to transmit precise spatiotemporally controlled instructions to cell, influencing their morphology and functions. Also, this cell culture platform

allowed to study the connection between cell morphology and nuclear internal organization, in terms of chromosome and heterochromatin domains arrangement, generated by the dynamic topography surface variation with the aim to examine the impact on the genomic materials as a consequence of nuclear deformation induced by the topographical signal. Eventually, the possibility to erase the imprinted pattern restoring the initial flat surface allowed to induce both single and multiple topography variation thus transmitting cyclic stimulation to cells, which resulted to be able recover their initial morphological configuration, paving the way to the use of a new class of cell-instructive biomaterials, on which topographic cues can be presented/removed "on-demand" allowing to unravel many biological processes involved in dynamic cell-topography interaction. Further, given that this photo-switchable platform represents a means to control cell functions in a spatiotemporal way, we propose for future experiments to exploit it in order to guide stem cell final fate for tissue growth and regeneration applications.

Aknowledgments

I want to say thank you to all people helped me to realize this PhD thesis and supported me and my research activity during these formative years.